Semi-continuous Extraction of Bio-alcohols using Supercritical Carbon Dioxide

---

A Major Qualifying Project
submitted to the faculty of
the Chemical Engineering Department at
WORCESTER POLYTECHNIC INSTITUTE
in partial fulfillment of the requirements for the
degree of Bachelor of Science.

March 24, 2017

Submitted by:

Cameron DiSpirito

Eric Stolz

Advisors:

Professor Michael Timko

Professor Geoffrey Tompsett

Abstract

Biofuels, especially ethanol, have become a competitive alternative to petroleum based fuels. Higher molecular weight alcohols, such as butanol, pentanol, and hexanol, are more effective fuels than ethanol due to their high energy density and low water solubility. However, these fuels are currently uneconomical to produce by fermentation because they are cytotoxic, which limits alcohol concentrations during fermentation to below 2%. Continuous or semi-continuous product removal, such as by supercritical fluid extraction (SFE) could help alleviate the limitations caused by end product inhibition. While most cells are unable to survive the high pressure conditions required for SFE, *Bacillus megaterium* SR7, a strain of bacteria recently discovered by an MIT research group and genetically modified to produce isobutanol, can grow under conditions required for SFE. To determine the feasibility of semi-continuous extraction of alcohol from fermentation broth, this project examined the extraction efficiency for n-butanol, isobutanol, n-pentanol, and n-hexanol at initial concentrations of 0.5 wt% and 1.0 wt% from aqueous solutions. Flow rates of 1.26, 3.2, 5.4, and 9.0 mL/min were tested for each alcohol, and the extraction efficiency for each set of conditions was determined. Extraction efficiency was defined as the amount of CO_2 required to extract a given mass of alcohol. By this metric, higher molecular weight alcohols were more efficient than lower molecular weight alcohols, and slower flow rates were more efficient than higher flow rates. Additionally, overall mass transfer coefficients were estimated for each case based on a two-film model of mass transfer. However, it was determined that for many of the conditions tested, the system was equilibrium limited. This was confirmed by calculating the distribution coefficient for each case, and comparing this value to literature predictions for partition coefficients. It was found that higher molecular weight alcohols were more likely to be equilibrium limited than lower molecular weight alcohols, and that slow flow rates were also more likely to be equilibrium limited compared to fast flow rates. Finally, to determine the growth rate of *B. megaterium* SR7 under SFE conditions, the bacteria was grown under 1500 psig $scCO_2$. Growth was primarily concentrated in a divot in the bottom of the reactor, indicating that cells in other parts of the reactor may be under shear stress. In response, the mixing profile in the reactor was modeled using both literature correlations and by mixing ultrafine cellulose in an acrylic model of the reactor. Results indicated that slower mixing speeds, as well as installing baffles and using impellers which generate less shear, would be beneficial.

Table of Contents

1. Introduction

As the world's population increases and various forms of technology become more abundant and accessible, energy demands also increase. In fact, energy demands have been increasing at a rate of 1.1% per anum and are predicted to follow a similar trend in future years (Shafiee & Topal, 2009). Currently, fossil fuels are the most abundant and widely used form of energy worldwide (Shafiee & Topal, 2009). Fossil fuels include various sources of non-renewable energy, such as coal, oil and natural gas. Such forms of energy are considered non-renewable because they take millions of years to form naturally and cannot be synthetically produced in short periods of time and as a result, natural reserves are rapidly depleting (Shafiee & Topal, 2009). Analysts predict that sources of crude oil will be completely diminished by the year 2050 (Shafiee & Topal, 2009). Oil accounts for 32.9% of energy consumption worldwide and is used commonly in the transportation industry (BP 2016). Keeping in mind the modern world's dependence on oil and its diminishing natural sources, it is clear that alternative forms of energy need to be explored in an attempt to find viable replacements.

Several alternative energy sources have been explored in response to the concerns with petroleum over the past several decades. These include solar, wind, nuclear, hydropower, and biofuels (Haugen & Musser, 2012). Of particular interest to the transportation fuels industry is the development of biofuels to supplement or replace gasoline and diesel. Ethanol has been established as an effective fuel extender, and has been added to gasoline in a 1:10 ratio as "E-10" since the 1970s (Haas, 2011). Ethanol is industrially produced by yeast fermentation of corn or sugar cane stock (Sukumaran, Gottumukkala, Rajasree, Alex, & Pandey, 2011). Additionally, due to their higher oxygen content, alcohol enriched fuels generally burn cleaner, with less particulate and carbon monoxide produced, than pure gasoline (Haas, 2011). One of ethanol's main limitation, however, is its low energy content of 76,330 BTU/gal compared to gasoline's 115,000 BTU/gal (*Fuel Properties Comparison*, 2014). Another major concern for ethanol-gasoline blends is water contamination, since ethanol is hydroscopic (Wallner, Miers, & McConnell, 2009). Water contamination can result in a phase separation between ethanol and gasoline, which can foul engine components and decrease efficiency (Wallner et al., 2009).

One alternative to ethanol additives is butanol. Butanol has an energy density that is only 15% less than that of gasoline, which is a significant improvement over ethanol (Wallner et al., 2009). Butanol is also less explosive and less volatile than ethanol, making it a safer alternative

(Teresa Moreno, Stephen J Tallon, & Owen J Catchpole, 2014). Butanol has been industrially produced via the acetone, n-butanol, ethanol (ABE) fermentation pathway since 1912 (Teresa Moreno et al., 2014). The ABE process generally produces a fermentation broth with an A:B:E ratio of 3:6:1, with a final butanol concentration of 1.2 wt% (Teresa Moreno et al., 2014). Due to this low butanol concentration, separation costs associated with butanol production have been a major challenge to the industrial production of biobutanol (Teresa Moreno et al., 2014).

Bacillus megaterium SR7 is a strain of bacteria which can withstand high pressure and can be genetically modified to produce isobutanol (Thompson et al., 2016). In contrast to the traditional ABE fermentation pathway, the modified *B. megaterium* SR7 produces isobutanol via a two enzyme pathway (Thompson et al., 2016). Of particular interest is *B. megaterium*'s ability to grow and produce isobutanol at pressures of 100 bar (Thompson et al., 2016). Under such high pressures, carbon dioxide is in the supercritical state, which allows for the possibility of supercritical fluid extraction (SFE) of the isobutanol from fermentation broth.

Cleary, butanol has potential as a source of renewable energy from a chemical properties perspective. However, in order to determine its feasibility for industrial use, other characteristics, such as its extractability from solution, must be taken into account. Conventional methods of purification usually implement distillation (Teresa Moreno et al., 2014). Although distillation has proven to be an effective method for removing alcohols from solution, it comes with certain limitations. Distillation is an energy intensive process which requires large and expensive pieces of equipment, especially for purification of feedstocks with low initial concentrations (Errico, Tola, Rong, Demurtas, & Turunen, 2009). Therefore, more efficient extraction processes must be studied to make bio-butanol economically feasible. One such process which could decrease the cost of butanol separation is super critical CO_2 extraction. CO_2 is non-toxic, non-flammable and inexpensive (Teresa Moreno et al., 2014). Furthermore, under supercritical conditions it acts as a strong solvent for alcohols, such as butanol. Recovery of solutes from $scCO_2$ simply requires a pressure drop, where the CO_2 leaves its supercritical state thus exiting as a gas and leaving behind solutes (Teresa Moreno et al., 2014). Another important aspect of $scCO_2$ extraction is that it allows for in situ product recovery (ISPR), which increases the productivity of the bacteria and thus the end yield of butanol (Li, Chiang, Tseng, He, & Chao, 2016). Taking these factors into account, $scCO_2$ extraction has the potential to make butanol separation a more efficient and economically viable process.

2. Background

2.1 Biofuels

Biofuels are energy sources derived from living matter. Unlike fossil fuels, biofuels serve as a source of renewable energy and are capable of being produced in relatively short periods of time. Additionally, biofuels are commonly considered carbon neutral since they are typically derived from plant matter. Consumption of CO_2 by crops used to produce biofuels offsets the CO_2 emissions released from combusting biofuels (Mathews, 2008). Biofuels also pose significant advantages from an economic standpoint since they reduce the U.S. reliance on foreign oil, thus stimulating local economic growth. Although typically perceived as liquid fuel sources, biofuels also exist in solid and gaseous states (Guo, 2015). Solid biofuels are generally wood based and include firewood, wood chips, wood pellets and charcoal. Such forms of biofuel are typically used for electricity generation and heating. Liquid biofuels, which tend to be used in the transportation industry, include bioethanol, biobutanol, and biodiesel. The most common form of biogas is methane, which serves as an energy source for heating and cooking (Guo, 2015). Currently, the U.S. uses fossil fuels as its primary energy source, as shown in Figure 2.1. Furthermore, biofuels make up 47% of the renewable energy currently being used.

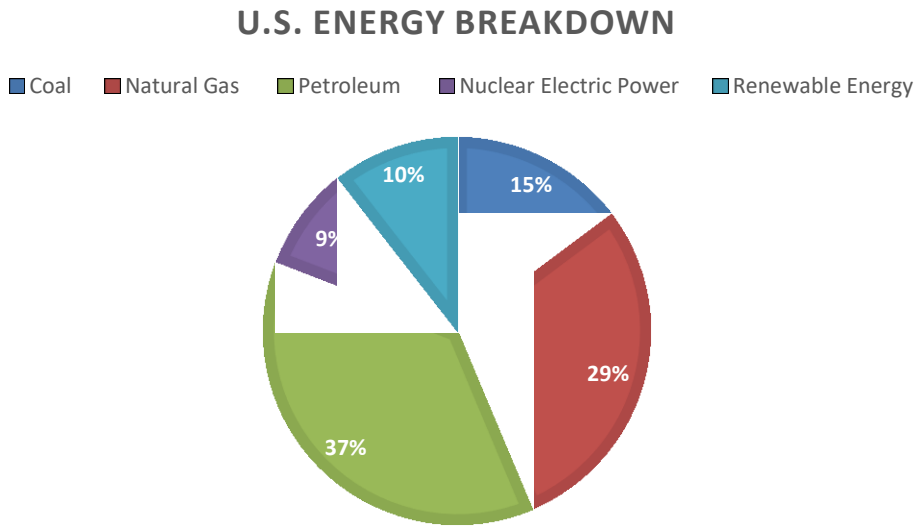

Figure 2.1: U.S. energy consumption. (Primary Energy Consumption by Source, 2016)

2.1.1 History of Biofuels

Older forms of biofuels, such as wood, have served as an energy source for humans for thousands of years. Originally, the combustion of wood and other cellulosic material provided

early humans with heat and light (Guo, 2015). With the dawn of the industrial revolution, wood and coal also served as an energy source for steam engines and electricity production. More recently, liquid biofuels, such as bioethanol, have gained attention from the scientific community as an alternative energy source for the transportation sector (Tyner, 2008). Liquid biofuels are prime candidates for the transportation sector because the current infrastructure uses liquid fossil fuels as the primary means of energy. Therefore, transitioning between the two will be easier. The Energy Policy Act of 1978 was instrumental in providing funding for the production of bioethanol as a fuel additive (Tyner, 2008). Thirty years later, the U.S. Energy and Security Act of 2007 called for an increase in biofuel production by establishing a goal of 136 billion liters of biofuel additive to gasoline by 2022; a 102 billion liter increase from 2008 (Guo, 2015). Such legislation catalyzed tremendous growth in the biofuel industry. In 1984 1.265 billion liters of bioethanol was produced; by 2004 12.85 billion liters of bioethanol was produced, a 56 million liter increase in bioethanol per year (Tyner, 2008). Between the years 2005 and 2008, the biofuel industry increased production tremendously, resulting in an 8.9 billion liter increase in production per year (Tyner, 2008). With strong government backing, the biofuel industry continues to grow at an astonishing rate, as shown in Figure 2.2. An outline of government legislation which has catalyzed growth of the industry is presented in Figure 2.3.

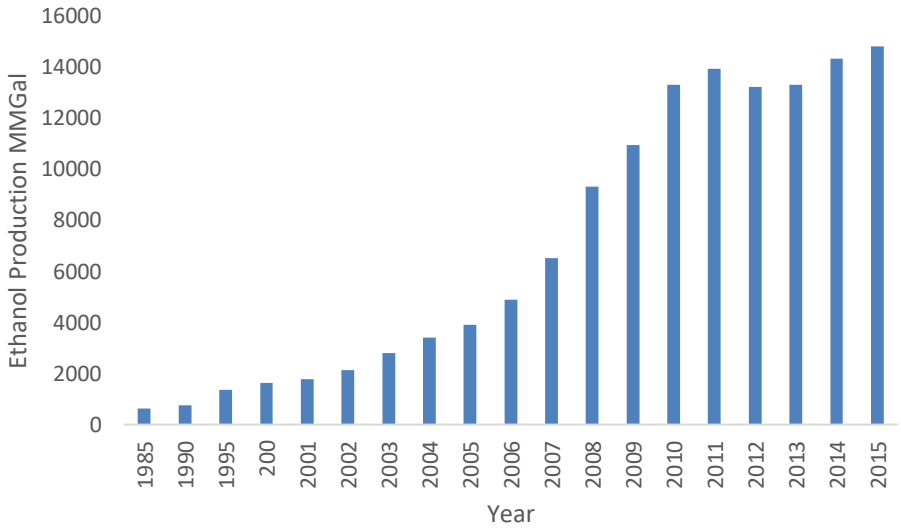

Figure 2.2: Ethanol production from 1985 to 2015. (Fuel Ethanol Overview, 2016)

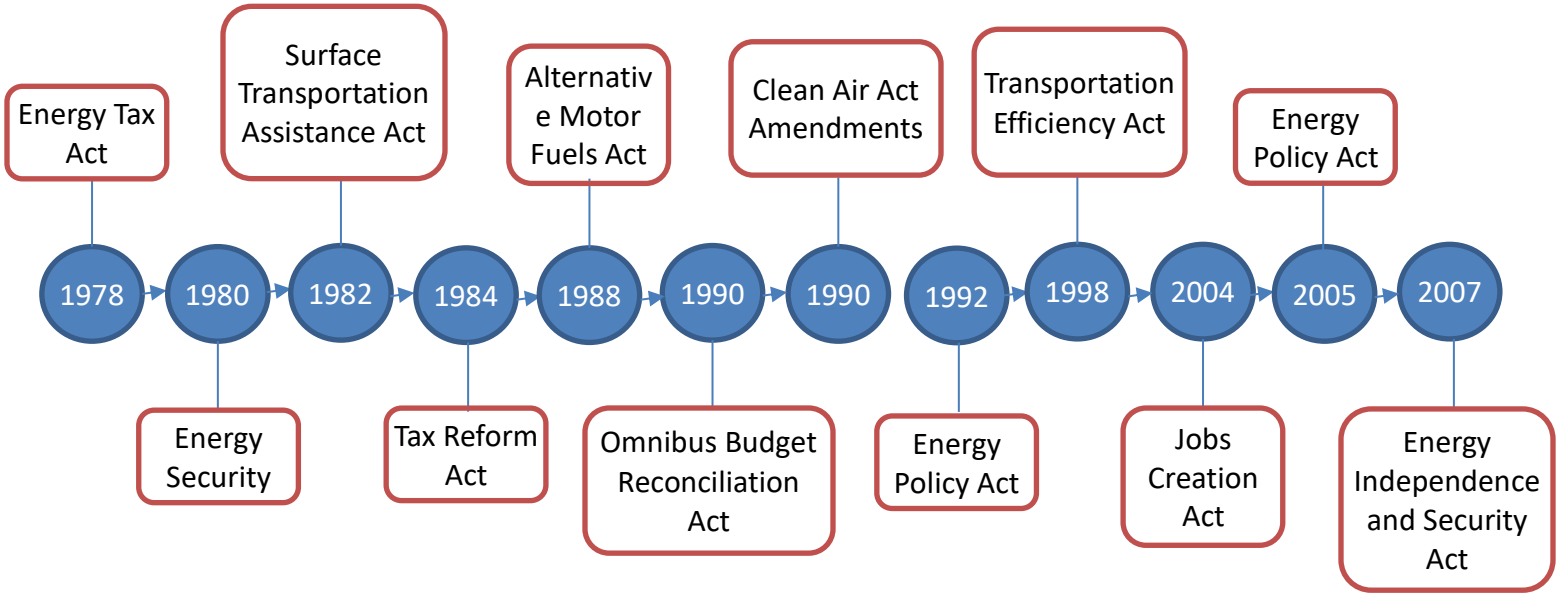

Figure 2.3: Timeline showing legislation which facilitated growth of bioethanol industry. (Tyner, 2008)

2.1.2 Biofuels Used in the Transportation Industry

There are several forms of biofuels used by the transportation industry. Bioethanol is the most common biofuel because it's currently the most cost effective option and the U.S. government has imposed regulations which ensure its use in small percentages (approximately 10%) as a gasoline additive. Two different feed stocks can be used for the production of bioethanol; material containing fermentable sugars or material containing difficult to digest polysaccharides (Cardona & Sanchez, 2007). Some examples of sugar containing feedstocks are sugar cane, molasses, and corn. Sugar containing feedstocks can be directly metabolized by yeast and other microorganisms to form bioethanol with minimal pretreatment. However, such feedstocks tend to be expensive since they are also used in the food industry and as feed for livestock (Cardona & Sanchez, 2007). Polysaccharide based feeds such as lignocellulosic biomass require extensive pretreatment in order to facilitate degradation, removal of indigestible lignin, hydrolysis of hemicellulose and the regulation of the ratio of crystalline cellulose to amorphous cellulose (Cardona & Sanchez, 2007). Therefore, producing bioethanol from lignocellulosic feedstocks is accompanied by higher processing costs. However, the raw feedstock is inexpensive since it is comprised mostly of agricultural byproducts or from plants which are fast growing and do not compete with the agricultural industry (Cardona & Sanchez, 2007). Biodiesel is a less common biofuel which is conventionally synthesized via the transesterification reaction of recycled

vegetable oil (Fangrui & Milford, 1999). More recently, researchers have explored the feasibility of producing biodiesel from microalgae. However, various engineering and economic obstacles must be overcome before this form of biofuel is marketable (Yusuf, 2007). Finally, biobutanol has gained recent attention from the scientific community as an alternative to other liquid fuels. Similar to bioethanol, biobutanol can be produced via the metabolic pathways of microorganisms or yeast. One such example is acetone-butanol-ethanol (ABE) fermentation. During this process, *solventigenic clostridia* converts sugar or starch into three products: acetone, butanol, and ethanol (Green, 2011). Although ABE fermentation is commonly implemented in industry, it has several drawbacks including high feedstock cost, low butanol yield, and high water consumption. Furthermore, the final products are conventionally separated from solution via distillation, which is an energy intensive process. Separation costs are further increased given the low titre of butanol in the final solution (Green, 2011). Biobutanol is a topic of growing interest because butanol has several more favorable fuel characteristics compared to ethanol (Rakopoulos, Rakopoulos, Giakoumis, Papagiannakis, & Kyritsis, 2014). A thorough comparison of bioethanol and biobutanol is presented in the following section.

2.1.3 Comparison of Bioethanol, Biobutanol, and Gasoline

As previously mentioned, bioethanol, biobutanol and gasoline have different chemical properties, thus posing certain advantages and drawbacks. Gasoline is a combination of various hydrocarbons which range widely in chain length (from C_7 to C_{11}) and chemical properties. As a result, the properties of gasoline are often quantified by a range of values (Wallner et al., 2009). Bioethanol is an alcohol possessing the following chemical formula: C_2H_5OH. Biobutanol is a higher order alcohol, with a longer chain length, since its chemical structure is capable of displaying several different isomers. The chemical formula of biobutanol is C_4H_9OH (Wallner et al., 2009). Clearly, bioalcohols are quite different from gasoline, but one of the most notable differences in chemical makeup is the presence of the alcohol functional group. This factor contributes to some differences in combustion properties, intensive properties, and other relevant fuel characteristics.

Bioethanol and biobutanol are 35% and 21.5% oxygen by mass, respectively, compared to gasoline which is 0% oxygen by mass. The presence of oxygenates in fuel results in more thorough combustion, thus reducing unhealthy and environmentally degrading emissions. More specifically, oxygenates reduces carbon monoxide emissions, which helps to regulate ozone formation in the

atmosphere (*Oxygenates Fact Book*). Additionally, they help reduce nitric oxide emissions, hydrocarbon emissions, and volatile organic compound emissions, which are known to form smog. Furthermore, oxygenates extend the shelf life of gasoline by helping to maintain proper octane levels (*Oxygenates Fact Book*). Conventionally, carcinogenic aromatic compounds have been used to increase the shelf life of gasoline. Oxygenates are a viable replacement for such compounds, which is an important aspect from a public health perspective (*Oxygenates Fact Book*). Therefore, bioethanol and biobutanol release lower amounts of harmful emissions into the atmosphere. Also, taking into consideration the prevalence of additives and other chemicals in conventional gasoline, such as methyl tert-butyl ether (MTBE), it clearly releases more degrading compounds into the environment upon combustion (Nadmin, Zack, Hoag, & Liu, 2001; Wallner et al., 2009). These are important figures from an environmental standpoint, especially considering the impact of harmful emissions on climate change.

Ethanol has a lower heating value (LHV) 37% less than gasoline and biobutanol has a LHV 22.5% less than gasoline (Wallner et al., 2009). The LHV is a measurement of heat available to do work upon combustion of a fuel source while also taking into account the heat lost during the vaporization of water byproducts. Therefore, when used in a combustion engine, a larger portion of the energy released from combustion is lost during the vaporization of water byproducts in both these bioalcohols compared to hydrocarbons. This poses a slight drawback for biobutanol and bioethanol from a thermal efficiency standpoint. Furthermore, higher LHVs mean more energy is released per mole of material upon combustion(Wallner et al., 2009). Both bioethanol and biobutanol have higher densities than gasoline, resulting in higher energy density values (Wallner et al., 2009). Higher energy density values are an advantage for the bioalcohols in question because they demonstrate that smaller quantities of fuel are needed to release the same amount of energy. Finally, ethanol has the highest octane rating, whereas the octane rating of biobutanol and gasoline fall into the same range. Octane rating is a measure of temperature and pressure needed to ignite a fuel source. Higher octane ratings are more ideal for spark ignition engines. Furthermore, high octane ratings allow more energy to be extracted from a fixed quantity of fuel when compared to low octane fuels (Wallner et al., 2009). Also, bioethanol is quite soluble in gasoline, but various additives are required to make it soluble in diesel (Rakopoulos et al., 2014). On the other hand, biobutanol is less hydrophilic, therefore, it is more soluble in gasoline and is less likely to solvate trace amounts of water, which can cause corrosion in engines and phase separations in the fuel

(Wallner et al., 2009). Biobutanol also has a higher viscosity when compared to ethanol. This point is important because it allows biobutanol to also serve as an alternative source to diesel fuels (Rakopoulos et al., 2014). Another advantage of biobutanol is its higher energy density value. Therefore, combustion of biobutanol releases more energy per a unit volume of fuel (Wallner et al., 2009). Finally, biobutanol has a lower oxygen content than ethanol, which means it produces less carbon dioxide upon combustion (Masum, Masjuki, Kalam, Palash, & Habibullah, 2015). Table 2.1 provides a comparison of the fuel properties of ethanol, gasoline and butanol described above.

Table 2.1: Comparison of Fuel Characteristics between ethanol, 1-butanol, and gasoline. (Wallner et al., 2009)

Property	Gasoline (C_4-C_{12})	Ethanol (C_2H_5OH)	1-butanol (C_4H_9OH)
Composition (C,H,O) wt%	86, 14, 0	52, 13, 35	65, 13.5, 21.5
LHV (MJ/kg)	42.7	26.8	33.1
Density (kg/m^3)	715-765	790	810
Octane number	90	100	87
Solubility in H_2O at 20ºC (ml/100 ml H_2O)	<0.1	Fully soluble	7.7
Reid Vapor pressure (psi)	7.8-15	2.32	0.48-0.77

2.2 Bacillus Megaterium

Bacillus megaterium SR7 is a relatively large strain of bacteria (10 mircometers in length), which, was discovered in a deep sub-surface $scCO_2$ well. As a result, *B. megaterium* is capable of withstanding unconventional growth conditions. Most notably, B. Megaterium can withstand high pressure environments, the acidic PH of $scCO_2$ and function properly under anaerobic conditions. Furthermore, upon genetic modification, this strain of bacteria can be used to synthesize bioalcohols. These characteristics makes it an ideal candidate for biobutanol production under SF conditions. (Thompson et al., 2016). Recently, scientists at MIT have analyzed *B. Megaterium* SR7 by performing genome sequencing, functional annotation and physiological growth characterization. Furthermore, they also employed a variety of genetic modifications, including an isobutanol production pathway. This feat was accomplished by the addition of two enzymes: 2-ketoisovalerate decarboxylase and alcohol dehydrogenase. In an effort to limit the production of isobutyraldehyde, an unwanted byproduct which has high affinity for $scCO_2$, an alternative alcohol

dehydrogenase was introduced and seemed to function with promising results. Exceptional growth was achieved at low pressure conditions (1atm) in the presence of CO_2 and further experimentation is underway to improve growth in high pressure systems (Thompson et al., 2016).

2.3 Supercritical Fluid Extraction

Over the past four decades, supercritical fluid extraction (SFE) technology has gained attention from both the scientific community and several industries as an alternative extraction process (Mohamed & Mansoori, 2002). SFE is commonly used in a variety of industries, including food, pharmaceutical, and cosmetic processing plants (Phelps, Smart, & Wai, 1996). This process is particularly attractive for products which are heat sensitive and might degrade in the conditions required by other extraction techniques (Mohamed & Mansoori, 2002). Also, SFE can be both more efficient and economical than conventional separation techniques(Mohamed & Mansoori, 2002). A common example of SFE can be found within the beverage industry, where it is an integral part of the decaffeination process for coffee grounds. Other common SFE applications include the extraction and fractionation of palatable fats and oils, the removal of toxic pesticides from agriculture products, and the extraction of nonpolar chemicals from fermentation broths (Mohamed & Mansoori, 2002).

2.3.1 Supercritical Fluids

Supercritical fluids are obtained by subjecting a given fluid to certain temperature and pressure conditions, at which point they surpass their critical point and become supercritical, as shown in Figure 2.4. Supercritical fluids (SF) possess a variety of important solvent characteristics. First, they have densities similar to liquids and viscosities and diffusivities similar to gases. Therefore, they flow similarly to fluids in a gaseous state, but possess the extraction capabilities similar to fluids in the liquid phase (Phelps et al., 1996). Typically, supercritical fluids are excellent at dissolving nonpolar chemicals. Furthermore, supercritical fluid's extraction properties can be drastically altered by controlling the pressure and temperature in the system (Phelps et al., 1996). This allows supercritical fluids to mimic a wide variety of liquid solvents. Additionally, SFE tends to be a faster process than liquid extraction systems since it possess better mass transfer properties. Liquid solvents tend to have lower solute diffusivities and higher viscosities, and these factors increase the time needed to complete extraction (Phelps et al., 1996). Also, modifiers can be added to SF's in order to increase their affinity for certain chemicals. Some examples of chemicals used

for SF extraction are carbon dioxide, ammonia, argon, Freon, propane, and water. A table comparing the pressure and temperature required to bring these chemicals to their supercritical states can be seen in Table 2.2. Such chemicals tend to be relatively inert, therefore, they are non-reactive (Phelps et al., 1996).

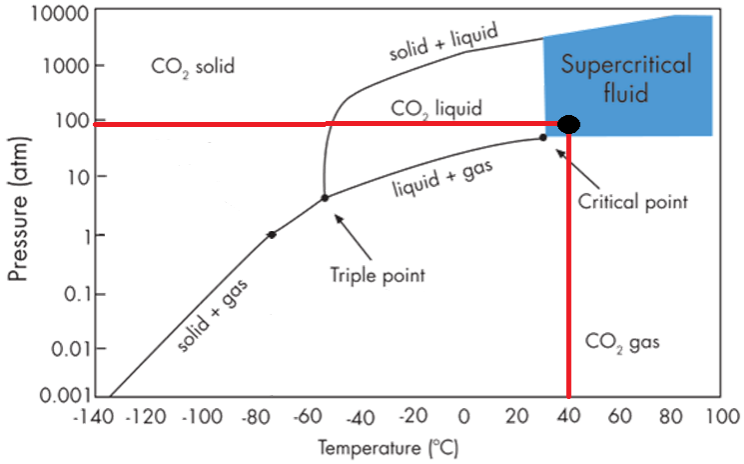

Figure 2.4: Phase Diagram of CO_2 showing operating conditions of reactor used for experimentation. (Hunter, 2010)

As previously mentioned, a variety of chemicals can be used in SFE systems, but CO_2 is one of the most commonly used fluids in industry. CO_2 is cheap, readily available, nonflammable, and nontoxic in comparison to other potential chemicals. Next, CO_2 possess a relatively low critical temperature and critical pressure (Phelps et al., 1996). This makes it easier and cheaper to initiate the phase changes required to bring CO_2 to its supercritical state. Supercritical CO_2 is good at solvating alkanes, terpenes, aldehydes, esters, fats and alcohols (Phelps et al., 1996). A drawback of CO_2 is that it has no permanent dipole moments and thus a small polarizability. However, the polarizability can be increased by an order of magnitude by adding modifiers such as acetone, methanol, propane or octane (Phelps et al., 1996).

Table 2.2: Critical pressure and temperature of fluids used in SFE. (Phelps et al., 1996)

Substance	Critical Pressure (atm)	Critical Temperature (°C)
CO_2	72.9	31.3
N_2O	72.5	36.5
CCl_2F_2	40.7	111.8
H_2O	217.7	374.1
Xe	58.4	16.6
Ar	48.0	150.9
NH_3	112.5	132.5

2.3.2 Supercritical Fluid Extraction Overview

SFE is a relatively simple process from a macroscopic perspective and can be carried out in batch or continuous processes. Heat exchangers and pumps are used to bring the fluid past its critical point. After the fluid is in its supercritical state, it's bubbled into the feed (Phelps et al., 1996). Theoretically, the supercritical fluid dissolves the necessary chemicals and exits the system, leaving behind the undesired (or in some cases the desired) materials. Next, the supercritical fluid undergoes a pressure drop, at which point it returns to its gaseous state, where the solute is less soluble. As a result, the majority of the solute is expelled from the SF into a collection vessel. Since most SFs are gases at ambient conditions, this step in the process occurs spontaneously. Finally, the extract-free fluid leaves the system and can be recycled (Phelps et al., 1996). Table 2.3 shows common uses of SFE in different industries.

SFE provides a variety of advantages over conventional extraction methods from both an environmental and economic standpoint. First, supercritical fluids can replace a variety of environmentally harmful chemicals which are commonly used for liquid-liquid extraction or gas stripping, such as benzene, toluene, and carbon tetrachloride (Phelps et al., 1996). Also, since SFs can be recycled back into the extraction process with minimal processing, chemical plants can save money on the storage, transportation, and processing of liquid solvent waste (Mohamed & Mansoori, 2002). In certain cases, such as the extraction of 1-butanol from aqueous solutions, SFE is significantly cheaper than conventional separation processes, such as distillation (Moreno, Tallon, Ryan, & Catchpole, 2012). Many supercritical fluids tend to be inexpensive to purchase when compared to conventional solvents used for extraction. Furthermore, SFE requires a small amount of equipment, with the most expensive part usually being the pump (Phelps et al., 1996). However, as previously mentioned, SFE requires high levels of pressurization, which is a potential drawback from an economic standpoint. (Phelps et al., 1996).

Table 2.3: Common uses of SFE in different industries. (Phelps et al., 1996)

Industry	Company	Materials being processed
Beverage	SKW Inc.	Hops
Tobacco	Fuji Flavor Co.	Tobacco
Beverage	Jacobs Suchard	Coffee
Pharmaceutical	Takeda	Acetone from antibiotics
Water Processing	Clean Harbors	Waste water
Military	U.S. Air Force	Aircraft gyroscopic components
Telecommunications	AT&T	Fiber optics rods

2.3.3 Supercritical Fluid Extraction of Butanol from Aqueous Solutions Using CO_2

Supercritical CO_2 is a strong candidate for butanol extraction from aqueous solutions. Compared to lower molecular weight alcohols, butanol is less polar. Therefore, it has a higher affinity for $scCO_2$ and a lower affinity for the aqueous solvent (Antero. Laitinen & Juha. Kaunisto, 1999). In $scCO_2$ systems, 1-butanol has a partition coefficient of 2.2, whereas ethanol has a partition coefficient between 0.05 and 0.125, as shown in *Table 2.4*. Therefore, 1-butanol is more soluble in $scCO_2$ than ethanol. Also, butanol is less volatile than lower molecular weight alcohols since it has a lower vapor pressure. This makes it easier to separate from the $scCO_2$ following depressurization (Antero. Laitinen & Juha. Kaunisto, 1999). This is an important characteristic for recycling the $scCO_2$ since small concentrations of alcohol can alter the mass transport properties of the system and decrease recovery efficiency. Lower weight alcohols, such as ethanol and methanol remain in the CO_2 in higher concentrations following the pressure drop, a significant drawback which hinders the feasibility of SFE in practical applications for such alcohols (Antero. Laitinen & Juha. Kaunisto, 1999).

SFE of butanol from aqueous solutions is a relatively new topic in the scientific community. However, several studies have been conducted on such systems with promising results. Research conducted by Moreno et al. demonstrated that high recovery of 1-butanol from aqueous solutions is possible under the proper conditions. This research team utilized a counter current flow tower, operated as both a spray column and a steel pall ring packed column (Teresa Moreno et al., 2014). They found that higher solvent to feed ratios resulted in better recovery of 1-butanol but also resulted in a more dilute extract. At solvent to feed ratios (S/F) ranging from 2-3, 92% of the initial 5wt% 1-butanol solution was capable of being recovered as product. They also observed that recovery of 1-butanol was significantly lower for lower feed concentrations (Teresa Moreno et al., 2014). When the solvent to feed ratio was held constant, and flow rates were slowed down, better recovery was achieved. Moreno also observed that 1-butanol was more soluble in $scCO_2$ at higher pressures. For a 0.5wt% solution, increasing the systems pressure from 100 to 200 bar resulted in a 1-butanol recovery increase from 51% to 61%. However, increasing the pressure of the system also increases water affinity for $scCO_2$ (Teresa Moreno et al., 2014). Therefore, more water is extracted when the pressure is increased, thus resulting in a more diluted product. Finally, Moreno also observed that increasing the columns packing with steel pall rings

improved both the separation efficiency of the system and allowed for higher flow rates while maintaining the same recovery efficiency. Such trends are likely a result of increased contact area between the $scCO_2$ and the aqueous solution (Teresa Moreno et al., 2014). Laitinen et al. operated a bench-scale, continuous counter-current Oldshue-Rushton column in an effort to extract 1-butanol using SF technology. They found that SFE was capable of extracting 99.7% of the initial 5wt% 1-butanol feed solution. In a separate study, Moreano et al. operated a hydrophobic polypropylene hollow-fiber membrane contractor, peered with a SFE system, in an attempt to extract 1-butanol from an aqueous solution. The team identified two parameters which impact extraction efficiency; $scCO_2$ flow rate and operating pressure. Operating at 100 bar, they were able to extract up to 89% of the original 1-butanol feed concentration (T. Moreno, S. J. Tallon, & O. J. Catchpole, 2014).

Table 2.4: Comparing mass transfer properties of different alcohols in $scCO_2$ extraction systems

Compound	Partition Coeff. m (Kc/w)	Reactor Type	Conditions	Extraction Efficiency at 90% (mol/mol)	Kla (s^{-1})	Ref.
ethanol	0.09	Pilot plant, counter-current column	100bar, 40°C 10wt% EtOH	~17:1	0.002-0.007	Medina et al.(Medina & Martinez, 1997)
ethanol	0.12	Counter current flow column	100 bar, 40°C	~12:1	0.004-0.012	Bernad et al.(Bernad, Keller, Barth, & Perrut, 1993)
isopropanol	0.23	Counter-current spray column	103.4 bar, 30°C, 5vol%IPA	4.5:1	0.007-0.019	Chun et al(Chun, Lee, Cheon, & Wilkinson, 1996)
isopropanol	0.2	small-scale continuous countercurrent extractor	102 bar, 40°C	11:1	0.01	Lahiere and Fair 1987(Lahiere & Fair, 1987)
n-butanol	2.2	mechanically agitated Oldshue–Rushton-type valve extraction column (Chematur Ecoplanning)	100 bar, 40°C, 5wt% butanol	1:1 to 3:1	0.0019–0.0034	Laitinen and Kaunisto 1999.(A. Laitinen & J. Kaunisto, 1999)
n-butanol	2.2	Column with membrane contactor	100 bar, 40°C, 10wt% butanol	5:1 w/w	0.0004-0.0012 cm/s	Moreno(T. Moreno et al., 2014)

2.3.4 Supercritical Fluid Extraction of Butanol from Fermentation Broths Using CO_2

Recently, SFE technology has gained the attention of researchers in the biotechnology industry as a potential means for extracting products from bioreactors. Many of the previously mentioned benefits also apply to SFE in bioreactors, however, several other advantages have been elucidated. First, SFs lower the viscosity and surface tension of fermentation broths, thus enhancing mass transfer and allowing more thorough penetration of small pores found in cell cultures (Khosravi-Darani & Vasheghani-Farahani, 2005). Also, SFE allows for low temperature

conditions, which is an important aspect for cell cultures sensitive to heat. Distillation of bio-broths is particularly expensive since products tend to exist in very low concentrations, thus increasing the energy requirements for the system. SFE might be a viable alternative to distillation in the case of extracting nonpolar products from bio-broths since it requires less energy input (Khosravi-Darani & Vasheghani-Farahani, 2005). Finally, SFE allows for in situ separation of products from cell cultures, which is particularly important for systems affected by end-product inhibition. Also, in situ SFE extraction allows for higher product purity than other conventional techniques, such as pervaporation and liquid-liquid extraction which use other forms of chemical solvents. Such chemical solvents are tough to remove from final products and sometimes damage the organisms in the broth (Khosravi-Darani & Vasheghani-Farahani, 2005). SFE also has several drawbacks when applied to bio-broths. First, the biotechnology industry lacks high pressure processing equipment, therefore, implementation of SFE would be accompanied by high capital costs. Furthermore, many organisms experience varying levels of membrane and protein degradation under high pressure conditions. Such effects can be mitigated by inoculating the original culture in high pressure environments and by carefully controlling pressure changes in the system (Khosravi-Darani & Vasheghani-Farahani, 2005). However, such techniques are limited in their ability to obtain cell culture growth under SF conditions. In SFE systems that use CO_2 as the solvent, PH levels of the broth have been reported to exhibit more acidic characteristics since CO_2 is soluble in aqueous solutions under high pressure. Increases in the acidity of bio-broths often hinder cell function, however such effects can be mitigated through the addition of a base or by switching to other solvents, such as ethane (Khosravi-Darani & Vasheghani-Farahani, 2005).

2.4 Reactor Geometry

2.4.1 Supercritical Fluid Extraction Units

One of the primary design factors considered when designing SFE units is effective surface area between the supercritical fluid and the liquid solvent. This is typically accomplished by designing the unit as a tall, thin tube so that there is a greater residence time for the CO_2 bubbles in solution (A Laitinen & J Kaunisto, 1999). Additionally, efforts are made to reduce the size of CO_2 bubbles in the extractor. Reducing the diameter of the CO_2 bubbles has the effect of increasing the surface area to volume ratio, thus increasing the surface area available for mass transfer in the same volume of CO_2 fed into the extractor (Westerterp, van Dierendonck, & de Kraa, 1963). This is typically accomplished via mechanical mixing inside the extractor or by feeding the CO_2 through

a sparger (A Laitinen & J Kaunisto, 1999). By increasing the surface area to volume ratio, the rate of diffusion of solute from the liquid to supercritical phase increases, since diffusion is proportional to surface area by Fick's Law of diffusion.

Table 2.5: Summary of extraction unit design

Species	**Reactor Design**	**Source**
Ethanol	Stirred semi-batch	(Tai & Wu, 2005)
Ethanol	Rotating Disk Column	(Laitinen & Kaunisto, 1998)
Ethanol, n-butanol	Oldshue-Rushton Valve extraction column	(A Laitinen & J Kaunisto, 1999)
Ethanol	Counter-flow packed column	(Lim, Lee, Lee, Kim, & Chun, 1995)
n-butanol	Membrane contactor column	(Teresa Moreno et al., 2014)

One of the simplest designs is the stirred semi-batch extractor, such as the one studied by Tai and Wu (2005). This design consists of a tank partially filled with a water/alcohol mixture and an impeller to provide mixing. While being operated, the headspace above the liquid is filled with $scCO_2$. $scCO_2$ is continuously pumped into the bottom of the tank, and bubbles up through the liquid. As the $scCO_2$ rises through the liquid phase, alcohol diffuses into the $scCO_2$ bubbles. $scCO_2$, which now contains extracted alcohol, is then removed from the headspace of the tank, and is depressurized to allow the alcohol to separate from the CO_2 phase. A diagram of Tai and Wu's extractor is shown in Figure 2.5.

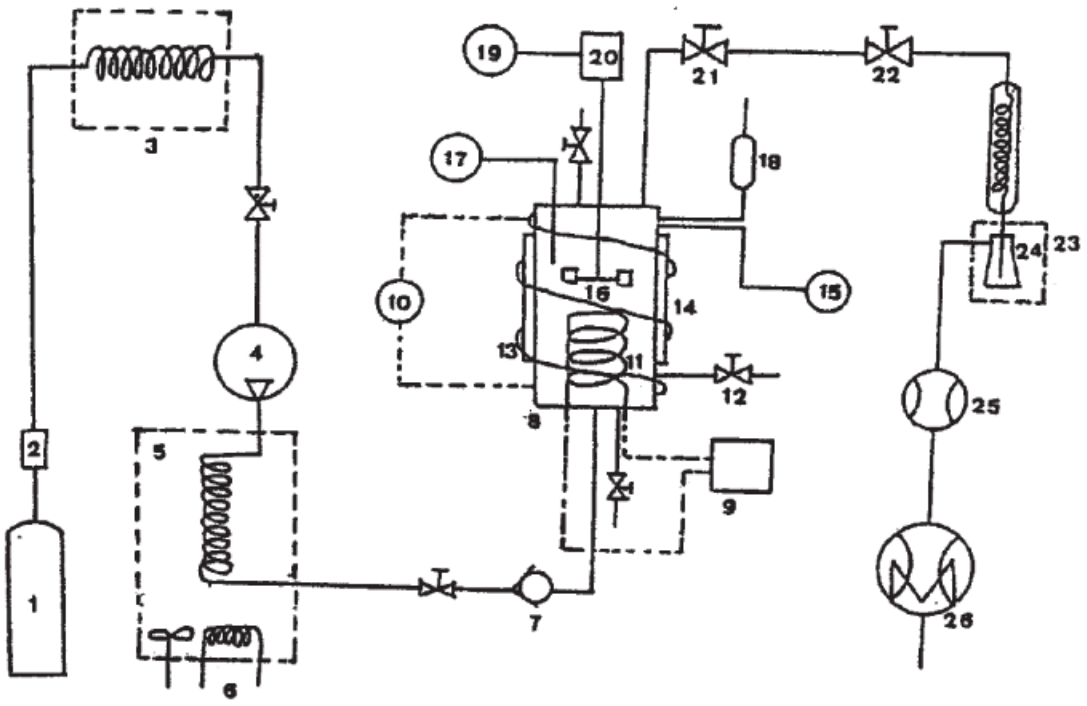

Figure 2.5: Process diagram of semi-batch extractor. 1. CO_2 tank, 2. filter, 3. chiller, 4. small pump, 5. preheater, 6. heater, 7. check value, 8. extractor, 9. voltage controller, 10. voltage controller, 11. coil, 12. sampling valve, 13. heating tape, 14. view port, 15. pressure gauge, 16. paddle, 17. temperature gauge, 18. safety valve, 19. tachometer, 20. motor, 21. ball valve, 22. metering valve, 23. cold trap, 24. collector, 25. rotameter, 26. dry test meter. (reproduced from Tai and Wu, 2005)

In industrial applications, continuous flow extraction columns are often employed because they are more cost effective to run in large scale applications. A diagram of a typical column extractor is given in *Figure 2.6*. Common SCF extractor designs include the rotating disk column, the Oldshue-Rushton valve extraction column, and the membrane contactor column. One advantage of using a rotating disk column, such as the one described by Laitinen and Kaunisto (1998), is that it provides effective mixing with low amounts of shear. This is due to the large contact area between the rotating disks and the fluid, which means that mixing at lower speeds provides a similar amount of mixing that traditional impellers would provide at high speeds. In an Oldshue-Rushton column, a vertical column is separated into many compartments by stator plates (A Laitinen & J Kaunisto, 1999). In each compartment, there is an impeller that ensures the fluid is well mixed. Having multiple impellers is important, considering the large aspect ratio (height/diameter of the tank) of the column (A Laitinen & J Kaunisto, 1999). Packed beds are also commonly used as SCF extractors. While packed beds are more efficient than spray columns such

as the rotating disk and Oldshue-Rushton columns, they are much more expensive because they require a large column diameter (A Laitinen & J Kaunisto, 1999).

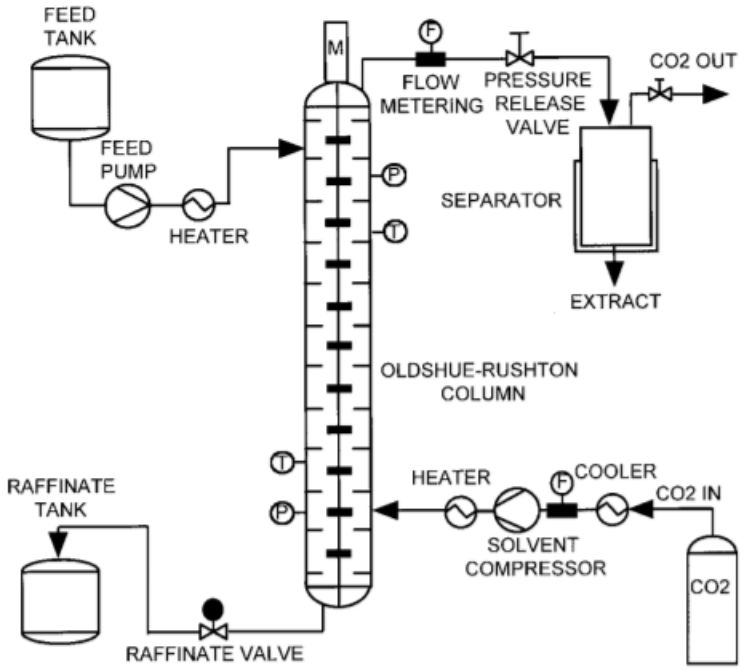

Figure 2.6: Process diagram of a column extractor (diagram of an Oldshue-Rushton column, reproduced from Laitinen and Kaunisto, 1999).

2.4.2 Bioreactor Design

Design of bioreactors differs in several ways compared to the design of extraction units. While the design of extractors is primarily focused on providing the greatest amount of contact area between phases, bioreactors are designed to provide conditions most appropriate for cellular growth (Doran, 2013; A Laitinen & J Kaunisto, 1999). While the aspect ratio (height of the tank divided by the diameter of the tank) of bioreactors generally vary from 1 to 6, taller columns experience several challenges, including a greater cost of manufacture and more challenging mixing requirements (Doran, 2013). As a result, most fermentation reactors have an aspect ratio of about 3 (Doran, 2013).

Sterilization and ensuring aseptic operation is also of particular concern while operating bioreactors. This requires cleaning, typically by steam or bleach, between batches to avoid contamination (Doran, 2013). Of additional consideration is the material used to make the bioreactor. Glass and stainless steel are most common as they are easy to sterilize, are non-reactive, and provide a clean, smooth surface (Doran, 2013). The reactor interior must also be carefully polished to avoid ridges where cells can accumulate and form biofilms, and divots in the bioreactor

should be avoided to avoid areas with little exposure to the bulk mixed medium (Shuler & Kargi, 2002).

Chemostats are bioreactors which use separation techniques to maintain a constant concentrations of substrate and product in the reactor (Shuler & Kargi, 2002). One method of accomplishing this is by connecting the bioreactor to a separation stream. In this stream, cells are filtered out, and product is separated from the liquid. New media is then added back to the bioreactor to maintain constant volume and substrate concentrations (Shuler & Kargi, 2002). There may also be a recycle stream, where the biomass and conditioned media which was removed is added back into the bioreactor (Shuler & Kargi, 2002).

2.5 Mass Transfer

Mass transfer is defined as the motion of molecules in a solution due to concentration gradients (Wankat, 2012). The primary mechanism of mass transfer of alcohol from the aqueous phase to the $scCO_2$ phase in the SFE unit is diffusion. Diffusion is mass transfer due to random, Brownian motion of particles, in contrast to convectional mass transfer, which is caused by bulk fluid motion (Wankat, 2012). By understanding the mass transfer properties of the alcohol-water-$scCO_2$ system, a model for extraction rate and efficiency can be developed.

One objective of this experiment is to determine the overall mass transfer coefficient (K_la) for the alcohols under different conditions. This will allow for scale up of the SFE system being studied to different reactor volumes and conditions. In modeling the mass transfer of alcohol from the aqueous phase to the $scCO_2$ phase, it was assumed that two boundary conditions existed. One boundary existed in the aqueous phase, and a second in the $scCO_2$ phase (see figure 1). The model for alcohol extraction follows the two-film model specified by Tai and Wu (2005). The two film model is applied to this system by applying a mass balance to the alcohol in the $scCO_2$ phase (equation 2.1) and the aqueous phase (equation 2.2).

$$V_s \frac{dC_{A,c}}{dt} = -GC_{A,c} + V_w K_s a\left(K_{C/W} C_{A,w} - C_{A,C}\right)$$

Equation 2.1

$$\frac{dC_{A,w}}{dt} = -K_s a\left(K_{C/W} C_{A,w} - C_{A,C}\right)$$

Equation 2.2

These equations have the initial conditions of $C_{A,s}(t=0) = 0$ and $C_{A,w}(t=0) = C_{A,w,0}$. Using Laplace transforms, these equations can be solved to obtain equation 2.3:

$$C_{A,w} = C_{A,w,0}[\beta_1 \exp(\alpha_1 t) + \beta_2 \exp(\alpha_2 t)]$$

Equation 2.3

Where:

$$\alpha_1 = \frac{-q_1 + \sqrt{q_1^2 - 4q_2}}{2}$$

Equation 2.4

$$\alpha_2 = \frac{-q_1 - \sqrt{q_1^2 - 4q_2}}{2}$$

Equation 2.5

$$\beta_1 = \frac{\alpha_1 + A}{\alpha_1 - \alpha_2}$$

Equation 2.6

$$\beta_2 = \frac{\alpha_2 + A}{\alpha_2 - \alpha_1}$$

Equation 2.7

$$q_1 = K_s a * K_{C/W} + \frac{G}{V_c} + \frac{V_w}{V_c} K_s a$$

Equation 2.8

$$q_2 = K_s a * K_{C/W} \frac{G}{V_c}$$

Equation 2.9

$$A = \frac{G}{V_c} + \frac{V_w}{V_c} K_s a$$

Equation 2.10

In most cases, it is safe to assume that the contribution from α_2 is negligible compared to α_1 (Tai & Wu, 2005). Therefore, equation 2.3 can be simplified to equation 2.11:

$$C_{A,w} = C_{A,w,0} \beta_1 \exp(\alpha_1 t)$$

Equation 2.11

$$\ln\left(\frac{C_{A,w}}{C_{A,w,0}}\right) = \alpha_1 t + \ln(\beta_1)$$

Equation 2.11 can be solved graphically by plotting $\ln\frac{C_{A,w}}{C_{A,w,0}}$ against time. The slope of the resulting line is equal to α_1. $K_l a$ can then be calculated using equation 2.12.

$$K_l a = -\frac{\alpha_1 (1 + \alpha_1 {}^{V_c}/_{G})}{K_{C/W}\left[\left(\alpha_1 {}^{V_c}/_{G}\right) + 1\right] + \alpha_1 {}^{V_w}/_{G}}$$

Equation 2.12

2.6 Non-Steady State Equilibrium Model

In some cases, such at low $scCO_2$ flow rates, the $scCO_2$ phase becomes saturated with alcohol during the extraction process. If this occurs, the extraction is no longer diffusion limited, but instead is limited by the equilibrium between the aqueous and supercritical phases. The equilibrium constant governing this system, $K_{c/w}$, is defined by equation 2.13:

$$K_{C/W} = \frac{C_{A,c}}{C_{A,w}}$$

Equation 2.13

In the case where the system is equilibrium limited, the time profile alcohol concentration in each phase is governed by equation 2.14.

$$V_w \frac{dC_{A,w}}{dt} = -GC_{A,c}$$

Equation 2.14

Using the definition of $K_{c/w}$ in equation 2.13, this becomes:

$$\frac{dC_{A,w}}{dt} = \frac{-GK_{C/W}C_{A,w}}{V_w}$$

Equation 2.15

Solving the differential equation with the initial condition of $C_{A,w}$ (t=0) = $C_{A,w,0}$, the time profile of alcohol in the aqueous phase becomes equation 2.16.

$$ln\frac{C_{A,w}}{C_{A,w,0}} = \frac{-GK_{C/W}}{V_w}t$$

Equation 2.16

The concentration of alcohol in the $scCO_2$ phase can be determined by solving equation 2.16 for $C_{A,w}$, and using equation 2.13 to find $C_{A,c}$.

If $ln\frac{C_{A,w}}{C_{A,w,0}}$ is plotted against time, then the slope of the resulting line of best fit is equal to $\frac{-GK_{C/W}}{V_w}$. This allows $K_{c/w}$ to be determined from the time profile of alcohol concentration in the water phase.

2.7 Mixing Effectiveness

In bioreactors, proper mixing is essential to ensure that nutrients and products are evenly dispersed throughout the reactor (Doran, 2013). This is important because without proper mixing, the area immediately surrounding the cells can become low in nutrient concentration and high in product concentration. An additional consideration is keeping the cells themselves dispersed in the reactor. At slow mixing speeds, the cells can settle to the bottom of the reactor. Planktonic growth,

where the cells are evenly dispersed throughout the reactor, is preferable, because it allows each cell more space to draw nutrients from fermentation broth (Doran, 2013).

Several factors impact the effectiveness of mixing in a stirred tank. These include mixing speed (n), impeller clearance from the bottom of the tank, the diameter of the impeller (D_i), the diameter of the tank (D_t), the height of the liquid in the tank (h), geometric shape of the tank, and the type of impeller used (Doran, 2013).

Impellers can create fluid flow in two dimensions: the axial dimension (top to bottom) and the radial dimension (center to wall). The flow profile varies depending on the type of impeller used. Flat, vertical blade impellers such as the Rushton turbine create a primarily radial flow profile because the impeller blades push water outwards (Doran, 2013). This can be a concern in large tanks, since without sufficient axial flow, stratification of fluid layers can occur, resulting in a concentration gradient in the vertical dimension (Visscher, van der Schaaf, Nijhuis, & Schouten, 2013). Other impeller designs have been made to create axial mixing. These include the pitched blade turbine and the marine propeller, which pump the fluid in both the radial and axial dimensions (Doran, 2013). Another method for avoiding concentration gradients in the axial dimension is to use multiple Rushton turbines on the impeller shaft, which ensures mixing throughout the vertical dimension. An example of this type of mechanical mixing design is given by the Oldshue-Rushton column described in the extraction unit design section (A Laitinen & J Kaunisto, 1999).

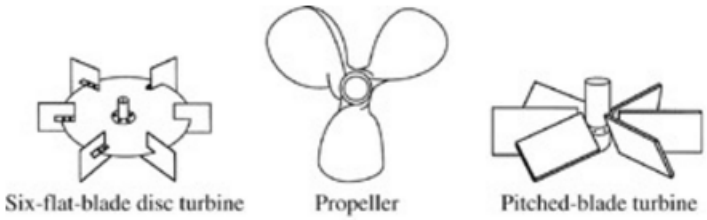

Figure 2.7: Representations of a Rushton turbine (left), propeller (middle), and pitched blade turbine (right). Taken from Doran, 2008.

One measure of mixing effectiveness is the time required to fully mix particles into solution after starting from a state where the particles are settled on the bottom of the reactor. This has been modeled by the Zwietering Equation (Zwietering, 1958).

$$n_{JS} = \frac{S{\nu_L}^{0.1}{D_P}^{0.2}[g(\rho_p - \rho_L]^{0.45}x_p^{0.13}}{D_i^{0.85}}$$

Equation 2.17

In this equation, S is a dimensionless parameter which depends on the reactor and impeller geometry. Typical values of S are given by Zwietering (1958) and by Doran (2013). For the reactor being examined in this report, an estimated S value of 4.25 is used base on reported values of S for similar tank and impeller geometries (Doran, 2013). The Zwietering Equation can be applied to determine the minimum mixing speed required to fully suspend bacterial cells in solution.

Another measure of mixing effectiveness is the mixing time, defined as the amount of time required to fully mix the suspension from a state where all the particles had settled out of solution (Marrone, 1998). Marrone (1998) suggests that while models of mixing time in liquid-liquid systems may not be completely accurate, due to differences in the densities and viscosities of the fluids being investigated, several models can be used to approximate the mixing time in a supercritical fluid system. Each of these models states that the mixing time is a function of the Reynolds number, the Froude number, and tank and impeller geometries. These models are summarized in **Error! Reference source not found.**.

$$Re = \frac{nD_i^2\rho}{\mu}$$

Equation 2.18

$$Fr = \frac{n^2 D_i}{g}$$

Equation 2.19

Table 2.6: Summary of literature correlations for mixing time.

Source	**Impeller Type**	**Correlation**
(Norwood & Metzner, 1960)	Flat blade turbine	$f_t = nt_{mix}\left(\frac{D_i}{D_t}\right)^2\left(\frac{D_t}{h}\right)^{\frac{1}{2}} Fr^{-\frac{1}{6}}$
(Moo-Young, Tichar, & Dullien, 1972)	Flat blade turbine	$f_t = nt_{mix}\left(\frac{D_i}{D_t}\right)^2\left(\frac{D_t}{h}\right)$
(Fox & Gex, 1956)	Propeller	$f_t = nt_{mix}\left(\frac{D_i}{D_t}\right)^{\frac{3}{2}}\left(\frac{D_t}{h}\right)^{\frac{1}{2}} Fr^{-\frac{1}{6}}$
(Landau & Prochazka, 1961)	Propeller	$nt_{mix} = 5.6\left(\frac{D_t}{D_i}\right)^2$
(van de Vusse, 1959)	General	$f_t = \left(\frac{nt_{mix}D_i^2 p}{V_L}\right)\left(\frac{\rho n^2 D_i^2}{(\rho_1-\rho_2)gh}\right)^y$

In these equations, f_t is a mixing time factor, which is a function of the Reynolds number.

Values of f_t are specific to each mixing time correlation and are published by the respective author for each correlation. The van de Vusse model is more general than the others, and can be used for several types of impellers. In this model, p is the pitch of the impeller blade, ρ_1 and ρ_2 are the densities of the two fluids being investigated, and the value of y is a function of the impeller type. The value of y is 0.25 for propellers, 0.35 for tilted blade turbines, and 0.30 for Rushton-type (vertical blade) turbines (Marrone, 1998). Solving these correlations allows for comparison of each impeller type at different rotational speeds.

An additional concern related to mixing in a bioreactor is the amount of stress imparted onto the cells by mixing. Kresta and Wood (1993) estimate the energy dissipation rate in a stirred tank per unit mass of fluid by the following equation:

$$\varepsilon = A\frac{\mathrm{v}^3}{L}$$

Equation 2.20

This equation assumes isotropic dissipation and that turbulent shear is a much greater than laminar shear. A in this equation is a constant of proportionality and in this case is about 1, v is the angular velocity, and L is the characteristic length equal to $\frac{1}{10}$ the diameter of the impeller (Kresta & Wood, 1993). This equation, therefore, can be used to compare the amount of energy imparted onto the fluid and cells by the impeller at different impeller velocities.

Stress is created by changes in fluid velocity, and is most prominent just off the tip of the impeller blades. The smallest possible length scale in a mixed tank system can be estimated by the Kolmogorov eddy length, λ (Doran, 2013).

$$\lambda = \left(\frac{\nu}{\varepsilon}\right)^{1/4}$$

Equation 2.21

The Kolmogorov eddy length is important for determining how cells will be impacted by fluid flow in the tank. An eddy is an area of rotational flow in a bulk fluid with a different flow profile. The Kolmogorov length, λ, is defined as the characteristic length of the smallest eddy in a mixed tank (Doran, 2013). At eddy lengths much greater than the cell diameter, the cells will be transported within the eddies, and will not be as strongly affected by shear caused by changes in the velocity profile (Doran, 2013). At eddy lengths less than the diameter of the cells, the cells are

more likely to become caught between two eddies which are at different velocities, thus imparting a strong shear on the cell (Doran, 2013). In some cases, this shear can be strong enough to damage or kill the cells.

Efforts to reduce the amount of stress created in a mixed tank system is a major goal in bioreactor design (Doran, 2013). One method of reducing the amount of shear in a mixed system is to mix at lower velocities. However, as predicted by the mixing time correlations above, reducing impeller velocity has the tradeoff of also increasing the mixing time (Marrone, 1998). Another approach is to change the type of impeller used to mix the tank. One impeller designed to reduce the amount of shear in mixed tanks is the centrifugal impeller (Wang & Zhong, 1996; Xia, Wang, Zhang, & Zhong, 2008). Due to its much larger surface area compared to traditional impellers such as the Rushton impeller, centrifugal impellers are able to provide effective mixing, even in large tanks, while creating much less shear compared to smaller impellers (Wang & Zhong, 1996).

In the supercritical CO_2-water system, cavitation may also be a concern. At the tip of the impeller, there will be a pressure drop in the fluid due to the rapid increase in velocity (Brennen, 1995). If this pressure drop causes the local pressure to be less than the saturation pressure of CO_2 in water, then CO_2 bubbles can form. When the bubbles move away from the impeller into the bulk fluid, the pressure once again rises and causes the bubbles to violently collapse. This collapse can create a jet of water that shoots out at high velocity, which can damage nearby cells. This process of bubble formation and collapse caused by changes in pressure is termed cavitation (Brennen, 1995). When the supercritical CO_2 reactor is at operating conditions of 1500 psi and 40^{o}C, the water is essentially saturated with carbon dioxide ("Materials Measurement Laboratories," 2016). Reducing the pressure also decreases the solubility of CO_2 in water, and as a result local pressure drops can cause CO_2 bubbles to form.

There are several negative consequences of cavitation in supercritical fluid extraction units and bioreactors. The high velocity jet produced by the collapse of cavitation bubbles has been shown to damage metal components in pumps and impellers (Brennen, 1995). As such, if cavitation occurs it can damage impellers and other internal mechanisms, and can create pitting on the walls of the unit (Brennen, 1995). Cavitation could also be severely damaging to organisms in bioreactors, as there would be more than enough force in the jets to kill impacted cells.

Figure 2.8: Cavitation off the tip of an impeller. Reproduced from Brennen, 1995.

According to the Bernoulli Equation, changes in velocity can cause a local deviation from the bulk reactor pressure. Assuming constant density and potential energy throughout the considered liquid phase, the Bernoulli Equation is:

$$P - P_l = \frac{1}{2}\rho(v_l^2 - v^2)$$

Equation 2.22

Where, the subscript *l* refers to local pressures and velocities, and P and v refer to bulk pressure and velocity. This equation predicts that if the local velocity is greater than the bulk velocity of the fluid, the local pressure will be less than the bulk pressure. As such, areas of concern are those where there is a significantly higher velocity than the bulk fluid. In the reactor being studied, the area of greatest concern therefore is the fluid immediately surrounding the impeller tips, since the fluid there will be travelling close to the angular velocity of the impeller blade.

Installing baffles is another common method of improving mixing effectiveness in stirred tanks. Baffles are long, thin strips attached to the walls of the tank which interrupt the fluid flow pattern in the tank. In an unbaffled tank, impellers tend to create circular flow, where the bulk fluid flows in a circular pattern around the tank in the same direction as the impeller is rotating (see *Figure 2.9*). This is disadvantageous, since it tends to create vortices and does not effectively mix the fluid in the axial direction (Doran, 2013). Baffles interrupt this type of circular flow by forcing the fluid to flow axially when it hits the baffle. *Figure 2.9* gives a simplified generalization of the flow profiles in an unbaffled tank and a baffled tank. As a result, baffles are desirable when designing mixed tanks in order to avoid vortices and fluid stratification in tall vessels.

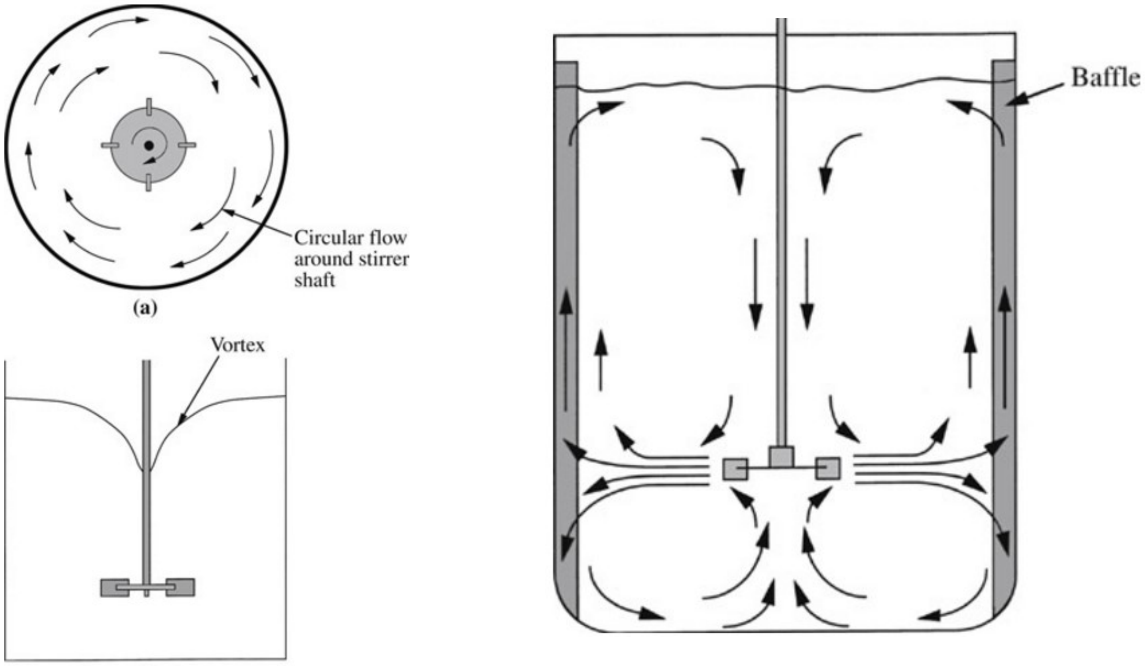

Figure 2.9: Simplified fluid flow profiles in an unbaffled tank (left) and a baffled tank (right). Taken from Doran, 2013

2.8 Extraction Safety Considerations

Several considerations were taken with regards to safety while prepping and running the extraction unit. One of the primary concerns was the high operating pressure (1500 psi) of the SFE unit. Most of the apparatus, including the extraction tank and lines leading to the pump, were made of stainless steel rated for pressures greater than the operating pressures. There was also a 3000 psi rupture disk on the extractor to release excess pressure in an emergency situation where the extractor becomes over pressurized. The areas of greatest concern for pressure ruptures are the plastic lines leading from the back pressure regulator to the glass collection vessels, as well as the glass collection vessels themselves. The rapid depressurization in this part of the reactor is accompanied by large decreases in temperature, which can cause ice to form in the lines. This was of greatest concern at high flow rates of CO_2 (9 mL/min or greater). Ice formation can cause line clogging, which results in dangerous pressure buildups in both the lines and the collection vessels, thus making both pieces of equipment susceptible to explosions. There was an incidence of a glass vessel exploding due to over-pressurization with last year's MQP group (Conlon, Knutson, Overdevest, & Rivard, 2016). This incident led to the implementation of new safety protocols in an effort to protect operators and improve system safety.

To mitigate this risk, heating tape was placed on the stainless steel tubing just before the plastic tubing of concern, in an attempt to prevent the fluid from freezing. A thermocouple located against this tubing was monitored, and if the temperature of the tubing dropped below 5°C the experiment was halted by turning off the CO_2 pump. During experimentation, operators were instructed to watch the plastic tubing for signs of freezing. In the event that freezing occurred, the experiment was paused until the ice melted. Additionally, PFA coated vessels were used and enclosed in plastic mesh to contain glass shards in the case of an explosion. Furthermore, the entire unit was enclosed behind polycarconate doors to block any shrapnel or fluid from hitting operators in case of a pressure failure. As an added precaution, operators wore safety glasses, gloves, and lab coats as personal protective equipment.

Of additional concern were the chemical hazards presented by the methanol used to recover the extracted alcohols, as well as the alcohols being extracted. Methanol is flammable, and is toxic if ingested, inhaled, or allowed to come into contact with skin ("Methanol Safety Data Sheet," 2017). As such, gloves, safety glasses, and lab coats were worn when handling methanol. Furthermore, methanol was transferred between vessels in a fume hood to limit exposure to vapors. n-butanol, isobutanol, n-pentanol, and n-hexanol each exhibit similar hazards to methanol, and were treated with the same care as methanol ("1-butanol Safety Data Sheet," 2017; "1-hexanol Safety Data Sheet," 2017; "1-pentanol Safety Data Sheet," 2017).

2.9 Biosafety Considerations

Bacillus megaterium is not known to cause infection in immunocompetent people, and is labeled as a biosafety level 1 microbe (*Biosafety in Microbiological and Biomedical Laboratories*). This is the lowest biosafety level, which simply requires standard biological lab protocols be followed. During growth of *B. megaterium* in the bioreactor in high pressure conditions, steps were taken to prevent exposure of the bacteria to researchers in the lab. Standard personal protective equipment, including safety glasses, lab coats, and nitrile gloves were worn at all times. All equipment and contaminated areas were sterilized with 10% sodium hypochlorite or with 70% isopropyl alcohol (*Biosafety in Microbiological and Biomedical Laboratories*). Precautions were also taken to prevent creating aerosols. To accomplish this, valves were opened slowly, and pressurized vessels were allowed to equilibrate before being opened to the atmosphere. Any potentially contaminated material was disposed of in institutional biohazard bags. Finally, all

researchers washed their hands before leaving the lab (*Biosafety in Microbiological and Biomedical Laboratories*).

3. Methodology

3.1 Supercritical Fluid Extraction Methodology

3.1.1 Experimental Design

The ultimate goal of this experiment was to develop a model of $scCO_2$ extraction rates and efficiencies for medium chain alcohols. In developing this model, there were five main objectives of the supercritical fluid extraction experiments. The primary objectives were to:

1. Compare the extraction efficiencies of n-butanol, isobutanol, n-pentanol, and n-hexanol. This was accomplished by was accomplished by running the extraction unit at a consistent initial alcohol concentration (0.5 wt%) and CO_2 flow rate (5.4 mL/min).
2. Compare the extraction rates and efficiencies of select alcohols at different CO_2 flow rates. This was accomplished by running the extractor with each alcohol at a consistent initial concentration and at different CO_2 flow rates.
3. Compare the extraction efficiency of n-butanol and isobutanol at different initial alcohol concentrations. This was accomplished by running the extractor with n-butanol or isobutanol at 1.0 wt% and 0.5 wt% at a constant CO_2 flow rate (5.4 mL/min).
4. Determine the effect of altering superficial $scCO_2$ surface area on extraction efficiency. This was accomplished by comparing the extraction rate of an alcohol with and without a stainless steel frit to produce smaller CO_2 bubbles.
5. Develop a model to predict extraction rates and efficiencies for the various alcohols based on the CO_2 flow rate and alcohol concentration.

3.1.2 Process Flow Diagram

The following is a process flow diagram of the SFE unit (Conlon et al., 2016).

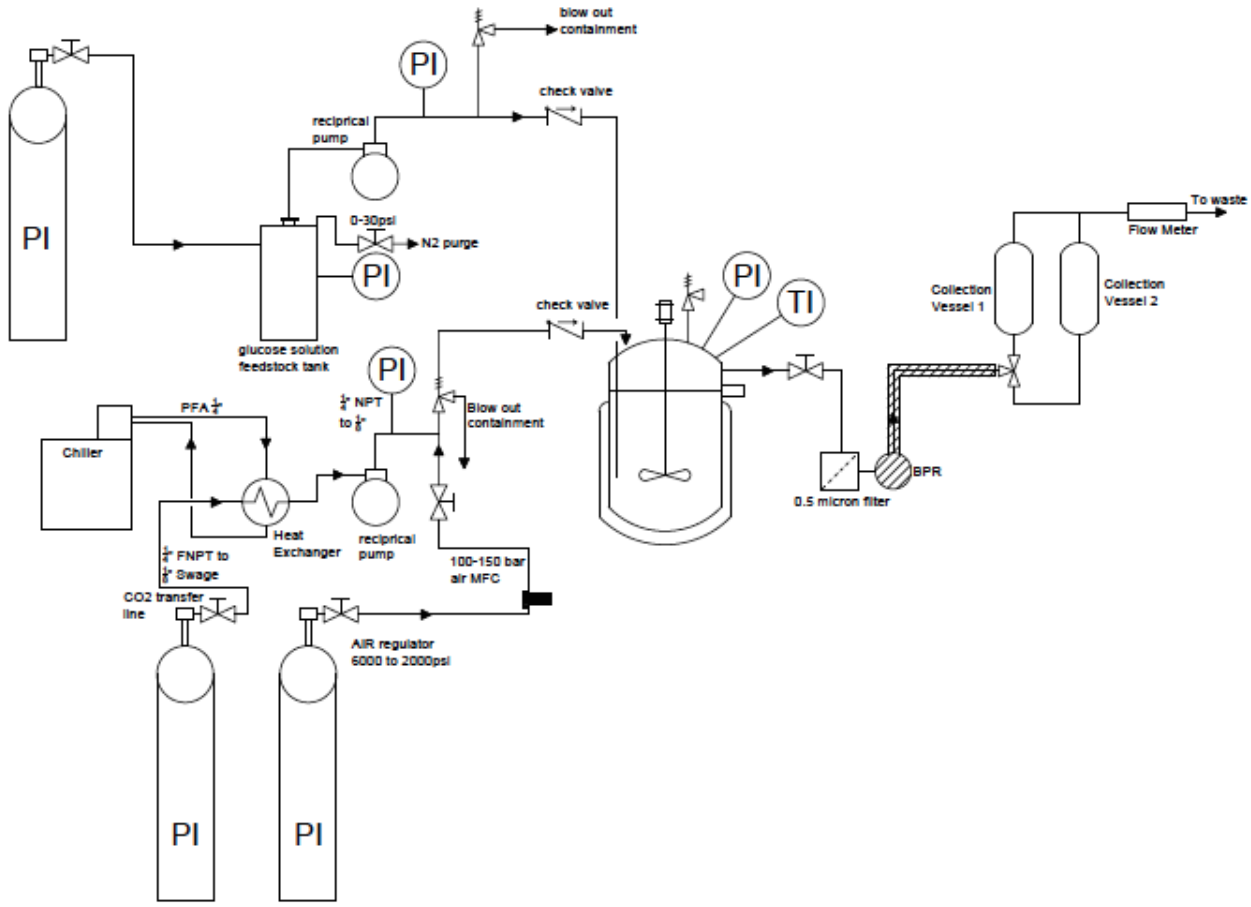

Figure 3.1: PFD of the SFE unit used in this report. Created by (Conlon et al., 2016).

CO_2 is fed from a high pressure cylinder into the extraction unit. The CO_2 is cooled to -1°C using a Fisher Scientific Isotemp chiller to maintain the CO_2 stream as a liquid. The stream is then pumped to high pressure using an Eldex BBB pump into a high pressure view cell partially filled with water, which saturates the CO_2 stream with water. The CO_2 stream then flows into a stainless steel Parr reactor, which includes a heating jacket and impeller shaft. The temperature and impeller velocity were controlled via a control panel linked to the reactor. Pressure in the reactor was controlled by an Equilibar back pressure regulator (BPR). After the BPR, the stream was depressurized in a heated stainless steel line set to 60°C. It then flowed to two methanol filled glass Pyrex collection vessels in series. Finally, the stream flowed through a wet test meter to measure the flow rate.

3.1.3 Setup

Several preparatory steps were taken before running the supercritical fluid extractor (SFE unit). First, personal protective equipment was donned. This included safety glasses, lab coats, and

nitrile gloves. Next, the chiller connected to the CO_2 line, located before the CO_2 pump, was set to -1°C, and the heating tape on the stainless steel line, located after the back pressure regulator, was set to 60°C. While the chiller and heating tape were allowed to equilibrate, the methanol collection jars were prepared. Ten clean 500 mL Pyrex jars were weighed to determine their empty dry mass. They were then each filled with 100 g of HPLC grade methanol (Sigma Aldrich, 99.9% pure). The filled bottles were weighed, capped, and placed in an ice bath to prevent evaporation of methanol. A 150 g initial aqueous alcohol solution charge was prepared by weighing an appropriate amount of the alcohol and adding this alcohol to the appropriate amount of deionized water.

Once the chiller and heating strips had reached their set temperatures, the SFE unit was prepared. First, all valves were checked to ensure they were in the appropriate open or closed position. The Parr reactor vessel was sealed to the rest of the system by a Teflon O-ring and set of clamps. This Teflon O-ring was visually inspected before operating the unit, to ensure it would still make a tight seal. Once these inspections were passed, the initial 150 g alcohol charge was added to the extraction vessel, and the vessel was connected to the rest of the SFE unit. At this point, the reactor heater was set to 40°C, and mixing was set to 200 rpm. Two alcohol collection vessels were attached to the unit in series. Once the reactor temperature reached its set point, the CO_2 pump was turned on, and pump stroke length was adjusted to provide the desired CO_2 flow rate. Pressure was increased in the reactor until it reached the set point of the back pressure regulator, which for these experiments was 1500 psi. Once the pressure reached 1500 psi, CO_2 flowed continuously through the unit, thus starting the extraction process.

3.1.4 System Operation

To measure the CO_2 flow rate, the effluent CO_2 stream was passed through a GCA/Precision Scientific wet test meter. If the CO_2 flow rate deviated from what was desired, the pump was adjusted accordingly. Alcohol was collected from the system in two methanol filled Pyrex jars connected to the extractor in series. To determine the time profile of alcohol concentration in the extract, these bottles were changed at regular intervals. For the low and medium CO_2 flow rates of 1.26, 3.2, and 5.4 mL/min, the bottles were changed at 5, 10, 20, and 40 minutes, and the experiment ended at 60 minutes. However, at higher CO_2 flow rates of 9 mL/min, icing in the line became a safety concern and an abbreviated schedule was followed. For 9mL/min, the bottles were changed at 5, 10, 15, and 20 minutes, and the experiment was terminated at 30 minutes. The Pyrex bottles were kept on ice to minimize the amount of evaporation.

3.1.5 Shutdown and Analysis

At the conclusion of the experiment, the CO_2 pump was turned off, and the alcohol collection vessels were removed. The system was depressurized slowly using the gas release valve at the top of the extractor and a heated line. The product containing vessels were weighed at the end of the experiment. Then, the contents of the two collection vessels which were in series on the extractor for the same time point were combined and mixed, and a sample was taken for analysis by gas chromatography (GC). The residual solution in the extractor was also weighed, and a sample was taken for GC analysis. These samples were analyzed for composition using a Shimadzu GC-MS-FID 2010. The GC was calibrated using standard solutions of n-butanol, isobutanol, n-pentanol, and n-hexanol prepared from pure stocks of these alcohols diluted in water and methanol to create calibration curves over the concentration range of 0.05 wt% to 1.0 wt% (see Figure 3.2). The glassware and extraction unit were rinsed three times with tap water to remove any alcohol residue, followed by triple rinsing with DI water and allowed to dry for several hours before the next run.

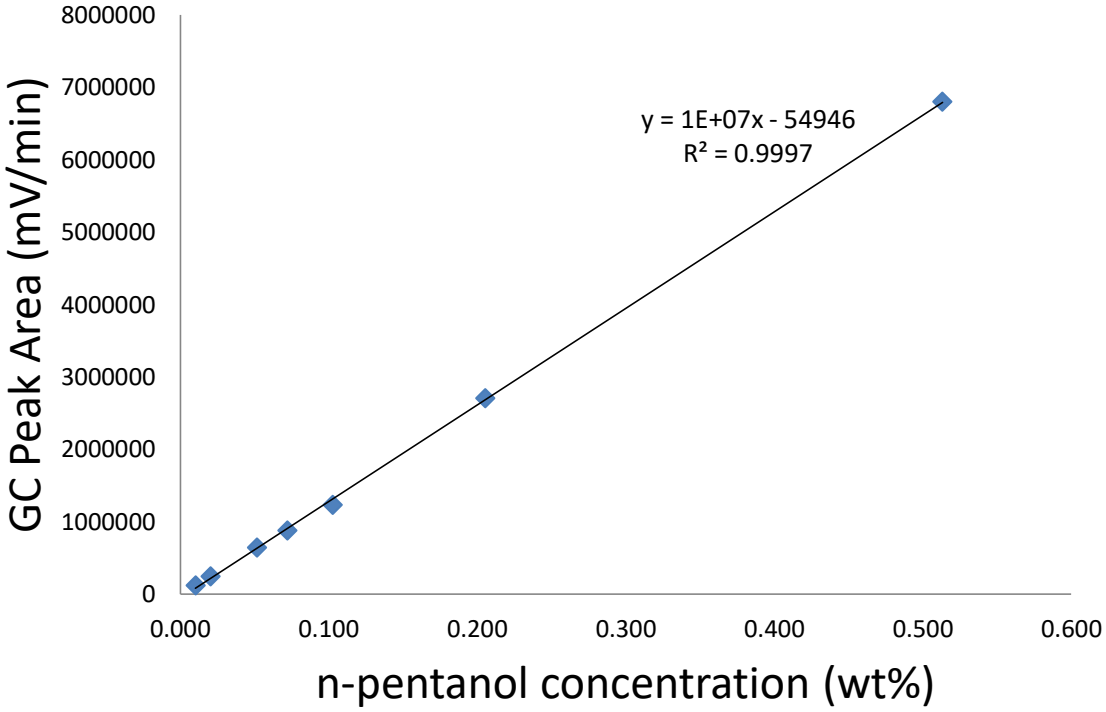

Figure 3.2: GC calibration curve for n-pentanol over a range of 0.05 wt% and 1.0 wt%.

3.2Mixing Methodology

Several experiments were designed in order to determine the mixing effectiveness inside the fermentation unit. Since the original fermentation-extraction unit is made of stainless steel,

an acrylic model of the fermenter was used for these experiments. The acrylic model had identical dimensions to the stainless steel reactor. The acrylic reactor model was created by Tom Partington of the WPI Chemical Engineering Department. The acrylic model is shown in figure 3.3.

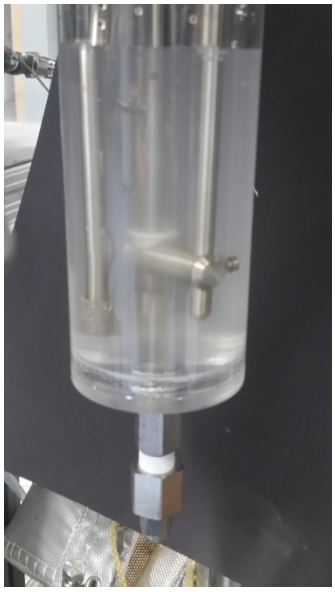

Figure 3.3: Picture of the acrylic reactor attached to the extraction unit and loaded with 200 mL of 0.1 wt% ultrafine cellulose.

Three different impellers were used for these experiments. The first is a vertical flat blade impeller similar to a Rushton Turbine. The vertical square paddle impeller had a total diameter of $1\ \frac{1}{16}$ inches, and four blades with lengths of $\frac{5}{16}$ inches each. The second is tilted flat blade impeller, which had a total diameter of 1 inch, and four blades tilted at a 45° angle, each with a length of $\frac{5}{16}$ inches (Figure 3.3, left). The third impeller used was a marine style impeller, which had a total diameter of 1 inch, and three blades with lengths of $\frac{5}{16}$ inches each (Figure 3.4, right). All impellers had a $\frac{1}{2}$ inch clearance from the bottom of the reactor.

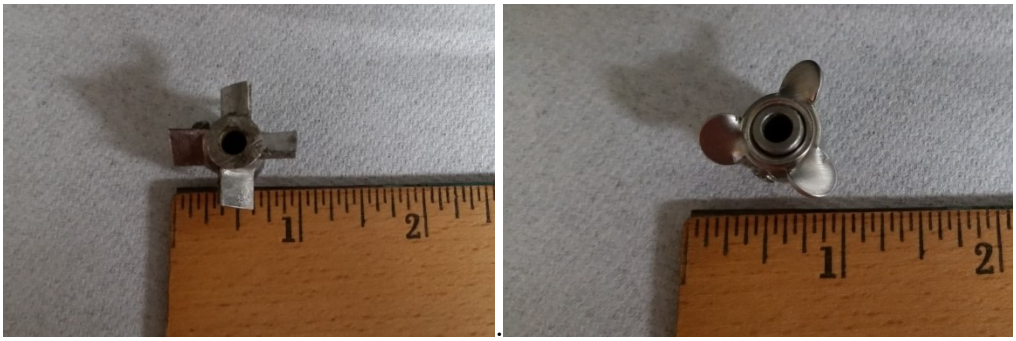

Figure 3.4: Picture of the tilted blade impeller (left) and marine propeller (right) used for the mixing experiments.

Due to safety and time considerations, *B. megaterium* was substituted for Sigma-Aldrich Sigmacell® microcrystalline 20 micron cellulose. Microcrystalline cellulose was selected due to its low cost, its hydrophilic properties, and its diameter being similar to that of *B. megaterium*. However, one drawback of using cellulose is that it tends to swell and clump together, forming some particles that are larger than the desired diameter.

Two types of mixing experiments were conducted in this study. The first set of experiments were measurements of the just stirred mixing speed, which was accomplished by loading the cellulose into the bottom of the reactor and measuring the amount of time required to fully mix the cellulose into suspension. The second set of experiments was measurements of the mixing time for different impellers. This was accomplished by starting with a solution where the cellulose had settled out of solution, and measuring the amount of time required to suspend all of the cellulose particles.

Due to the mixing experiments being carried out in an acrylic reactor rather than the pressure rated stainless steel reactor, all of the mixing experiments were carried out at ambient pressure and temperature. For the just stirred mixing speed experiments, the initial cellulose was loaded into the divot created by the sparging port on the reactor. This was done by first filling the reactor with 197 mL of water. In a beaker, 0.06 grams of cellulose was mixed with 3 mL of water. This concentrated solution of cellulose was carefully placed into the divot of the reactor using a Pasteur pipette. The reactor was secured to the reactor controller by stainless steel clamps, and the impeller was set to the desired mixing rate and allowed to stir the solution for three hours. After three hours, the turbidity of the mixture was observed. If the reactor was uniformly turbid and no cellulose was observed in the sparging port, then the reactor was assumed to be well mixed. If there were areas of the reactor more turbid than others, or if there was excess cellulose left in the

divot, then the reactor was not well mixed. This was repeated for each impeller type. The first mixing rate studied for each impeller was 100 rpm. If the solution was not well mixed at 100 rpm, the experiment was repeated with a mixing speed 100 rpm greater than the previous experiment until the reactor was well mixed. The minimum impeller speed needed to fully mix the cellulose mixture was determined to be the just stirred mixing speed.

For the mixing time experiments, 0.06 grams of cellulose was mixed with 200 mL of water and placed in the acrylic reactor. The reactor was attached to the controller by stainless steel clamps, and the cellulose was allowed to fully settle out of solution for five minutes between runs. After five minutes of settling, the impeller was set to the desired mixing speed. The speeds which were tested were 100, 200, 400, and 600 rpm. The time required to fully mix the solution, which was defined the same way as in the just stirred mixing experiments, was recorded for each stirring rate. This was repeated for each type of impeller.

3.3 Biotic Runs

First, the bioreactor must be inoculated with *B. megaterium* and filled with the M9+ growth medium. The growth medium was prepared one day in advance by mixing 50 mL of 5xM9 salts, 500 uL of 1M MgSO4, 2.5 mL of 5g/L Yeast extract, 6.25 mL of 40% glucose solution, 250 uL of 100x Metals, 16.6 mL of 1.5 M Alanine, 25 uL of $CaCl_2$ and 163 mL of H_2O. Next, 12.5 mL of 20x Na_2S and 220 uL of anaerobic indicator were prepared. Before inoculation commenced, the chiller was turned on. Next, the reactor was filled with 200 mL of the M9+ media and assembled. During this step it's important to keep all ports closed, add the heating jacket and ensure that all controls are functioning properly. Next, the temperature and stirring rate were set to 37°C and 350 RPM. Subsequently, CO_2 was bubbled through the reactor for approximately 1.5 hours. Following this step, the CO_2 inlet valve was closed and Na_2S and anaerobic indicator were added using a syringe through the inlet sampling valve. The reactor was also degassed for approximately 15 minutes during this step. Next, the sample coil was attached to the reactor. Before the reactor was inoculated with the bacteria, a 5 mL sample was taken from the reactor, 100 uL of which was used to test for sterility and the rest for glucose concentration. To test for sterility, the sample was spread on a LBA plate. Next, bacteria spores were added to the reactor using a syringe and allowed to mix for 10 minutes. The back pressure regulator was set to the desired specifications and the reactor was pressurized to 1500 psi by pumping $scCO_2$ into the system. Once the system reached

1500 psi, the CO_2 inlet valve was closed and the CO_2 tank was shut off. Next, the reactor was sampled in an effort to obtain the initial cell count. To accomplish this, a sample was drawn from the reactor following the sampling procedure specified below. A 100 uL portion of the sample was plated on a LBA plate and a separate 100 uL portion was heated to 80C (in order to kill the bacteria cells) for 10 minutes and spread on a LBA plate. Following this, 750 uL of the original sample was added to 250 uL of formaldehyde solution and mixed. This sample was stored at 4C. The final portion of the sample was centrifuged in a 1.7 mL tube and 1 mL's of the remaining supernatant were dispersed into a separate 1.7 mL tube and store at -20C to test for glucose and fermentation products. Finally, the sampling valve was sterilized using the method mentioned below.

While operating the inoculated bioreactor, a meticulous methodology was followed in an effort to mitigate cell damage from depressurization and to collect accurate samples to determine cell growth in the reactor. First, clean Lysogeny Broth (LB) agar plates were always stored in a fridge at 4C. Before samples were withdrawn from the reactor, the LB agar plates were transferred from the refrigerator to the incubator, which was operated at 37 ^{o}C. Next, sampling equipment and the reactor outlet valve were sterilized using 70% isopropanol solution and allowed to dry before sampling. Next, the sampling apparatus was attached to the outlet needle-valve of the reactor. Subsequently, the needle valve was opened very slowly in an effort to prevent cell rupture from the associated pressure drop. Approximately 10 mL of broth was allowed to accumulate in the first section of the sampling apparatus, before the needle valve was closed. Subsequently, the next needle valve of the sampling apparatus was opened slightly to allow the 10 mL sample to enter the larger chamber of the apparatus. Next, a sterile 15 mL collection tube was placed beneath the sampling apparatus. The final valve of the sampling apparatus was opened slightly, which allowed the sample to slowly drip out into the collection vessel. This step of the process was perhaps the slowest, taking approximately 20 minutes to allow the sample to exit the apparatus without undergoing a rapid pressure drop. Once the sample was extracted from the reactor, sample color and turbidity were observed. Finally, five samples, three at different dilutions, one using paraformaldehyde to fix the cells, and one to be centrifuged, were prepared.

3.3.1 Dilution, Microscopy and Centrifuge Samples

As previously mentioned, three diluted samples were prepared for each run, including 1:50, 1:500, 1:5000, or 1:50,000 dilutions. In order to prepare these dilutions, a specified amount of M9 buffer was added to 1.7mL vessels. Next, the original sample in the 10mL vessel was mixed by

hand to ensure equal dispersion of all components. A specified amount, depending on the dilution being performed, was withdrawn from the collection vessel and inserted into the 1.7mL tube containing the M9 media. Next, the 1.7mL tube was mixed and a 50µL sample was withdrawn using a graduated pipette and expelled onto the agar plate and spread around the plate. The agar plates were allowed to dry, before being placed in the incubator upside down. The agar plates were stored in the incubator for one day, before being analyzed. Storing the samples for one day allowed the cultures to grow, and the bacterial colonies on each plate were counted. All contaminated materials were disposed of in institutional biohazard containers.

Samples were prepared to be analyzed with a microscope by fixing the cells with paraformaldehyde. To accomplish this, 750 µL of sample was inserted into 1.7mL tubes using a graduated pipette. Next, 250 µL of 12% paraformaldehyde solution was added to the same tube to fix the cells. These samples were stored a refrigerator at 4C.

Samples were also prepared to be analyzed for substrate conversion. Glucose concentration and fermentation products were the two sought after parameters. To accomplish this, 1000 µL of sample was added to 1.7 mL tubes. Subsequently, the tubes were placed in a centrifuge which was balanced by placing a 1.7 mL water filled tube opposite to the sample. The centrifuge was set to 15,000 RPM and allowed to operate for 5 minutes. Upon completion of the spinning cycle, samples were removed from the centrifuge and cell pellet formation was noted. The supernatant was then poured into a separate 1.7 mL vessel which was stored, along with the remaining cell pellet in a refrigerator at 4 ^{o}C.

3.3.2 Sterilization

After the samples were taken, the needle exit valve of the reactor were sterilized a second time with 70% isopropyl solution. The sampling apparatus was disassembled flushed using 10% bleach solution for at least 2 hours. Finally, the sampling apparatus was flushed with water, sprayed with 70% isopropyl alcohol and allowed to air dry for one day. Following sterilization, the reactor was topped off with $scCO_2$ to maintain a pressure of 100 bar.

4. Results and Discussion

4.1 Alcohol Extraction

During experimentation, we tested four flow rates, 1.26 ml/min, 3.2 ml/min, 5.4 ml/min and 9 ml/min, for each alcohol at a fixed initial concentration of 0.5 wt%. All runs were conducted for 60 minutes, except the 9 mL/min runs, which was only conducted for 30 minutes due to safety concerns.

4.1.1 Effect of Altering Flow Rate on Extraction Efficiency

Mass transfer theory dictates that slower flow rates should extract the most alcohol per gram of CO_2, since the residence time between the CO_2 and aqueous solution phase is greater. Therefore, the alcohol is allowed more time to diffuse into the scCO_2 phase at lower flow rates. After conducting numerous runs with different alcohols, the raw data for each alcohol at each given flow rate of CO_2 was averaged. Based on these averages, the mass of alcohol extracted was plotted against the cumulative amount of CO_2 used in the experiment. An example of this plot is given in Figure 4.1, which shows the amount of n-pentanol extracted per gram of CO_2. This type of graph gives one measure of extraction efficiency. Runs that extract more alcohol per gram of CO_2 would be more efficient. Our data tended to align with the theory mentioned above; the slowest flow rate extracted the most alcohol per a gram of CO_2 and the fastest flow rate extracted the least. As seen in Figure 4.1, 1.26 ml/min, extracted the most alcohol per gram of CO_2 whereas, 9 ml/min, extracted the least. Therefore, 1.26 ml/min is the most efficient CO_2 flow rate. Also, 1.26 ml/min and 3.2 ml/min seemed to overlap significantly, suggesting that the phase CO_2 was saturated with alcohol at these flow rates.

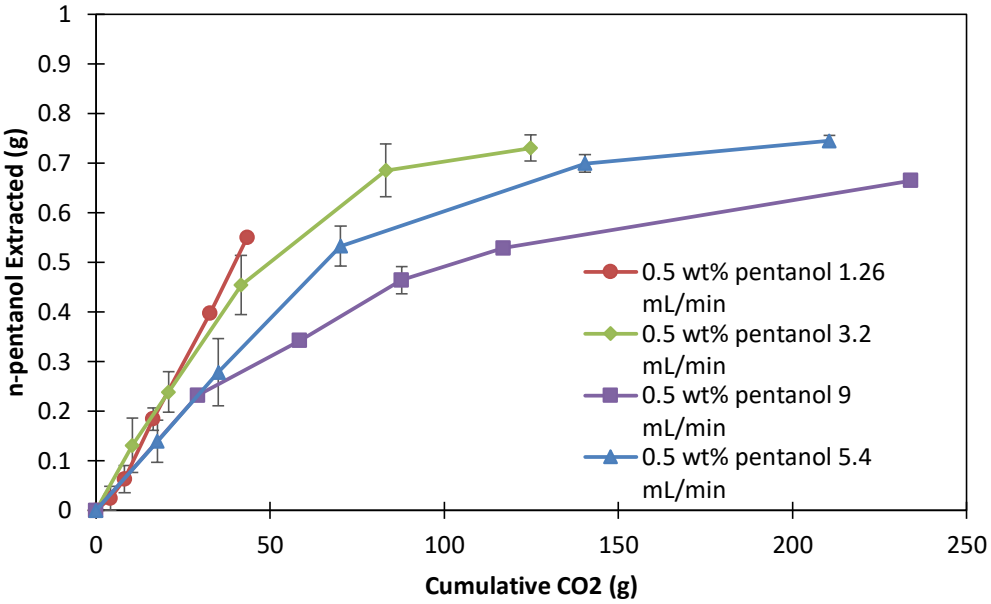

Figure 4.1: Mass of alcohol extracted as a function of the cumulative mass of CO_2 used for an initial concentration of 0.5 wt% n-pentanol, 1500 psi, 400 rpm, and CO_2 flow rates of 1.26 (red), 3.2 (green), 5.4 (blue), and 9 (purple) mL/min.

Examining the percent of the initial alcohol solution extracted per a gram of CO_2 at different flow rates is another method for examining the system's efficiency. This analysis can be performed by plotting percent alcohol extracted vs cumulative CO_2. Following the same logic mentioned above, slower flow rates should extract a larger percent of the initial alcohol per gram of CO_2. Figure 4.2 shows the percent of the initial n-hexanol solution extracted at varying flow rates. As expected, slow flow rates extracted the largest percent of n-hexanol per gram of CO_2. Also, the 5.4 ml/min and 9 ml/min flow rates appear to follow a similar trend. This suggests that the same amount of $scCO_2$ is required to extract a given percent of the initial hexanol at flow rates past 5.4 ml/min. This point is further exemplified in Figure 4.3 which shows the amount of CO_2 required to extract 80% of n-butanol at different flow rates. Both 5.4 ml/min and 9 ml/min require approximately the same amount of CO_2 to extract 80% of the initial solution. This suggests that this trend is consistent with different alcohols, and that the system should be operated at 9 ml/min instead of 5 ml/min if high flow rates are desired because it requires less time without sacrificing efficiency.

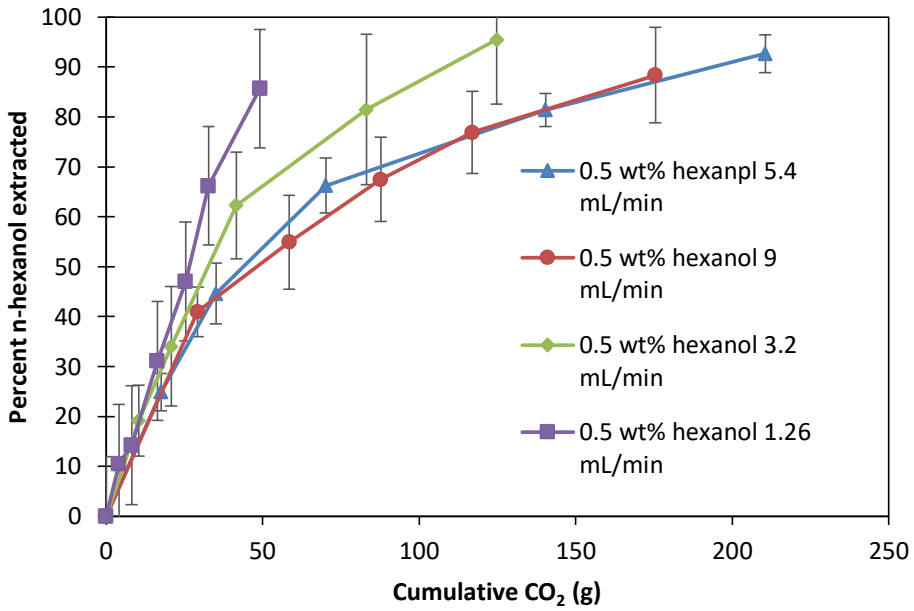

Figure 4.2: Percent n-hexanol extracted vs $scCO_2$ consumed for an initial concentration of 0.5 wt% n-hexanol, 1500 psi, 400 rpm, and CO_2 flow rates of 1.26 (purple), 3.2 (green), 5.4 (blue), and 9 (red) mL/min.

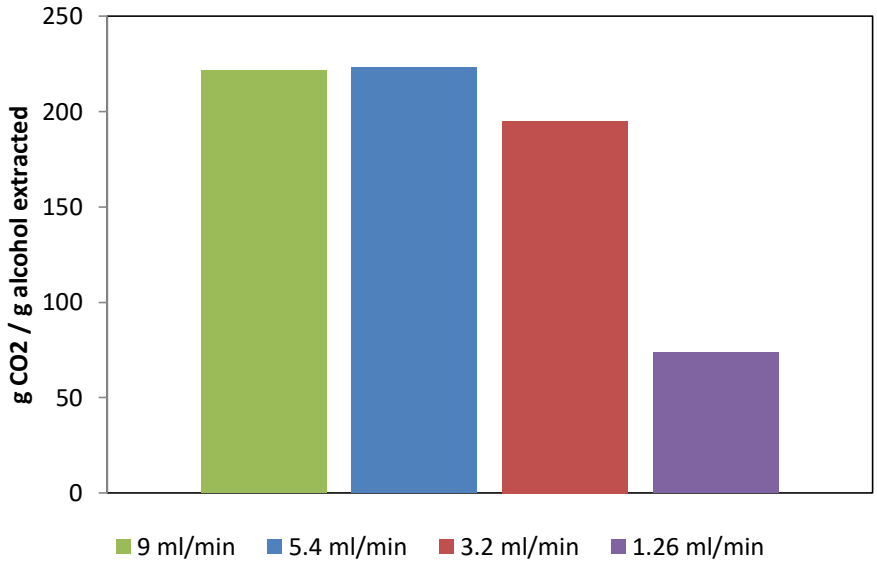

Figure 4.3: Amount of CO_2 required to extract 80% of the initial alcohol solution for an initial concentration of 0.5 wt% n-butanol, 1500 psi, 400 rpm, and CO_2 flow rates of 1.26 (purple), 3.2 (red), 5.4 (blue), and 9 (green) mL/min.

4.1.2 Effect of Alcohol Chain Length on Extraction Efficiency

We also compared different alcohols at the same $scCO_2$ flow rate and initial concentration. Higher chain length alcohols are less polar because the electrostatic potential of the hydroxyl group is negligible compared to the non-polar carbon chain in higher chain alcohols. As a result, they

should have a greater affinity for the nonpolar $scCO_2$ phase. Out of the four alcohols we examined, n-hexanol should result in the most effective extraction, followed by n-pentanol, n-butanol, and finally isobutanol. We speculate that isobutanol should be the worst extraction candidate since it is slightly more polar than n-butanol due to its branched form. This decreases its affinity to the $scCO_2$ phase and increases its affinity to the aqueous phase. Figure 4.4 compares the percent of n-hexanol, n-pentanol and n-butanol extracted with $scCO_2$, each at an initial concentration of 0.5 wt% and for a flow rate of 9 ml/min. The data plotted follows our predictions mentioned above. For example, at 50% extraction, hexanol required the least amount of $scCO_2$, followed by pentanol and then butanol. Unfortunately we were not able to collect extraction data for isobutanol at a 0.5 wt% initial concentration due to time constraints. However, we did several runs for isobutanol and butanol at an initial concentration of 1 wt% and a flowrate of 9ml/min. Figure 4.5 represents this data by showing percent of alcohol extracted vs cumulative CO_2. Our data did not follow the prediction mentioned above, rather, the two alcohols performed with nearly the same efficiency.

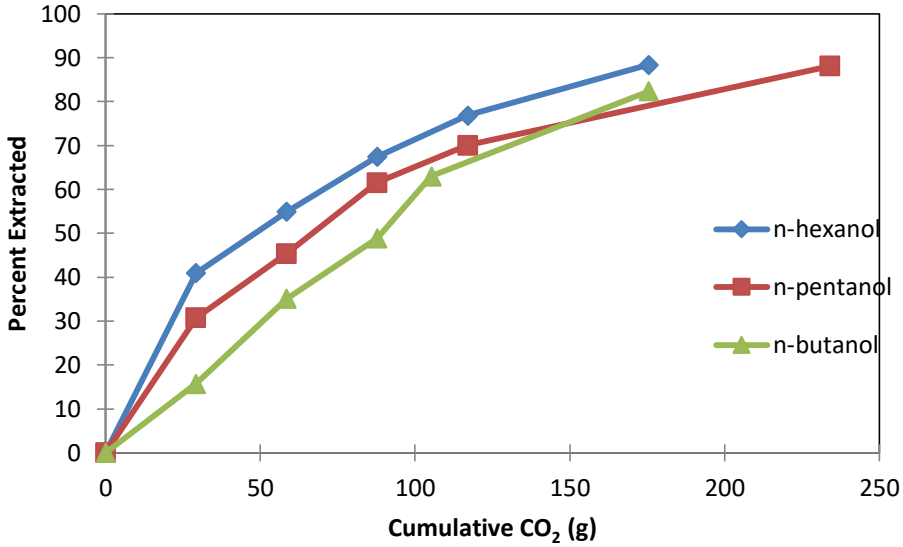

Figure 4.4: Comparison of extracting n-hexanol (blue), n-pentanol (red), and n-butanol (green) from aqueous solution at 9 ml/min $scCO_2$ flow rate, 400 rpm, and initial alcohol concentration of 0.5 wt%.

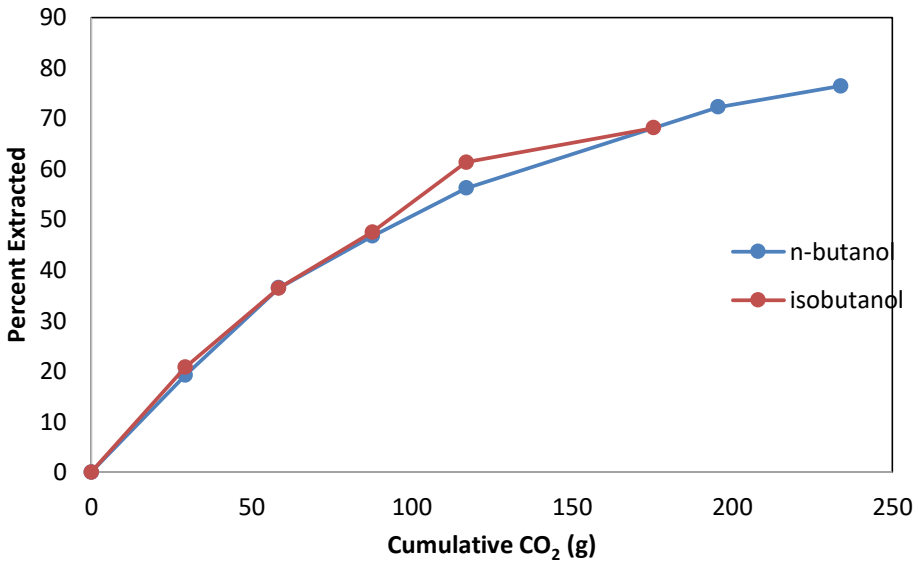

Figure 4.5: Comparison of percent extracted of n-butanol (blue) and isobutanol (red) at an initial concentration of 1 wt%, 400 rpm and a scCO₂ flow rate of 9 ml/min.

In an effort to further illustrate the theory mentioned above, several charts showing the amount of CO_2 required to extract a given percent of the initial alcohol concentration. Figure 4.6 shows the amount of $scCO_2$ needed to extract 60% of n-hexanol, n-pentanol, and n-butanol, at initial concentrations of 0.5 wt% and a flow rate of 9 ml/min. As seen in Figure 4.6 butanol required the most CO_2 to extract 60% of the initial solution, followed by pentanol and then hexanol. This follows the theory mentioned above.

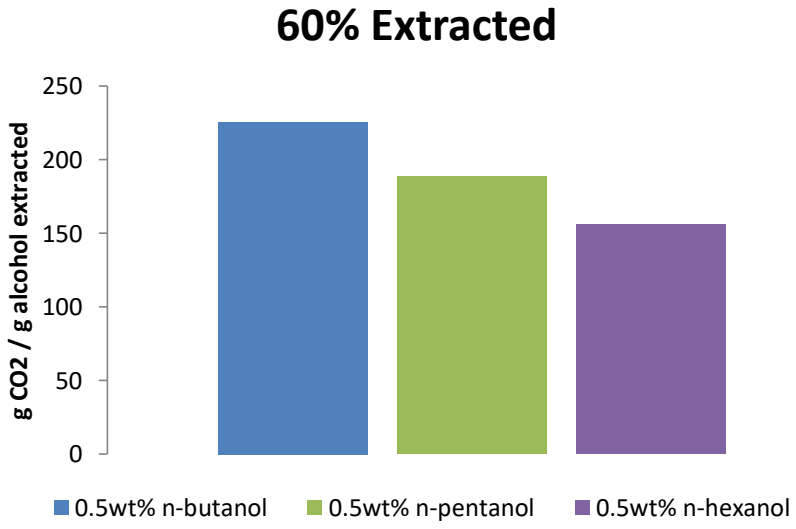

Figure 4.6: Ratio of weight of CO_2 to weight of alcohol to extract 60% of initial alcohol solution. Flow rate of $scCO_2$ held constant at 5.4 ml/min and initial alcohol concentration was 0.5wt%.

4.1.3 Effect of Initial Concentration of Alcohol on Extraction Efficiency

Assuming that the partition coefficient between alcohol in the aqueous phase and the $scCO_2$ phase does not vary with concentration, altering the initial concentration of alcohol in the system should not affect extraction efficiency. However, we predict that a higher initial concentration of alcohol should result in a larger concentration gradient, thus a larger driving force for the alcohol to diffuse into the CO_2 at a faster rate. Since the initial alcohol concentration is higher, the percent extracted should not be affected. However, when the initial concentration of alcohol is greater, more alcohol should be extracted per gram of CO_2 extractant. Our data, for runs conducted at 0.5 wt% and 1 wt% for both isobutanol and n-butanol, supports this hypothesis. As seen in Figure 4.7, the 1 wt% n-butanol initial solution resulted in more alcohol being extracted per a gram of CO_2.

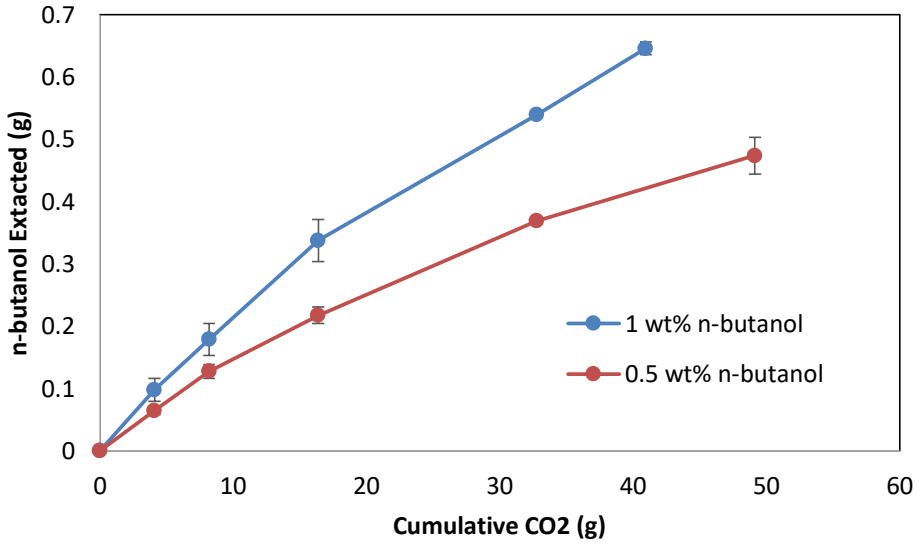

Figure 4.7: Mass of n-butanol extracted cumulative CO_2 at a $scCO_2$ flow rate of 5.4 mL/min, 400 rpm, 40°C, 1500 psi.

4.3.4 Summary of Alcohol Extraction Efficiency Results

In summary, the efficiency of alcohol extraction generally followed the expected results based on the two-film model of mass transfer. First, slower flow rates were more efficient at extracting alcohol from solution based on the amount of CO_2 used to extract a given amount of alcohol. This follows the mass transfer model because slower flow rates have a greater residence time in the reactor, meaning there is more time for alcohol to diffuse from the aqueous phase into the $scCO_2$. Second, longer chain length alcohols were more efficient at being extracted than small chain length alcohols. This likely because longer chain alcohols are less polar, so they have greater

affinity for the $scCO_2$ phase compared to the aqueous phase. Finally, increasing the initial alcohol concentration also increases the efficiency of extraction, because there is a greater driving force caused by the larger concentration gradient between the aqueous phase and the $scCO_2$.

4.2 Mass Transfer of alcohol into $scCO_2$

The mass transfer coefficient was determined experimentally by first plotting the natural logarithm of the ratio of alcohol concentration in the aqueous phase at different time points during the extraction runs ($C_{a,w}$) to the initial alcohol concentration in the aqueous phase ($C_{a,w,0}$). Runs of the same alcohols at the same initial concentrations and using the same CO_2 flow rate were averaged. A linear regression line was generated for each condition. An example of this type of plot is shown in Figure 4.8.

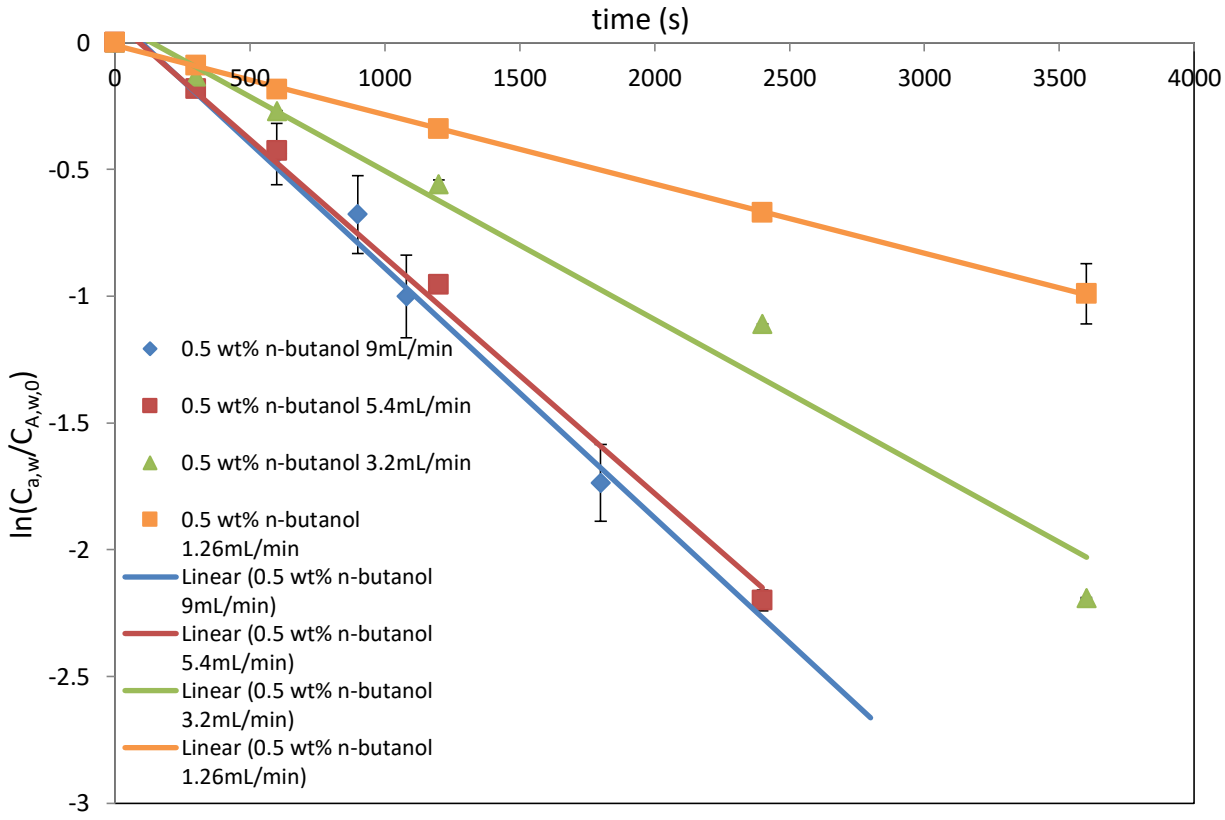

Figure 4.8: Natural logarithm of the ratio of alcohol concentration in the aqueous phase to the initial concentration of alcohol in the aqueous phase as a function of time for n-butanol at an initial concentration of 0.5 wt%, $scCO_2$ flow rates ranging from 1.26 to 9 mL/min, 400 rpm, and 40°C. Similar plots were generated for isobutanol, n-pentanol, and n-hexanol.

Recall Equation 10, which states that the slope of the linear regression in Figure 4.8 will be equal to α_1. Using the graphically determined value of α_1, the value of $K_s a$ can be determined using Equation 4.1.

$$\ln\left(\frac{C_{a,w}}{C_{a,w0}}\right) = \alpha_1 t + \ln(\beta_1)$$

Equation 4.1

$$K_s a = -\frac{\alpha_1(1 + \alpha_1 {}^{V_c}/_{G})}{K_{CW}\left[\left(\alpha_1 {}^{V_c}/_{G}\right) + 1\right] + \alpha_1 {}^{V_w}/_{G}}$$

Equation 4.2

The value of $K_l a$ was then determined from the value of $K_s a$ using Equation 3.

$$K_l a = K_s a * K_{CW}$$

Equation 4.3

This method was applied to all the conditions tested in this experiment. A summary of the values of $K_s a$ and $K_l a$ are given in Table 4.1.

Table 4.1: Experimentally determined values of $K_s a$ and $K_l a$ for n-butanol at 0.5 and 1.0 wt%, isobutanol at 1.0 wt%, n-pentanol at 0.5 wt%, and n-hexanol at 0.5 wt%. Asterisks indicate that the extraction of alcohol is equilibrium limited under the specified conditions.

Alcohol	Initial Alcohol Concentration (wt%)	Flow rate (mL/min)	$K_s a$	$K_l a$
n-butanol	1.00	12.5	0.00052	0.00114
	1.00	9	0.00389	0.00857
	1.00	3.2	0.00003*	0.00006*
	1.00	1.26	0.00005*	0.00011*
n-butanol	0.50	9	0.00011	0.00025
	0.50	5.4	0.00029*	0.00064*
	0.50	3.2	0.00015*	0.00032*
	0.50	1.26	0.00007*	0.00016*
isobutanol	1.00	9	-0.00052	-0.00104
	1.00	5.4	0.00012*	0.00023*
	0.50	5.4	0.00016*	0.00032*
	1.00	3.2	0.00013*	0.00027*
	1.00	1.26	0.00008*	0.00016*
n-pentanol	0.50	9	0.00002	0.00011
	0.50	5.4	0.00016	0.00080
	0.50	3.2	0.00019*	0.00095*
	0.50	1.26	0.00006*	0.00031*
n-hexanol	0.50	9	0.00016	0.00082
	0.50	5.4	0.00007	0.00036
	0.50	3.2	0.00011	0.00055
	0.50	1.26	0.00008	0.00042

Before interpreting these values, it is important to consider whether the system is mass transfer or equilibrium limiting. If the $scCO_2$ becomes saturated with alcohol as it passes through the aqueous phase, the measured value of the overall mass transfer coefficient will be smaller than

the actual value of the mass transfer coefficient. This is because once the $scCO_2$ reaches saturation, the net diffusion rate of alcohol into the $scCO_2$ phase becomes zero. As a result, less mass transfer occurs than if the system were not at equilibrium. A full discussion of situations where the extractor is equilibrium limited is given in subsequent sections.

The calculated values of K_sa are, for most conditions, within the same order of magnitude as those found for ethanol by Tai and Wu (2005). We expect that K_la will increase with increasing CO_2 flow rate and with increasing carbon number. It is expected to increase with carbon number because as the number of carbon-carbon bonds per hydroxyl group in an alcohol increases, the polarity decreases. As a result, the molecule has less solubility in water and a higher affinity for $scCO_2$, so the alcohol is more strongly attracted to the $scCO_2$ phase. It is also expected to increase with increasing CO_2 flow rate, since at a greater flow rate there should be a greater amount of contact area and convective mixing between the $scCO_2$ and aqueous phases (Tai & Wu, 2005).

A summary of all the calculated overall liquid side mass transfer coefficients is given in Figure 4.9. Figure 4.9 indicates that there is no apparent trend in K_la. This is also seen in Figure 4.10, which plots K_la only for cases where the extraction is not equilibrium limited. Again, there is no obvious trend in K_la as a function of CO_2 flow rate or the alcohol carbon number. One possible explanation for this is that there is no measureable difference between mass transfer coefficients based on flow rate or carbon number. There may also be complicating factors affecting trends in K_la. For example, although higher alcohols have a greater affinity towards the $scCO_2$ phase since they are less polar, they also have a lower value of diffusivity because they have a larger molar volume (Wankat, 2012). Additionally, although there is greater convective mass transfer at higher CO_2 flow rates, there is also a lower surface area to volume ratio since larger CO_2 bubbles form. These potentially offsetting factors could explain the lack of a general trend in K_la seen in Figures 4.9 and 4.10.

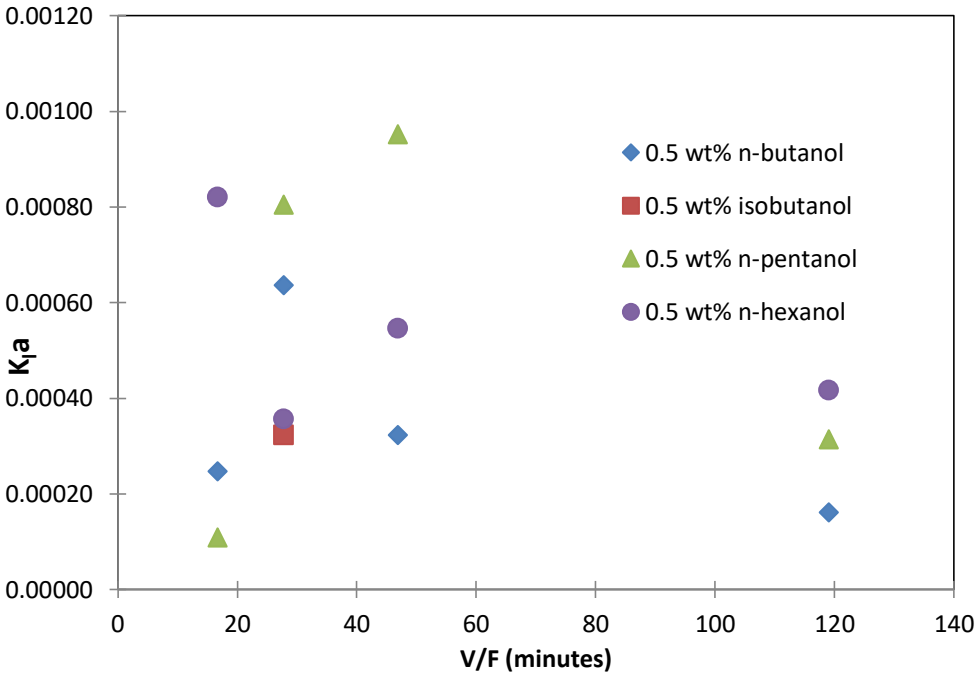

Figure 4.9: Overall mass transfer coefficient on the liquid side (K_la) as a function of the ratio of liquid volume to $scCO_2$ flow rate for n-butanol (diamonds), isobutanol (squares), n-pentanol (triangles), and n-hexanol (circles). All data points are at an initial alcohol concentration of 0.5 wt%, and a mixing speed of 400 rpm.

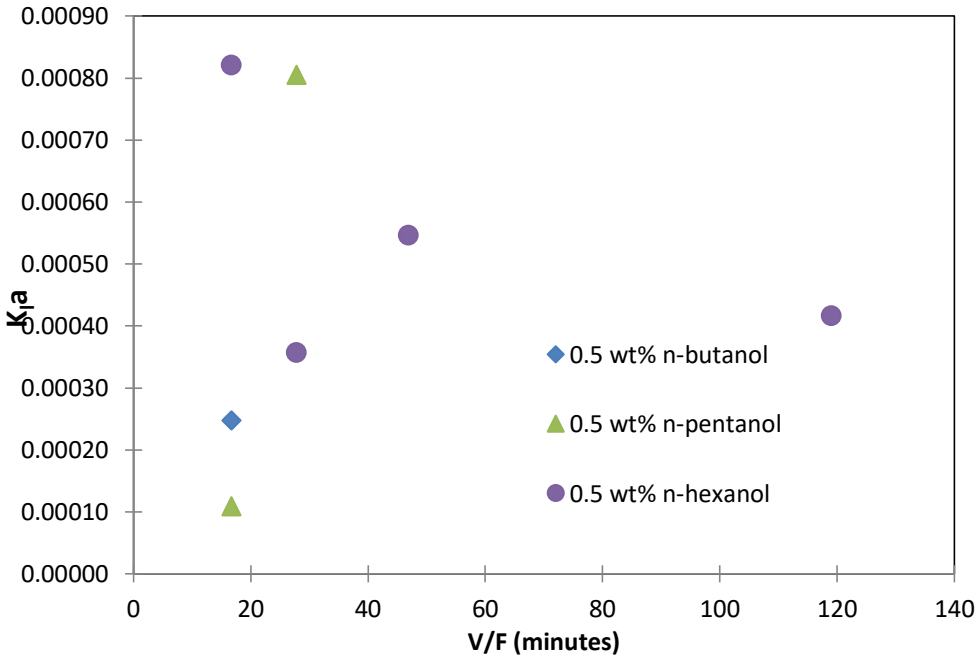

Figure 4.10: Overall mass transfer coefficient on the liquid side (K_la) as a function of the ratio of liquid volume to $scCO_2$ flow rate for n-butanol (diamonds), isobutanol (squares), n-pentanol (triangles), and n-hexanol (circles). Only data for conditions which were not equilibrium limiting were included. All data points are at an initial alcohol concentration of 0.5 wt%, and a mixing speed of 400 rpm.

Another possible reason for the lack of trends in Figures 4.9 and 4.10 is the assumption made to graphically solve for $K_s a$. It was assumed that in Equation 4 that the contribution of α_1 was much greater than the contribution of α_2 because according to the definition of α_1 and α_2, α_1 is always greater than α_2 (see methodology section). If this simplifying assumption is invalid, then the method of graphically solving for $K_l a$ based on the plots of $\ln\left(\frac{C_{A,w}}{C_{A,w,0}}\right)$ would be incorrect. It may be worth considering, in future analysis, either the full two-film model, or another model of mass transfer which better describes the mass transfer in the system (Equation 4.4).

$$C_{A,w} = C_{A,w,0}[\beta_1 \exp(\alpha_1 t) + \beta_2 \exp(\alpha_2 t)]$$

Equation 4.4

4.3 Determination of the Distribution Coefficient

Under certain conditions, the $scCO_2$ in the reactor becomes saturated with alcohol. In these cases, extraction efficiency is limited by the equilibrium between alcohol in the aqueous phase and alcohol in the $scCO_2$ phase. In the case where extraction is equilibrium limited, the concentration profile of alcohol in the aqueous phase is governed by Equation 4.5:

$$(V_W)\frac{dC_{A,w}}{dt} = -GK_D C_{A,w}$$

Equation 4.5

In Equation 4.5, G corresponds to $scCO_2$ flow rate, K_D is the distribution coefficient, $C_{A,w}$ is the concentration of alcohol in the water phase and V_W is the volume of the water phase. Since the partition coefficient represents the ratio of alcohol in the two phases, multiplying this by the flow rate of CO_2 and the concentration of water in the alcohol phase, and finally, dividing by the volume of the water phase, this gives us the change of concentration in the water phase with time.

$$\frac{dC_{A,w}}{C_{A,w}} = \frac{-GK_D}{V_W}dt$$

Equation 4.6

Next, Equation 4.2 was rearranged, as seen above in Equation 4.6, and integrated, resulting in Equation 4.7:

$$\ln\left(\frac{C_{A,w}}{C_{A,w2}}\right) = \frac{-GK_D}{V_W}t$$

Equation 4.7

K_D was determined by plotting $\ln\left(\frac{A_W}{A_{W2O}}\right)$ against time and finding the slope of the resulting trend lines. Based on Equation 4.7, the slope of these trend lines will be equal to $\frac{-FK_{CW}}{V_W}$. A representative example of this graph is seen in Figure 4.11 for isobutanol at different flow rates. This process was performed for each alcohol at each respective flow rate. Each alcohol exhibited similar trends, but with different slopes.

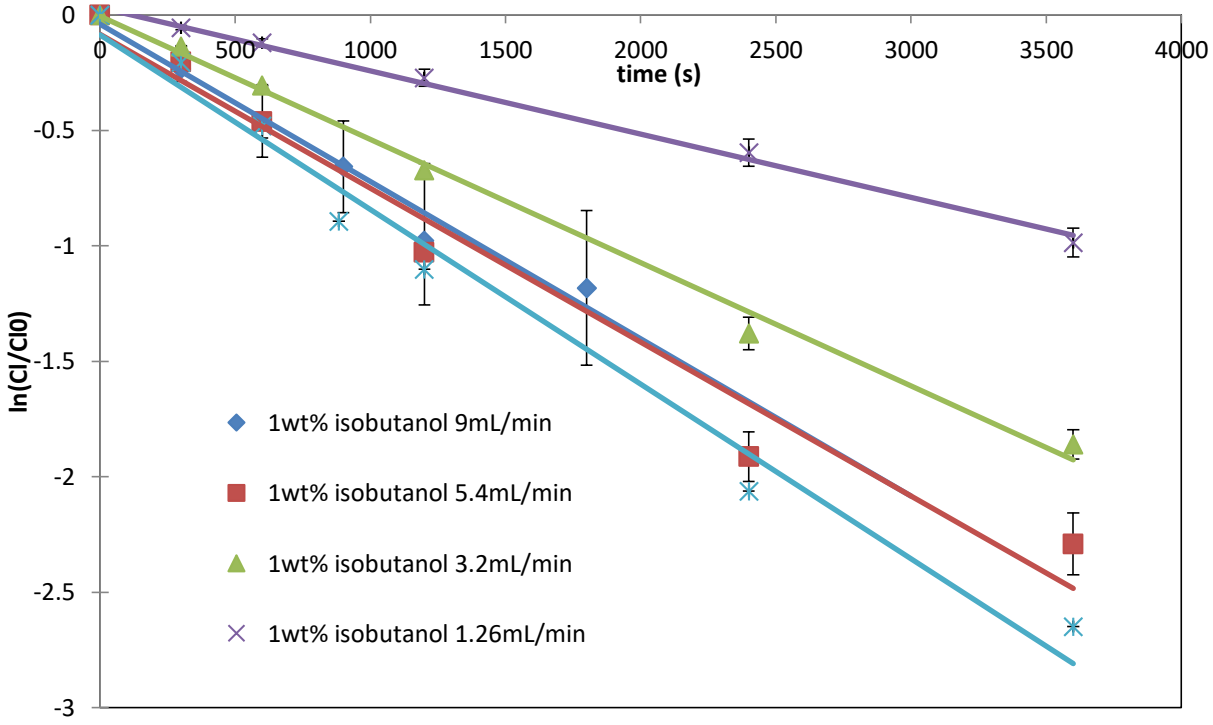

Figure 4.11: Plot of ln(Cl/Clo) vs time for isobutanol at flow rates ranging from 1.26 to 9 mL/min, 400 rpm, 40°C. The slope of these lines were used to determine K_{CW}.

At equilibrium, the $scCO_2$ phase is saturated with alcohol and the distribution coefficient, K_D, equals the partition coefficient, K_{CW}. Therefore, we were able to ascertain K_{CW} when the system is in equilibrium. Values of K_D were calculated to allow us to model the system. This is important because such models can be used to scale up the process to industrial standards. As seen in Table 2, K_D tended to increase with decreasing flow rate for a given alcohol at a fixed initial concentration. Since K_D is a ratio of alcohol in the $scCO_2$ phase to alcohol in the water phase this

trend was expected. Slower flow rates correlate with higher residence time between the $scCO_2$ phase and the aqueous solution. Therefore, more alcohol can diffuse into the $scCO_2$ phase, meaning there is more time for the alcohol to diffuse into the $scCO_2$ phase. For extraction runs governed by mass transfer instead of equilibrium, the K_D is less relevant, and the mass transfer model used in Section 4.2 should be followed.

Table 2: K_D of different alcohols, at varying flow rates and varying initial concentration. Conditions were 400 rpm, 40°C, and 1500 psi.

alcohol	Initial Concentration (wt%)	flow rate (mL/min)	K_D
n-butanol	1.00	12.5	0.4569408
	1.00	9	0.60398
	1.00	3.2	0.936315
	1.00	1.26	1.513428571
n-butanol	0.50	9	0.986026
	0.50	5.4	1.836525
	0.50	3.2	1.648215
	0.50	1.26	1.955421429
isobutanol	1.00	9	0.680845
	1.00	5.4	1.111216667
	0.50	5.4	1.260515
	1.00	3.2	1.500463125
	1.00	1.26	1.959257143
n-pentanol	0.50	9	0.87849
	0.50	5.4	1.784083333
	0.50	3.2	3.2990625
	0.50	1.26	2.794071429
n-hexanol	0.50	9	1.26
	0.50	5.4	1.083333333
	0.50	3.2	1.996875
	0.50	1.26	3.642857143

4.4 Comparison of the Mass Transfer and Equilibrium Limited System

4.4.1 Determining when the system is equilibrium limited

Depending on the conditions in the extraction run, the system was either limited by mass transfer or by equilibrium between alcohol concentration in the aqueous phase and alcohol concentration in the $scCO_2$ phase. In the case of mass transfer limitations, the rate of extraction of alcohol from the aqueous phase should be governed by the overall mass transfer coefficient, K_sa or K_la. However, in the case where the aqueous phase has time to fully reach equilibrium with the $scCO_2$ phase, the extraction rate is governed by the partition coefficient, K_{CW}. The method for determining whether the extraction rate was governed by mass transfer or equilibrium is by first calculating the distribution coefficients and overall mass transfer coefficients as explained in the previous sections. These values are summarized in Tables 4.1 and 4.2. The calculated distribution coefficient is expected to remain constant with decreasing $scCO_2$ flow rate if the system is equilibrium limited. This is because with a slower $scCO_2$ flow rates there is a greater residence time per gram of CO_2, so there is more time for alcohol to diffuse into the $scCO_2$ phase and a greater likelihood that the $scCO_2$ will become fully saturated with alcohol. This assumption was confirmed by comparing the values of K_D to literature predictions for K_{CW}. Specifically, the K_{CW} is expected to be 2.2 for n-butanol (Antero Laitinen & Juha Kaunisto, 1999), 2 for isobutanol, and 5 for n-pentanol and n-hexanol (Dooley, Cain, & Carl Knopf, 1997; Stahl, Quirin, & Gerard, 1988). A comparison of conditions where the system is equilibrium or mass transfer limited is shown in Figure 4.12.

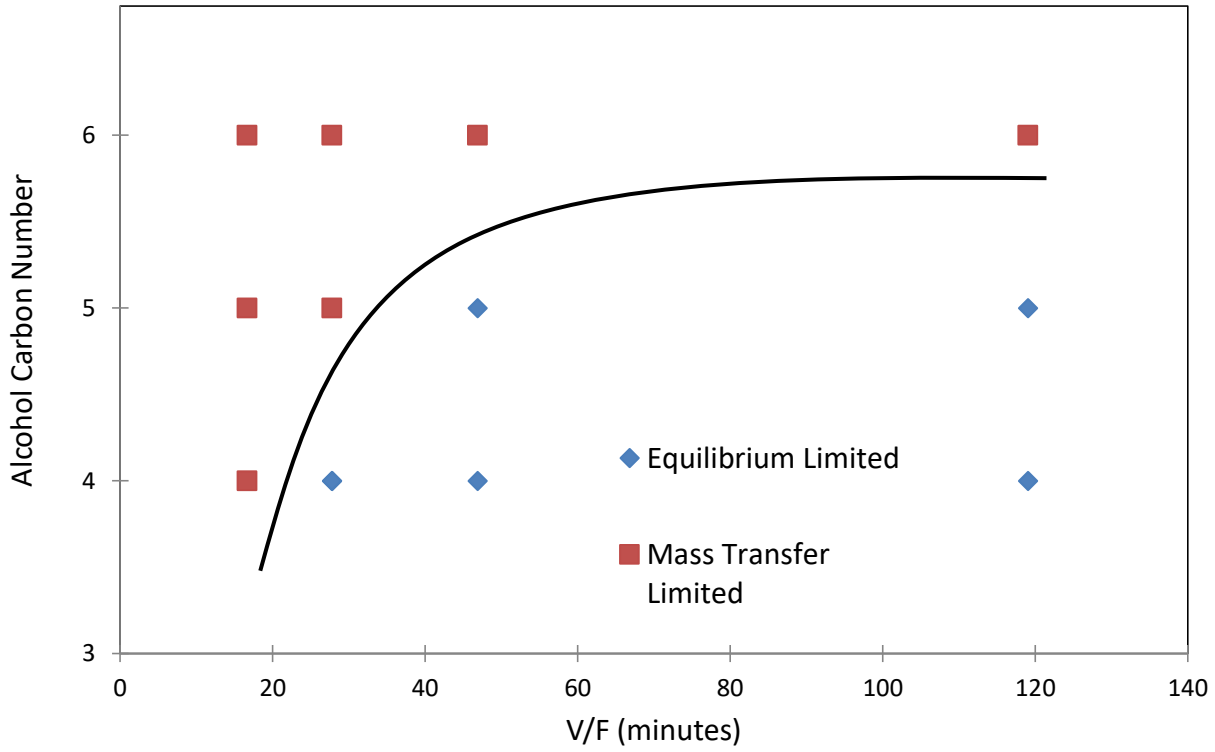

Figure 4.12: A comparison of conditions where alcohol extraction is equilibrium limited or mass transfer limited. All points are at an initial alcohol concentration of 0.5wt%, 1500 psi, 40°C and a stir rate of 400 rpm. The carbon number of the alcohol is plotted on the y axis, and the ratio of liquid volume to CO_2 flow rate is plotted on the x axis. Red squares indicate cases where the system is limited by mass transfer, and blue diamonds indicate cases where the system is limited by equilibrium. The line is a representation of the border between mass transfer and equilibrium limitation drawn by eye.

It is evident from Figure 4.12 that increasing the ratio of liquid volume to CO_2 flow rate pushes the system towards being equilibrium limited. This correlates well with the expectation that at a constant liquid volume, decreasing the flow rate of CO_2 increases the likelihood of being equilibrium limited. Also evident from Figure 4.12 is that increasing the alcohol carbon number also pushes the system towards being mass transfer limited. This is likely because the diffusivity of solvents generally decreases with increasing molar volume (Wankat, 2012). Larger molecules will generally diffuse more slowly, meaning that they would require a longer residence time to fully reach saturation in the $scCO_2$ phase.

4.4.2 Peclet Number

The Peclet number is defined as the rate of advective mass transfer to the rate of diffusive mass transfer. In this case, it is useful to define the Peclet number as Equation 4.8:

$$Pe = \frac{F}{V_l K_l a}$$

Equation 4.8

This relationship may be useful for future analysis of determining a measure of mass transfer using an adapted mass transfer model. In this case, it is noted that the Peclet number at the point where the system changes from being equilibrium to mass transfer limited (the line on Figure 4.12) is approximately 1.7 for n-butanol and 1.1 for n-pentanol.

4.4.3 Results of Sparging $scCO_2$ through a frit

This conclusion is also supported by an experiment where the $scCO_2$ was fed through a frit to produce smaller CO_2 bubbles. The results of this run, compared to another run which is under the same conditions except it lacks the stainless steel frit, is given in Figure 4.13. We would expect that in the case where extraction is limited by mass transfer the inclusion of a frit would improve efficiency. This is because the frit generates smaller bubbles, so there is a larger area available for mass transfer between the aqueous and $scCO_2$ phases. This would result in a larger overall mass transfer coefficient, making the diffusion of alcohol from the aqueous phase to the supercritical phase faster. However, as evident in Figure 4.13, there was no difference in extraction efficiency for n-butanol at 5.4 mL/min between the run with a frit and the run without a frit. This supports our conclusion that extraction of n-butanol under these conditions is equilibrium limited, since the rate of mass transfer is not improved by increasing the area available for mass transfer.

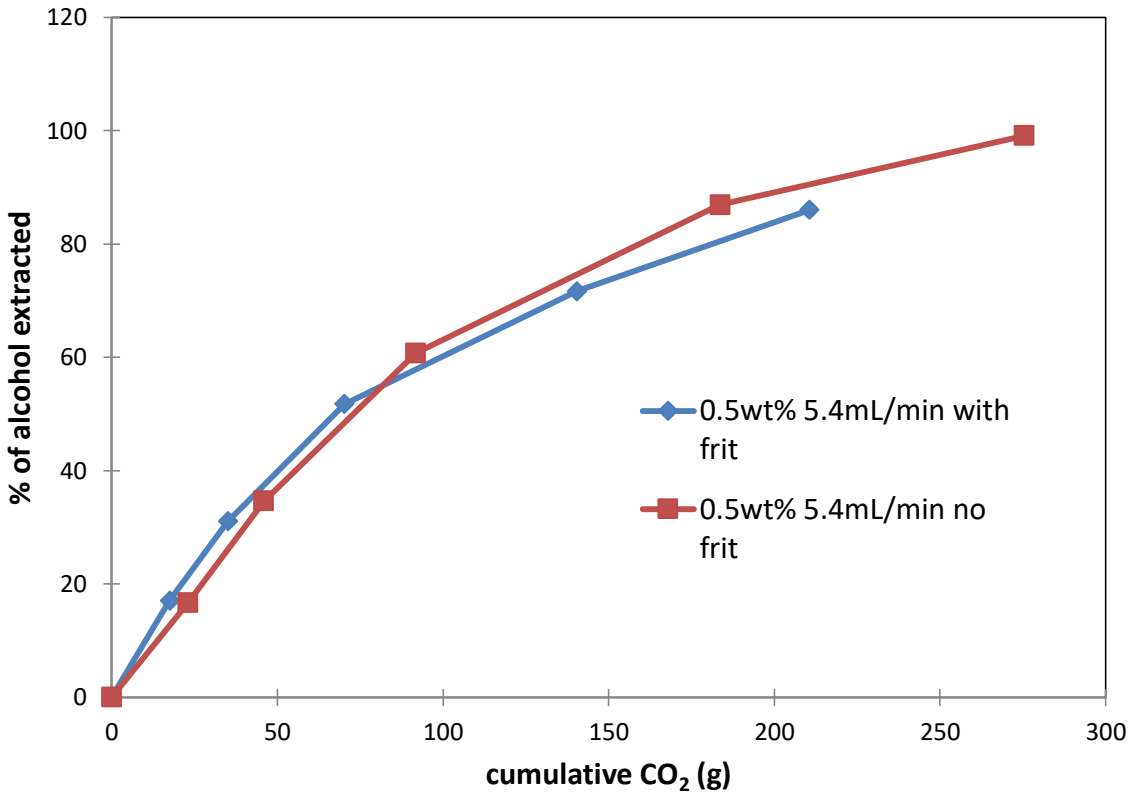

Figure 4.13: Comparison of the extraction efficiency for n-butanol at 5.4 mL/min scCO$_2$ flow rate, 400 rpm, 1500 psi, and 40^{0}C with a sparging frit (blue) and without a sparging frit (blue).

4.4.4 Comparison of the Mass Transfer and Equilibrium Limited Models

In order to further confirm whether the mass transfer or equilibrium model was more appropriate, the experimental data was compared to a plot of the predictions from the mass transfer model and the equilibrium model. The equilibrium predictions were obtained by solving for $C_{a,w}(t)$ in Equation 4.7 using the values of K_D from Table 4.2. The mass transfer predictions were similarly obtained by numerically solving for $C_l(t)$ using Mathcad software with the values of K_sa from Table 4.2. Figure 4.14 is a representative case of the system when extraction is equilibrium limited, and Figure 4.15 is a representative case of the system when it is mass transfer limited. These plots generally indicated that the equilibrium model was superior to the mass transfer model, such as in Figure 4.14. In fact, even in cases where the process is not equilibrium limited, the mass transfer model under-predicts the amount of alcohol extracted per gram of CO_2 consumed (Figure 4.15). This may indicate that the mass transfer analysis is not appropriate for estimating the overall mass transfer coefficient for this system.

These results indicate that the equilibrium model does an adequate job at predicting the extraction of alcohols using supercritical CO_2. However, the two-film mass transfer model adapted

from Tai and Wu (2005) fails to accurately predict the time profile of alcohol concentration in the aqueous phase (see Figures 4.14 and 4.15). This failure in the mass transfer model may be attributed to the simplifying assumption used to calculate $K_s a$. Recall from the background section that in order to graphically solve for $K_s a$, it was assumed that the contribution due to α_1 was much greater than α_2. In making this assumption, the mass transfer Equation takes the same exponential form as the equilibrium model. It is possible that this assumption is invalid, which would explain the discrepancy between the mass transfer and the equilibrium model.

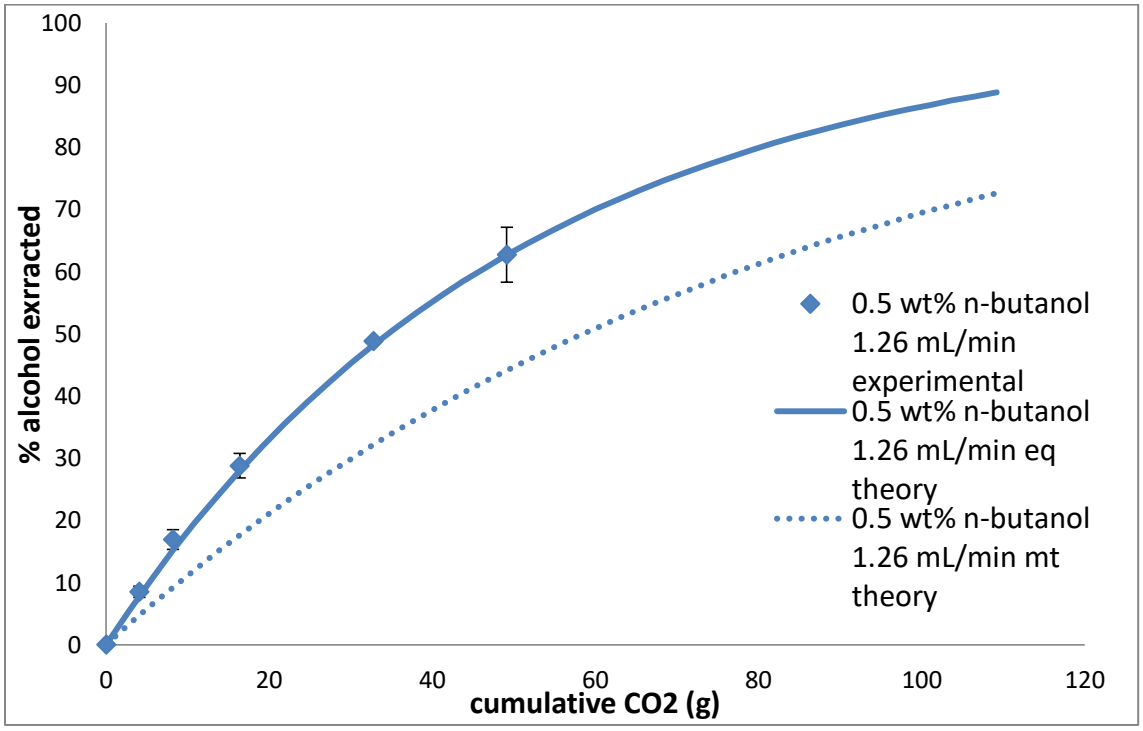

Figure 4.14: Comparison of the experimental (diamonds), equilibrium model (solid line), and mass transfer model (dotted line) for 0.5 wt% n-butanol and a CO_2 flow rate of 1.26 mL/min.

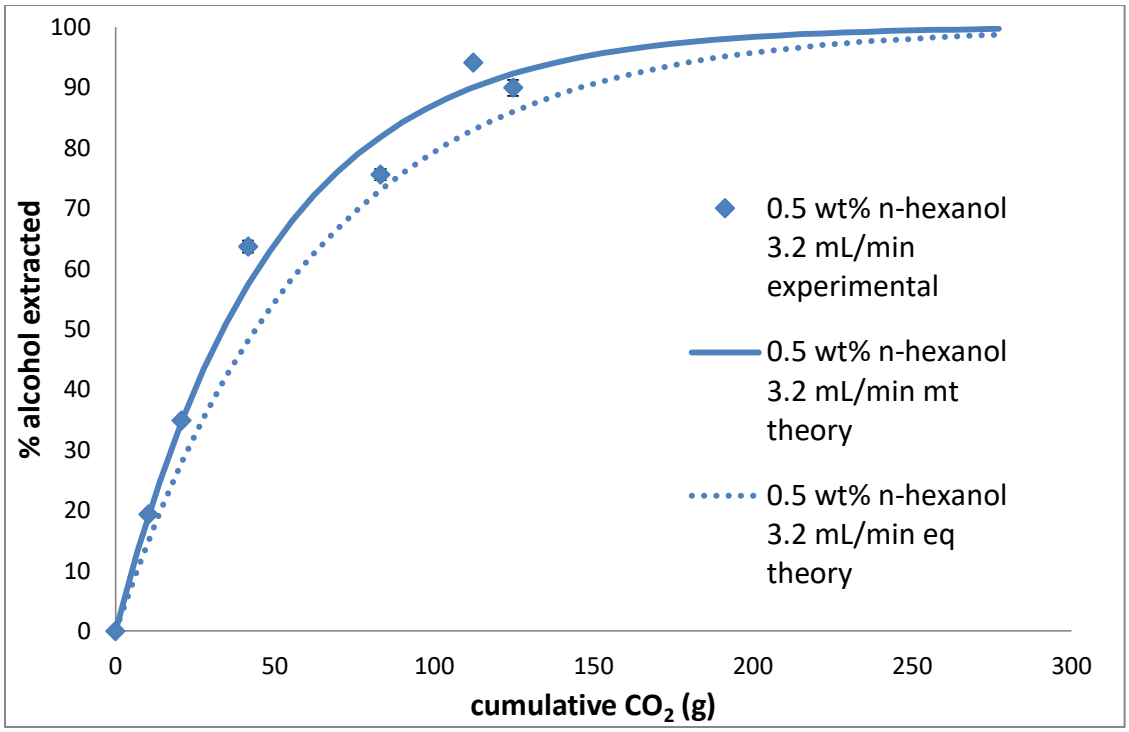

Figure 4.15: Comparison of the experimental (diamonds), equilibrium model (solid line), and mass transfer model (dotted line) for 0.5 wt% n-hexanol and a CO_2 flow rate of 5.4 mL/min.

4.5 Mixing Results

4.5.1 Just Suspended Velocities

Several experiments were conducted to determine the impeller velocity required to prevent settling of particles in the reactor. This value will be referred to as the just suspended velocity (JSV). To test this, 0.1 wt% Sigma Aldrich 20 micron ultrafine cellulose was loaded into the sparging port in the bottom of an acrylic model of the reactor. The impeller was turned on, and allowed to mix the fluid for three hours. After three hours, the turbidity of the reactor was observed to determine if the cellulose was well mixed. The picture on the left of Figure 4.16 is an example of the reactor that was well mixed, and the picture on the right of Figure 4.16 is an image of the reactor that is not well mixed. The results of these experiments are summarized in Table 4.3.

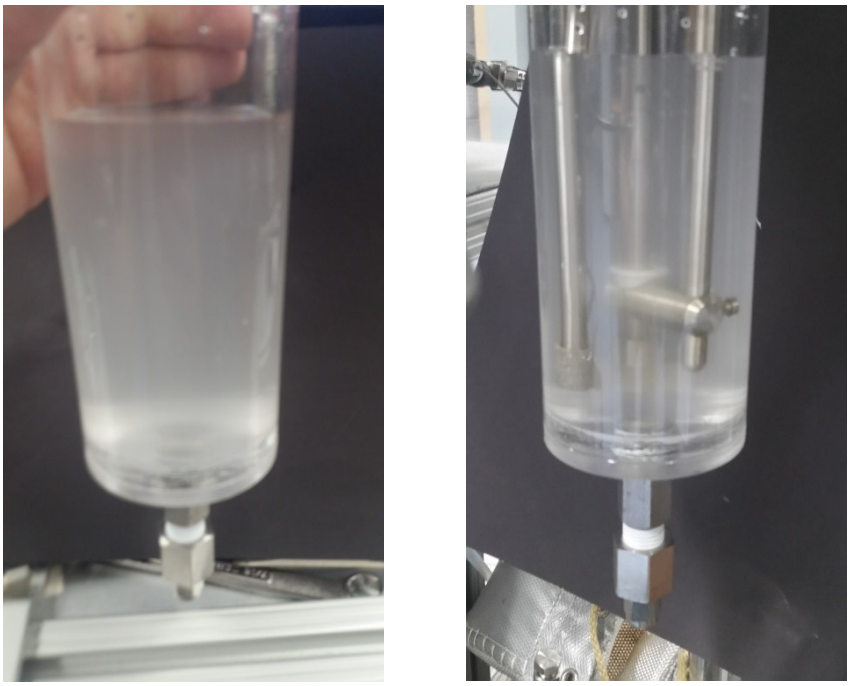

Figure 4.16: The reactor when it is well mixed (left) vs not well mixed (right). Note that the image of the well mixed reactor is much more turbid throughout the reactor, and that the not well mixed reactor (right) still has cellulose at the bottom of the reactor (the white ring at the bottom of the image on the right).

The experimental results in Table 4.3 can also be compared to the Zweitering Equation. Recall from the background section that the Zweitering Equation (Equation 4.9) considers reactor and impeller geometry, fluid properties, and particle concentrations. As a result, it is unable to predict changes in JSV based on different impeller designs. The contributions of reactor geometry and impeller design are lumped in the dimensionless term S in this model (Doran, 2013). Values of S for impeller and reactor geometries similar to the ones being examined are taken from Doran (2013).

$$n_{JS} = \frac{S{\nu_L}^{0.1}{D_P}^{0.2}[g(\rho_p - \rho_L]^{0.45}x_p^{0.13}}{D_i^{0.85}}$$

Equation 4.9

Table 4.3: Comparison of the experimentally determined just suspended velocities for each tested impeller type.

Impeller Type	Just Suspended Velocity (rpm)	S (Doran, 2013)	Prediction by Zweitering Eqn
Vertical flat blade (Rushton)	400 ± 100	4.25	90
Tilted Blade	200 ± 100	5.7	120
Marine Propeller	400 ± 100	6.6	140

Due to time constraints, these experiments were carried out in increments of 200 rpm. As a result, there is a large error range in the experimentally determined JSV. The results shown in Table 4.3 suggest that the tilted blade impeller is more effective at keeping particles suspended in this reactor system compared to the Rushton impeller and marine propeller because it has a smaller JSV. This does not follow the predictions of the Zweitering Equation, which predicts that the Rushton impeller is the most effective, followed by the tilted blade, and lastly the marine propeller. Also, the experimentally determined JSV are between two and four orders of magnitude greater than those predicted by the Zweitering Equation. This discrepancy is likely due to the non-ideal environment inside the reactor tank being examined. The Zweitering Equation assumes a baffled tank with no other entities to influence mixing. In contrast, the reactor being examined has no baffles, and there are several sampling and support arms inside of the reactor, as well as a large valve connection on the bottom of the reactor. These arms and the port could impact the mixing profile, resulting in the deviation observed from the Zweitering Equation. Also, it is likely that lifting the cellulose out of the sparging port would require much more mixing energy than if the reactor had a flat bottom.

4.5.2 Mixing Time

The amount of time taken to fully mix particles which had settled out of solution for different impeller types and velocities was also considered by measuring the time required to fully mix particles which had settled to the bottom of the reactor. These are also compared to literature correlations for mixing time, which are covered in depth in the background section. For sake of simplicity and ease of comparison, all of the experimental mixing results will be compared to the van de Vusse model. This is because the other models are specific to certain impeller types,

whereas the van de Vusse model can be applied to each of the impellers being studied. The experimental results and the van de Vusse model are plotted in Figure 4.17.

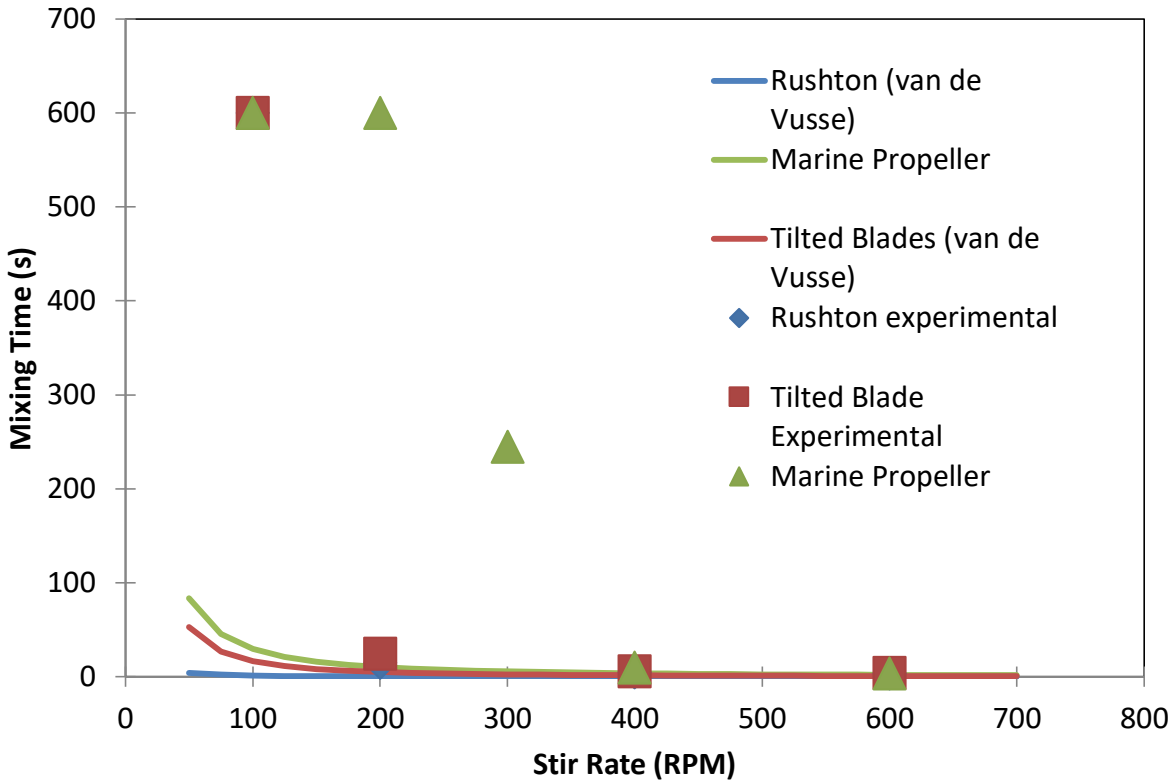

Figure 4.17: Comparison of mixing time for the Rushton, tilted blade, and marine propeller at different stirring rates.

Based on the experimental results, the mixing time becomes small (<50 seconds) at stirring rates of 200 rpm or greater for the Rushton and tilted blade impellers, and 400 rpm or greater for the marine propeller. While the van de Vusse model accurately predicts that the marine propeller takes longer to fully mix the solution, it does a poor job predicting the mixing time for all impellers at low mixing rates. This may be due to limitation in the theoretical model, as well as non-ideal conditions in the reactor including a lack of baffles and the presence of sampling and support arms. Based on the experimental and theoretical result, the Rushton or tilted blade impellers are superior at mixing solution in this reactor compared to the marine style impeller.

4.5.3 Shear

Shear was estimated using theoretical models for the velocity profile at the tip of the impeller. First, the Kolmogorov eddy length was estimated for this reactor. The Kolmogorov length is a measure of the smallest distance between eddies. Larger eddies impart smaller amounts of shear on the cells, since the cells are less likely to be caught between two eddies of different velocity. An explanation of the calculation of the Kolmogorov length is given in the background, but recall that the eddy length λ can be determined by Equation 4.10. The Kolmogorov eddy length for this system is shown in Figure 4.18.

$$\lambda = \left(\frac{\nu}{\varepsilon}\right)^{1/4}$$

Equation 4.10

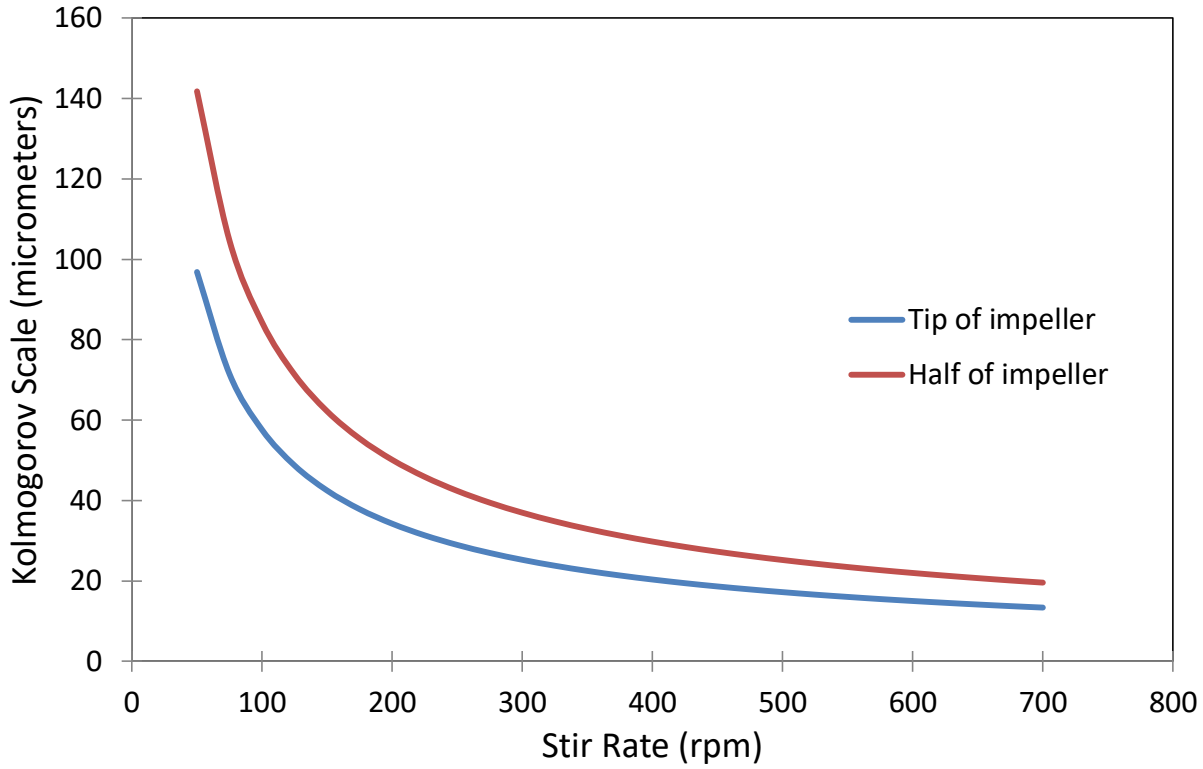

Figure 4.18: The Kolmogorov eddy length for the reactor at the tip of the impeller and at a distance half the radius of the impeller.

As expected, the Kolmogorov length decreases with increasing stir rate, indicating that the amount of shear imparted on cells will increase as the stir rate increases. Also, moving away from the impeller increases the eddy length, indicating that the cells will experience the most

shear at the tip of the impeller, and there will be less shear as the distance from the impeller increases.

4.6 Biotic Results

B. megaterium was grown at 1500 psi to determine the growth rate of this bacteria under the conditions required for supercritical fluid extraction. Growth of *B. megaterium* was analyzed over several weeks by taking samples from the 0.3L reactor, which was operated at 1500 psi and 37°C. The bacteria were fed with minimal media and the broth was mixed at 250 rpm. This experiment should give an indication of whether growth of the bacteria and production of butanol under these conditions is possible or not.

One measure of growth is plating the fermentation broth at different time points on agar plates. A description of the methodology related to this plating technique is given in the methodology section. Figure 4.19 shows colony growth from day 9 to day 23 at 1:500 dilutions. Each white dot on the plate represents a colony forming unit, which is equivalent to one viable cell inside the reactor. Therefore, more dots are indicative of better cell growth. As mentioned in the methodology, two samples were taken from the reactor. Cell count appeared to peak at day 16 and declined slightly for days 21 and 23. An interesting trend depicted in Figure 4.19 is that the first sample shows better cell growth than the second sample for a given dilution. This suggests that growth was localized around the exit stream of the reactor. We speculate that cell growth was primarily limited to a small divot just above the sampling valve, as seen in Figure 4.20. As indicated in the mixing results section, this divot likely disrupted the fluid flow pattern, thus shielding the bacteria from the detrimental effects of shear induced by the impeller and preventing them from being swept into the bulk fluid. Therefore, when the first sample was taken, large amounts of *B. megaterium* were flushed out of the reactor. Since *B. megaterium* did not grow well in the rest of the reactor, the second sample had small amounts of the bacteria.

The MIT research group (Jason Book and Adam Freeman) also grew *B. megaterium* at ambient pressure on a shaker table. Under such conditions, growth was significantly better. Ideally, cell growth should be evenly distributed throughout the reactor. In order to reach this goal, we must first validate that cell growth was poor as a result of impeller shear and not high pressure. First, the bacteria should be grown under the same conditions and in the same reactor, however, it should be run at 1 atm. If cell growth follows a similar trend, this will verify that shear forces are indeed the result of poor cell growth. Next, steps must be taken to mitigate shear related cell death.

This can be accomplished in several ways. First, slower impeller stirring rates should be tested. Next, baffles should be added to the reactor. Baffles can help reduce shear by increasing mixing effectiveness, which means that the reactor can be mixed at lower mixing speeds.

Figure 4.19 shows B. megaterium growth on agar plates. Each picture is labeled with the day and sample#

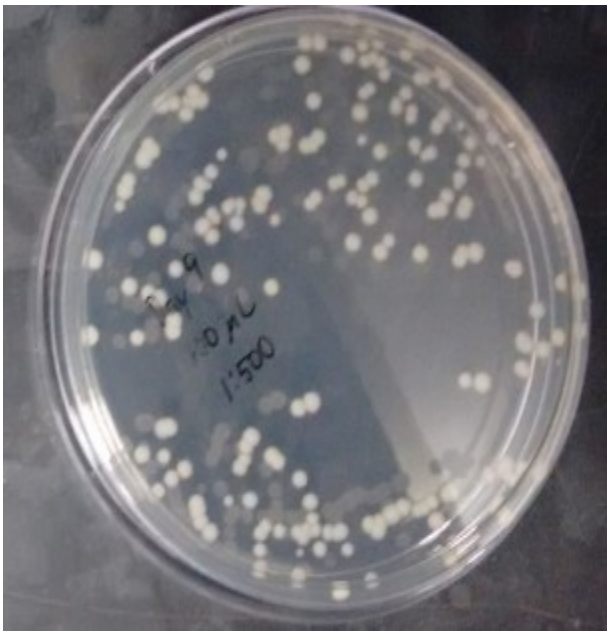

Day 9, sample 1

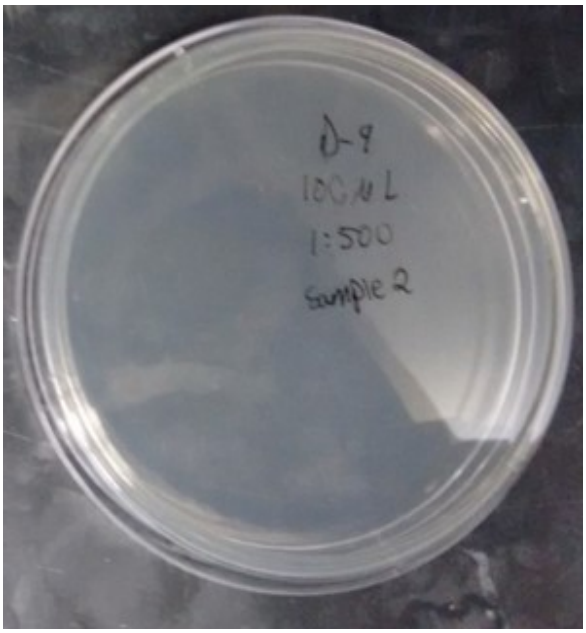

Day 9, sample 2

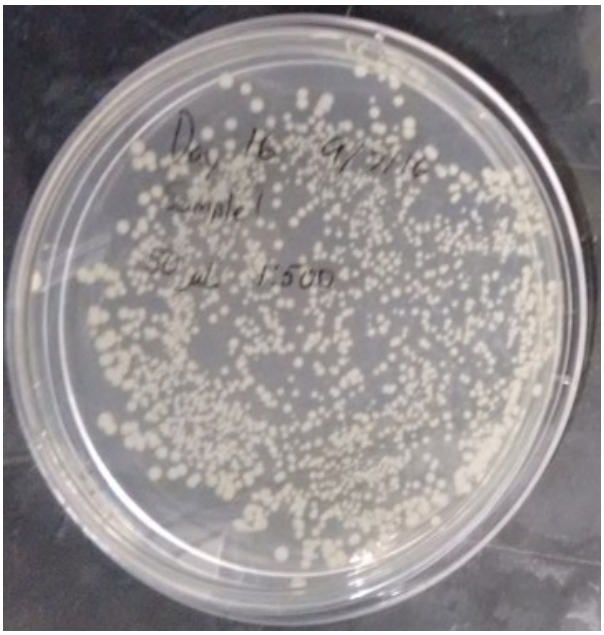

Day 16, sample 1

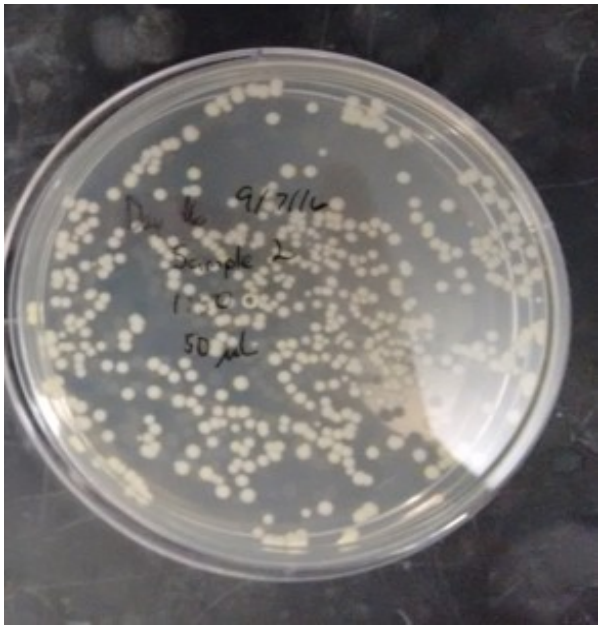

Day 16, sample 2

Day 21, sample 1

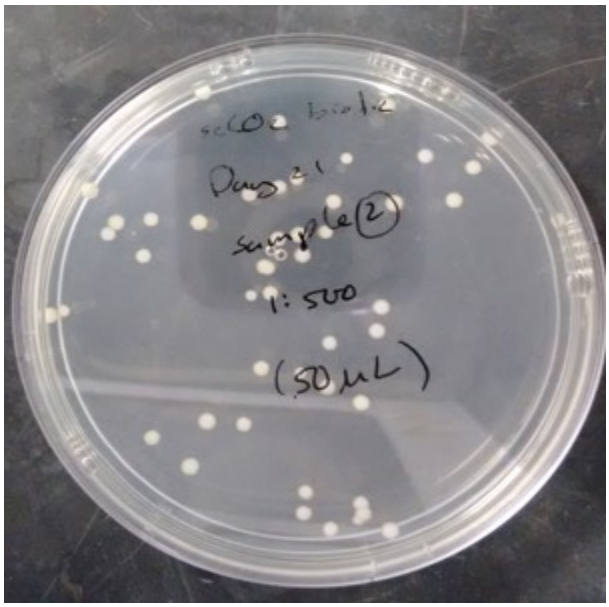

Day 21, sample 2

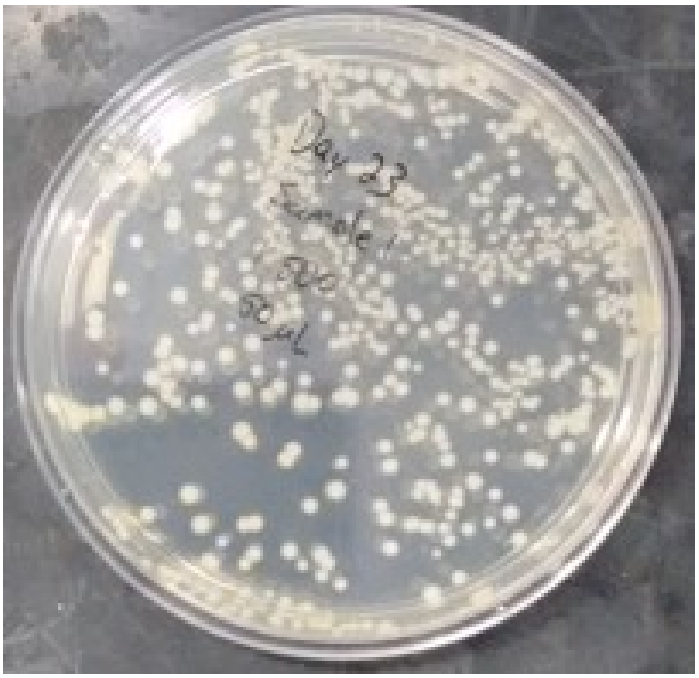

Day 23, sample 1

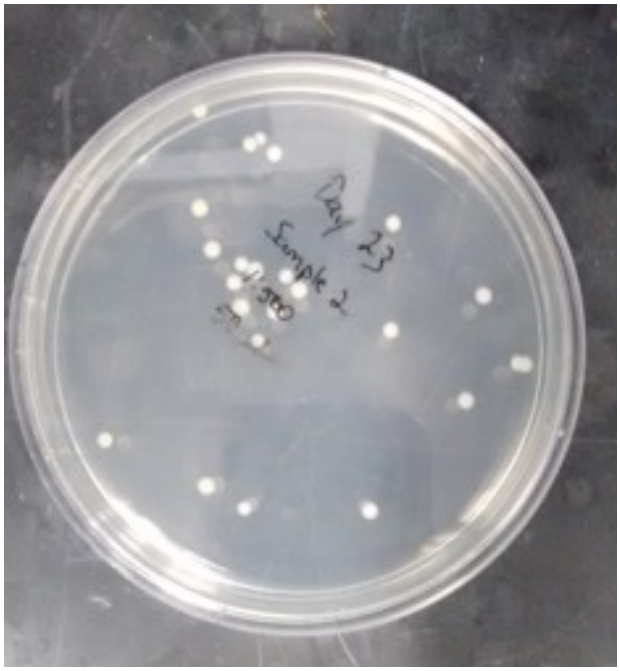

Day 23, sample 2

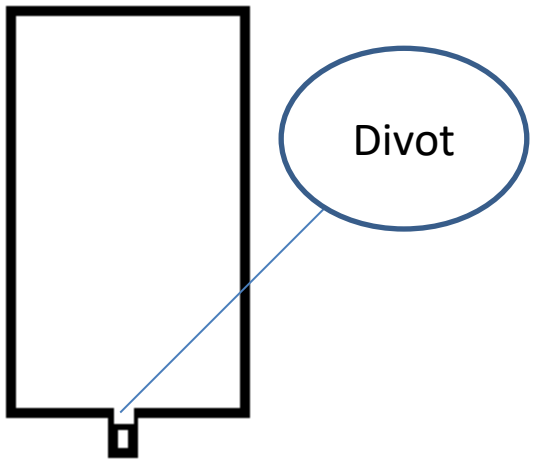

Figure 4.20: Divot in the bottom of the reactor.

5. Conclusions

In summary, this report examines the extraction of n-butnaol, isobutanol, n-pentanol, and n-hexanol from water using $scCO_2$. It also examines the mixing profiles and mixing effectiveness of the reactor based on different impeller types and mixing speeds. Finally, this report qualitatively examines the growth of *B. megaterium* SR7 in the reactor at a pressure of 1500 psi.

Several models of extraction efficiencies and rates for the extraction of n-butanol, isobutanol, n-pentanol, and n-hexanol were developed over the course of this study. The first model of alcohol efficiency examined in this paper is the amount of alcohol extracted per gram of $scCO_2$. This measure of efficiency can be used to determine the amount of CO_2 required to extract larger amounts of alcohol from solution, and can also be used to compare the relative amounts of CO_2 required to extract the various alcohols from solution. Based on this measure of efficiency, higher $scCO_2$ flow rates were less efficient, as they required more CO_2 to extract the same amount of alcohol compared to slower flow rates of CO_2. However, this comes at the cost of longer residence time and a lower time rate of extraction. Also, higher chain alcohols were more efficient based on this measure of efficiency, as n-hexanol required the least amount of CO_2 to extract 80% of the initial alcohol charge, followed by n-pentanol, and finally n-butanol.

The second extraction effectiveness model examined in this report is the overall mass transfer coefficient, K_sa. Comparing the overall mass transfer coefficients between different runs gives a measure of the relative effectiveness of diffusive and convective mass transfer of alcohol from the aqueous phase to the $scCO_2$ phase. Also, since the overall mass transfer coefficient is an intrinsic parameter of the system, it allows for predictions of the rate of extraction of alcohol for conditions other than the ones studied here. It also allows for scale up of the system to larger volumes and CO_2 rates. Unfortunately, the two-film model of mass transfer used in this report to estimate mass transfer coefficients from the extraction data was ineffective at calculating the true mass transfer coefficients. This may be the results of invalid simplifying assumptions in the derivations used to calculate K_sa. We recommend that future studies consider alternative models of mass transfer in order to accurately predict the value of K_sa.

The third model of extraction effectiveness was the calculation of distribution coefficients, K_D, for the alcohols and $scCO_2$ flow rates studied. The distribution coefficient is a measure of the ratio of alcohol concentration in the $scCO_2$ phase to concentration of alcohol in the aqueous phase. At equilibrium, K_D is equal to the partition coefficient, K_{CW}. The operating conditions are where

the system is barely at equilibrium, such that the maximum amount of alcohol is extracted into the $scCO_2$ phase, but there is no extra residence time of CO_2 where there is no net diffusion of alcohol due to the system having reached equilibrium. Based on the experimental results, lower chain alcohols are much more likely to be limited by equilibrium constraints. This suggests that smaller extraction units, or units with multiple equilibrium stages, are required by smaller chain alcohols such as butanol compared to higher chain alcohols such as pentanol and hexanol. Additionally, slower flow rates were more likely to be limited by the equilibrium constraints. Based on these trends and the calculated values of K_D, the optimal $scCO_2$ flow rate is between 5.4 and 9 mL/min for n-butanol, between 3.2 and 5.4 for isobutanol and n-pentanol, and less than 1.26 mL/min for n-hexanol. However, other considerations should be made in deciding the optimal flow rate for the system, such as the amount of carbon dioxide consumed and the overall mass transfer coefficient at those flow rates.

In the mixing experiments, three main findings were made. First, the mixing effectiveness in severely limited by the presence of a sampling port divot on the bottom of the reactor. This makes it difficult for mechanical mixers to lift particles out of the recessed space. Second, the square paddle impeller and tilted blade impeller are superior in terms of just stirred velocity and mixing times compared to the marine propeller. Finally, the mixing time is relatively small (less than one minute) for the square paddle and tilted blade impellers at mixing speeds greater than 200 rpm. Therefore, in order to minimize stress imparted on the cells by mechanical mixing, we recommend the system be mixed at lower speeds than at present, specifically around 200-300 rpm for the square paddle impeller which is used in biotic growth experiments.

Finally, the *B. megaterium* growth experiments showed promising results for the growth of *B. megaterium* SR7 under high pressure conditions. It was evident that *B. megaterium* was able to survive and grow under conditions necessary for supercritical CO_2 extraction. However, it raised concerns about the mixing effectiveness within the reactor and tolerance to shear by *B. megaterium*. *B. megaterium* grew best in the divot caused by the sparging port, where it was shielded from the bulk mixing regime. This could either indicate that planktonic growth was limited by shear caused by mechanical mixing, or that the cells settled into the divot and the mixing profile was insufficient to force the cells back into the bulk fluid.

6. Recommendations

6.1 Supercritical Fluid Extraction Scale Up

As shown in the results section, slower CO_2 flow rates are capable of extracting more grams of alcohol per gram of CO_2. Based on this metric of efficiency, slower flow rates are the most efficient, when time is not accounted for. Faster flow rates require more CO_2 to remove a given quantity of alcohol. However, they do so in less time, as seen in Figure 6.1. Therefore, for future research, we recommend identifying whether the system should be optimized to extract the solute in the least amount of time, or using the least amount of CO_2. Also, the 5.4 mL/min and 9 mL/min CO_2 flow rates followed the same trend. Therefore, they are equally as efficient, from both a time and CO_2 standpoint. As a result, we recommend that the system is not operated at 9 ml/min since it uses more CO_2 without making the process quicker. From our research, 3.2 mL/min seems to be the ideal CO_2 flow rate since it is CO_2 efficient and takes significantly less time than the 1.26 mL/min flow rate. Finally, we found that higher initial concentrations are more efficient. Therefore, we recommend that the system is operated with the highest possible concentration of solute.

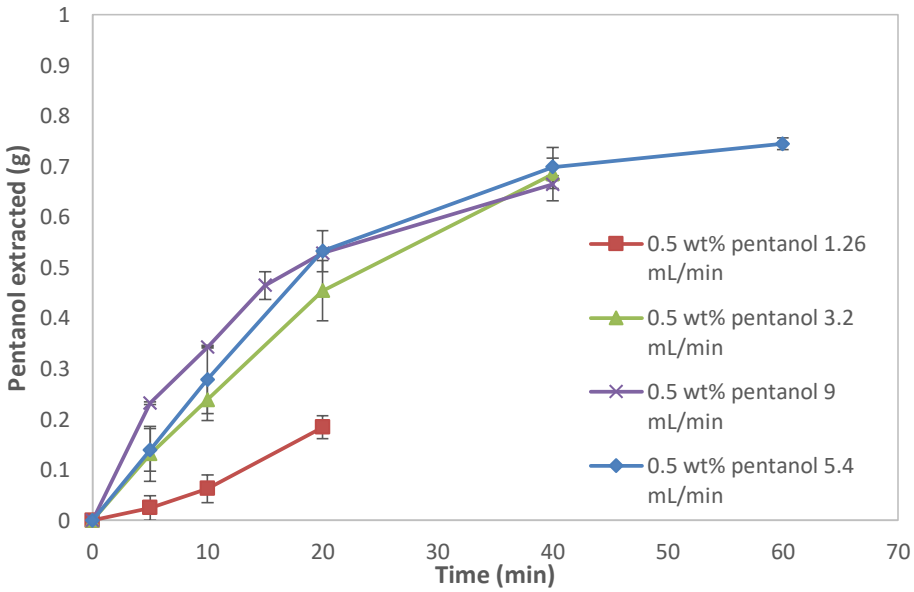

Figure 6.1: Percent of Pentanol extracted vs time with a set initial concentration of 0.5 wt% and varying flow rates.

Another important aspect which must be considered is the type of solute being extracted. We studied four alcohols (listed in order of increasing efficiency) isobutanol, n-butanol, n-

pentanol, and n-hexanol, where both isomers of butanol resulted in similar efficiencies. From our findings, we concluded that higher ordered alcohols tend to result in better extraction efficiencies. Therefore, we recommend that future researchers or companies planning on using this extraction method take careful note of the solute's chemical features, since they impact extraction efficiency. The most important characteristic that we examined was thepolarity of the compound. Less polar alcohols were extracted the most efficiently by $scCO_2$. Due to the solubility in scCO2. Based on these results, and the fact that higher alcohols generally have better fuel properties compared to ethanol, we recommend investigating the potential for biotically producing higher alcohols such as pentanol or hexanol.

Biotic Growth and Mixing

It was evident from the biotic growth and mixing experiments that either cells were being damaged by mechanical mixing or that the provided mixing was ineffective at lifting cells out of the bottom of the tank. Based on these results, we recommend that steps be taken to reduce sheer related cell death in the bio reactor. To start, we examined the following topics: impeller type, mixing rate and reactor geometry. Through our research we recommend that the titled blade impeller is used because it's capable of producing a well-mixed solution at 200 rpm in under 50 seconds. Impellers that are effective at slow rpms are less likely to kill bacterial growth in the reactor and require less energy to operate. We also recommend that a reactor without divots around the sampling port are used in an effort to obtain more accurate growth measurements and to prevent bacterial growth in unwanted regions in the reactor. Next, we recommend that a reactor with rounded edges, as seen in Figure 6.2, is utilized because it provides for better mixing profiles and helps to eliminate stagnant zones in the reactor. Furthermore, we recommend the addition of baffles to improve turbulent mixing within the reactor. We also recommend that future scientists analyze the feasibility of using bacteria growing surfaces and a nontraditional impeller if cell growth cannot be maintained through varying impeller specs and reactor geometry. Centrifugal impellers, as seen in Figure 6.3, have shown promising results with mitigating shear induced cell death in sensitive cultures.

Additionally, we recommend future research into the design of a bioreactor system where the reactor and extraction units are separate. In this design, fermentation broth would be removed from the bioreactor, filtered, and sent to the supercritical fluid extractor. After the alcohol is extracted, the growth media is recycled back to the bioreactor along with fresh media. This system

has the advantage of allowing the engineers to design the reactor and extractor separately. As discussed in the background section, bioreactors are generally designed with a much smaller aspect ratio (height/diameter) compared to SFE units. Additionally, it would allow for the addition of fresh media to the fermenter, which could prolong the production time of the bioreactor. An example of this design is shown in Figure 6.4.

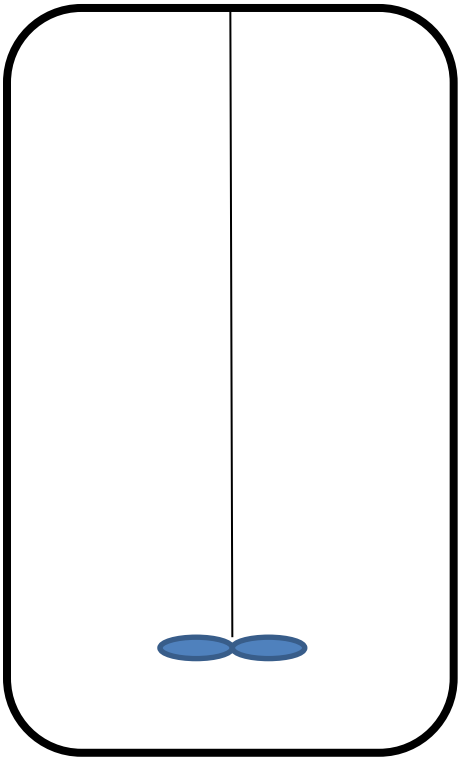

Figure 6.2: *Rounded edge reactor tank*

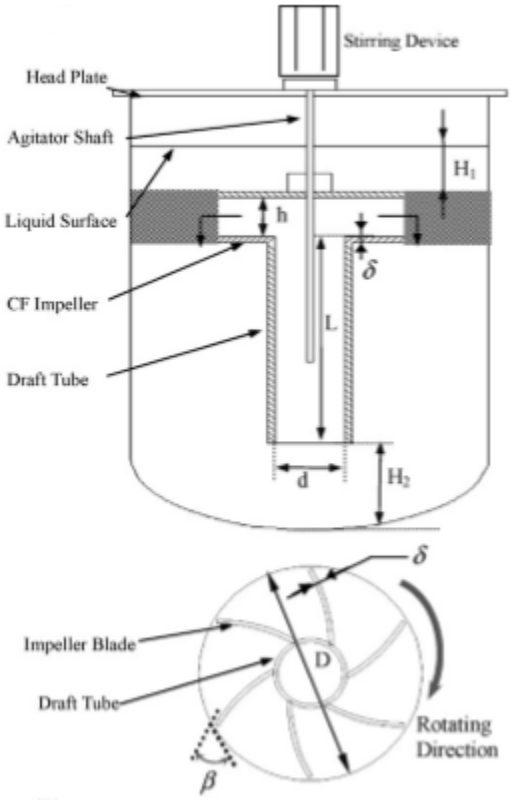

Figure 6.3: Centrifugal impeller design (Xia et al., 2008)

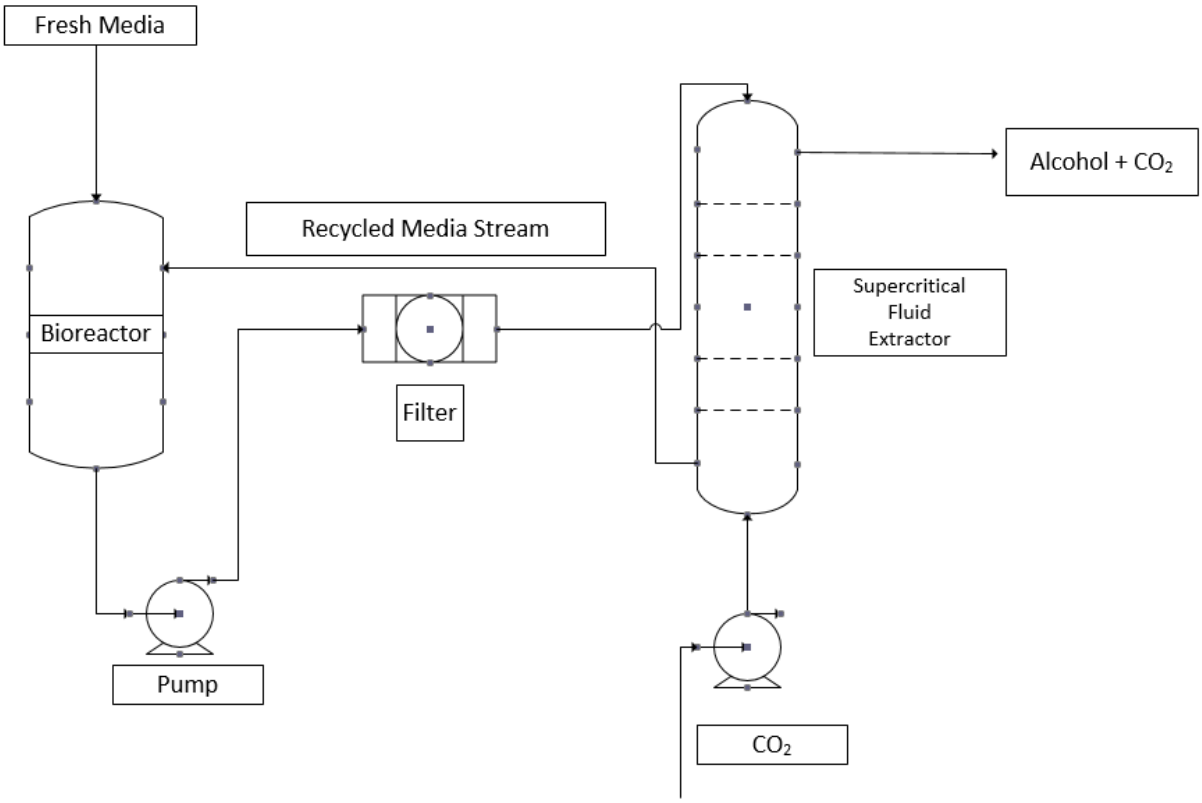

Figure 6.4: A simplified pfd of the proposed product removal with recycle system.

Acknowledgements

We would like to thank our advisors, Professor Michael Timko and Geoffry Tompsett for their assistance setting up and running the experiments in this report, and for their advice in writing this report. We would also like to thank our collaborators at MIT, especially Dr. Jason Boock and Dr. Adam Freedman for their expertise in running the biotic growth experiments. Furthermore, we would like to thank Tom Partington for making the acrylic model of the reactor used for the mixing experiments. Finally, we would like to acknowledge funding from the Department of Energy Grant DE-SC0012555 6930635.

Nomenclature

$C_{a,c}$	Concentration of alcohol in $scCO_2$
$C_{a,w}$	Concentration of alcohol in the aqueous phase
C_c	Concentration of alcohol in the CO_2 phase
C_l	Concentration of alcohol in the aqueous phase
D_i	Diameter of the impeller
D_t	Diameter of the tank
Fr	Froude number
f_t	mixing time factor
g	acceleration due to gravity (9.8 m/s^2)
G	$scCO_2$ flow rate
h	height of liquid in tank
K_{cw}	Partition coefficient of alcohol in the CO_2 phase/aqueous phase
$K_l a$	overall mass transfer coefficient on the aqueous side
$K_s a$	overall mass transfer coefficient on the CO_2 side
n	Stirrer Speed
p	Impeller blade pitch
Re	Reynolds number
S	Dimensionless parameter dependent on impeller and reactor geometry
V_s	Volume of $scCO_2$
V_w	Volume of aqueous phase
x	weight fraction
y	exponential factor
α	Factor in the two film mass transfer model
β	Exponential factor in the two film mass transfer model
ρ	Density
μ	Dynamic viscosity
ν	Kinematic Viscosity

Appendix 1: SFE Procedure

Preparation and Start Up

1. Set chiller temperature to -1°C.
2. Weigh and record the empty weight of each of the ten 500 mL Pyrex collection jars.
3. Fill each of the Pyrex collection jars with 100 grams of 99.9% pure methanol.
4. Prepare the initial alcohol charge using the appropriate amount of DI water and alcohol to make 150 mL solution at the desired concentration.
5. Place the collection vessels in an ice bath.
6. Load the initial alcohol charge into the reactor. Check the O-ring seal on the reactor for damage, and secure the reactor using stainless steel clamps.
7. Secure the CO_2 sparging line to the bottom of the reactor.
8. Secure the heating jacket to the reactor, and set the reactor temperature to 40°C. Set the stirring rate to 400 rpm.
9. Secure the first and second pairs of Pyrex collection vessels to the gas exhaust lines.
10. Open the regulator and valves on the CO_2 feed tank. Check pressure gages to ensure the tank is at the proper pressure (approximately 800-900 psig).
11. Open CO_2 release valve for 2 seconds to purge any gas from the line.
12. Set the back pressure regulator to the desired operating pressure (1500 psig).

Open the CO_2 valves to the reactor. Allow the pressure inside the reactor to equilibrate with the tank pressure.

13. Turn on the CO_2 pump. Observe flow of CO_2 through the view cell.
14. Once the reactor pressure reaches 1500 psig and flow is measured by the wet test meter, start the timer.

Operating Procedure

1. At the desired time intervals (5, 10, or 20 minutes), switch the collection vessels.
2. Throughout the experiment, observe pressure gages for pressure spikes and watch for freezing in the plastic lines.
3. If line freezing or pressure spikes are observed, immediately turn of the CO_2 pump.

Shut down

1. At the end of the desired extraction time, turn of the CO_2 pump and close the CO_2 tank regulator and valves leading up to the reactor.
2. Remove the sample collection vessels.
3. Weigh each collection vessel, and record their mass after completion of the run.
4. Mix the liquid in each sample vessel from the same time point.
5. For each time point, take two samples using a Pasteur pipette. Place one sample in a GC vial and the second in a 5 mL vial.
6. Depressurize the reactor using the CO_2 release valve at the top of the reactor. Unclamp the reactor from the unit.
7. Remove and weigh the remaining liquid residue from the reactor. Take two samples, one in a GC vial and one in a 5 mL vial.
8. Refrigerate the liquid samples. Dispose of remaining liquid according to WPI EHS standards.
9. Clean the reactor using DI water spray.
10. Triple rinse all collection vessels with tap water then triple rinse with DI water.
11. Analyze samples for alcohol concentration using the Shimadzu GC-FID system.

Appendix 2: Graphs

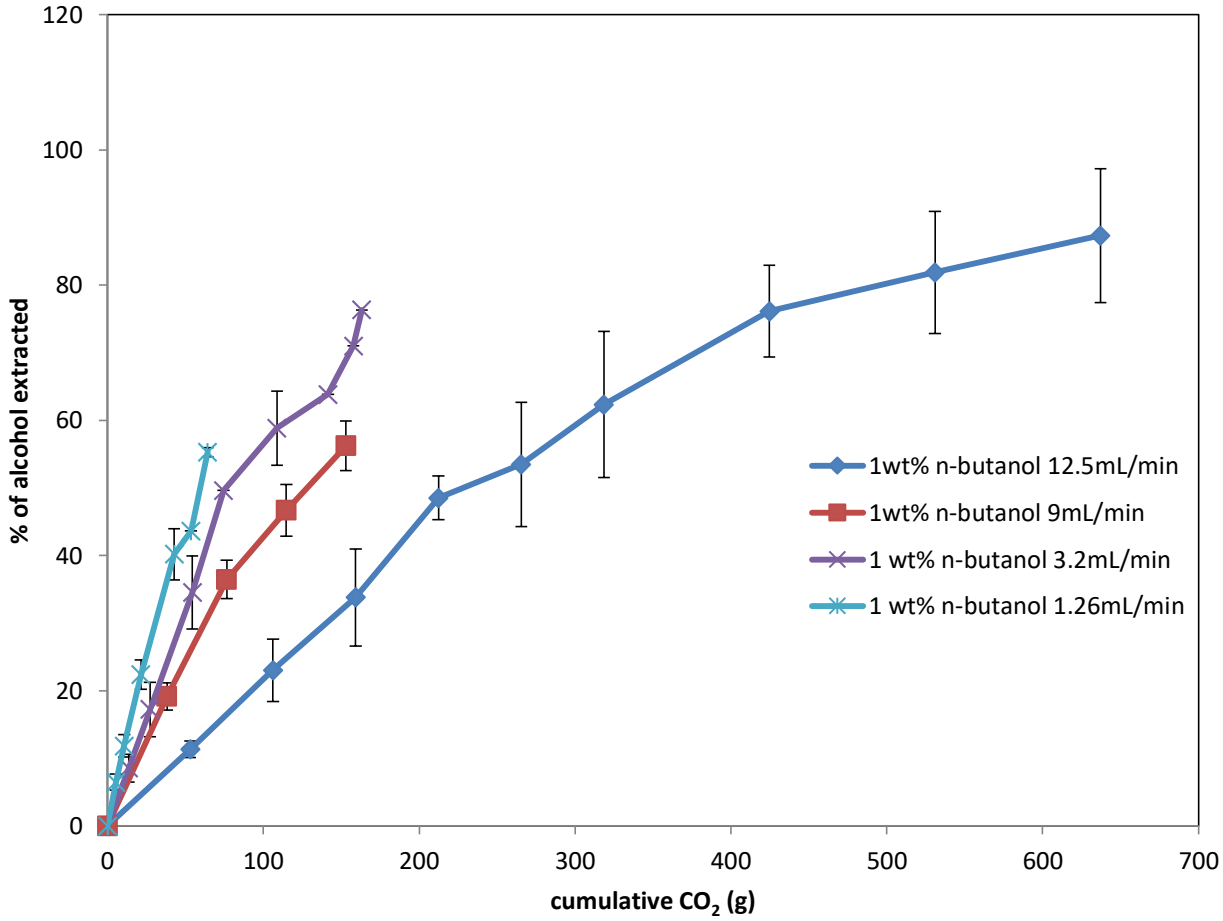

1 wt% n-butanol extraction efficiency at 400 rpm, 1.26 to 12.5 mL/min, 1500 psi, and 40°C.

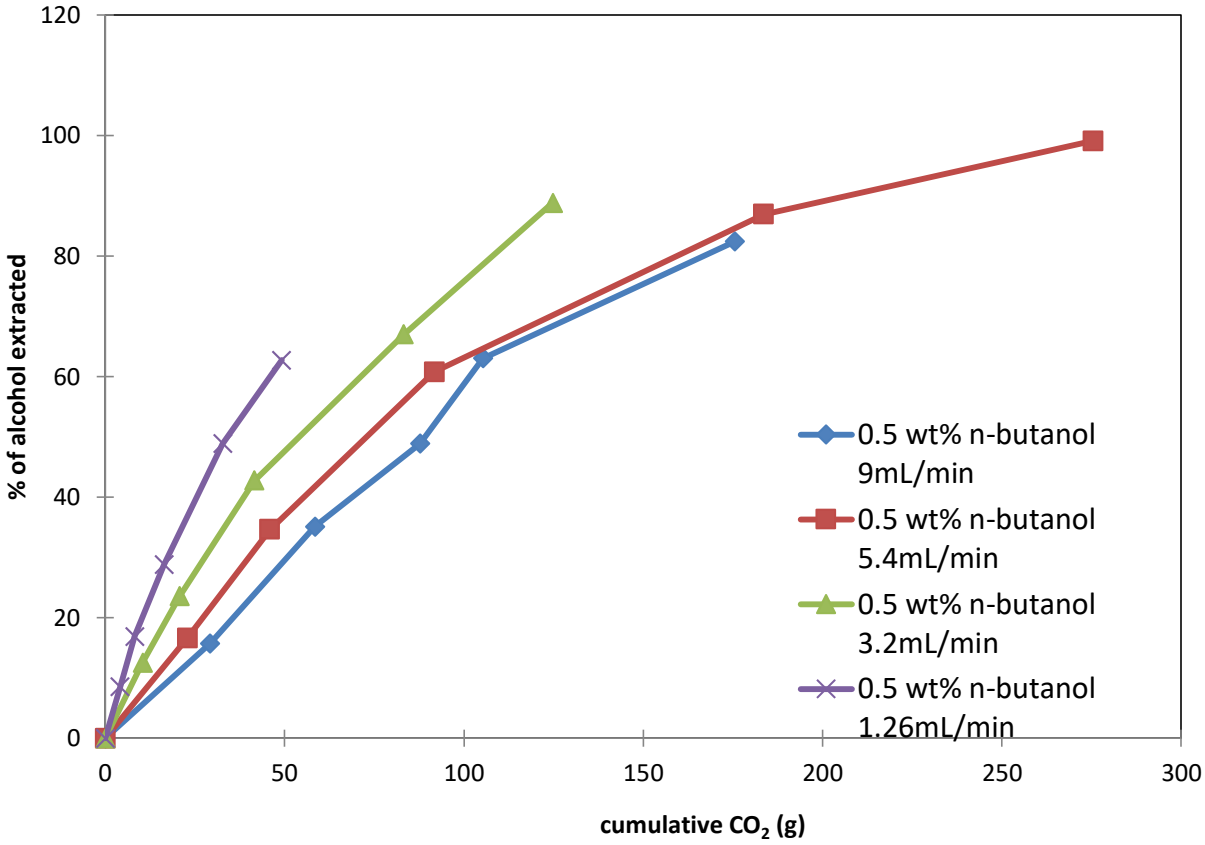

1 wt% n-butanol extraction efficiency at 400 rpm, 1.26 to 12.5 mL/min, 1500 psi, and 40°C.

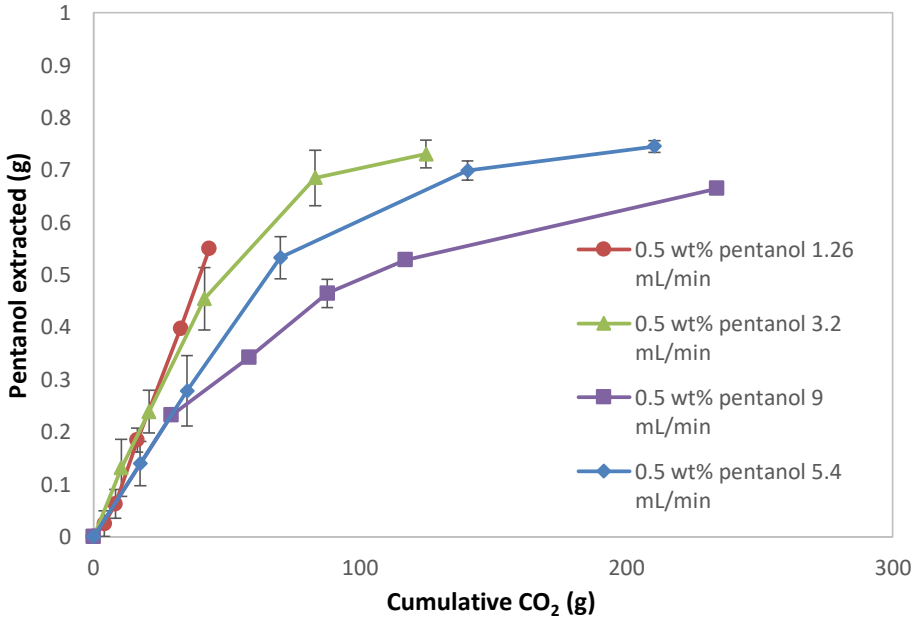

0.5 wt% n-pentanol extraction efficiency at 400 rpm, 1.26 to 12.5 mL/min, 1500 psi, and 40°C.

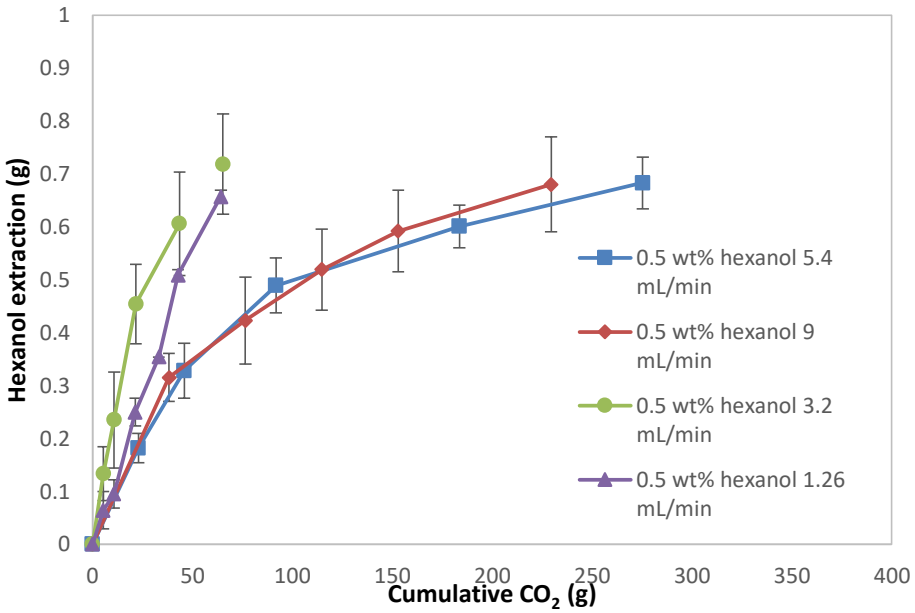

0.5 wt% n-hexanol extraction efficiency at 400 rpm, 1.26 to 12.5 mL/min, 1500 psi, and 40°C.

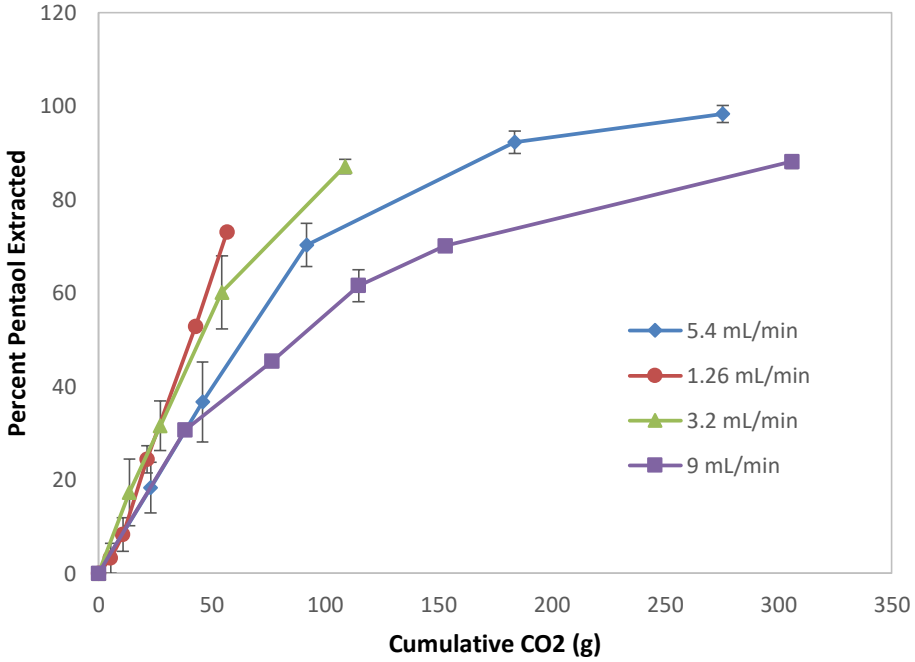

0.5 wt% n-pentanol extraction efficiency at 400 rpm, 1.26 to 12.5 mL/min, 1500 psi, and 40°C.

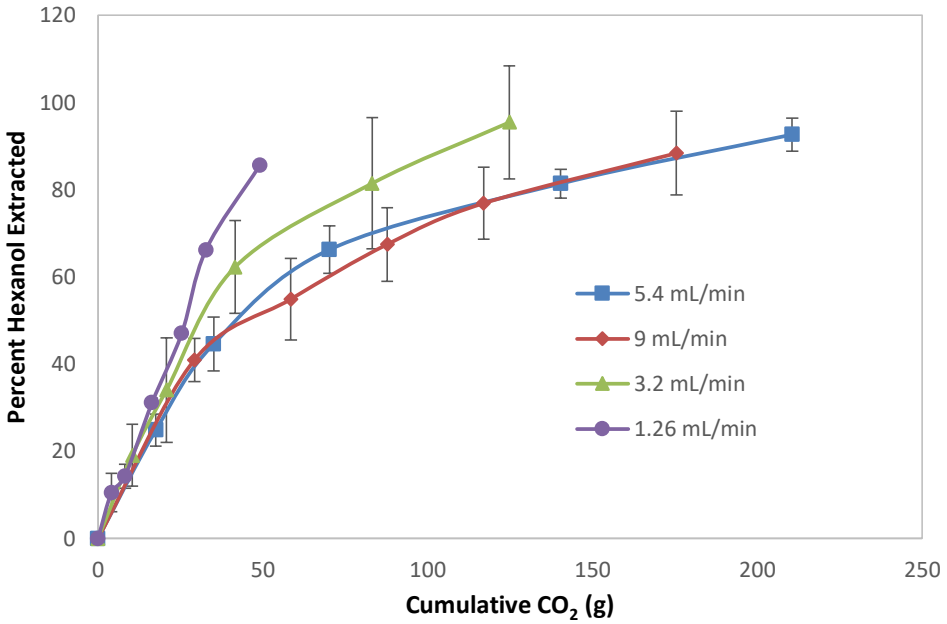

0.5 wt% n-hexanol extraction efficiency at 400 rpm, 1.26 to 12.5 mL/min, 1500 psi, and 40°C.

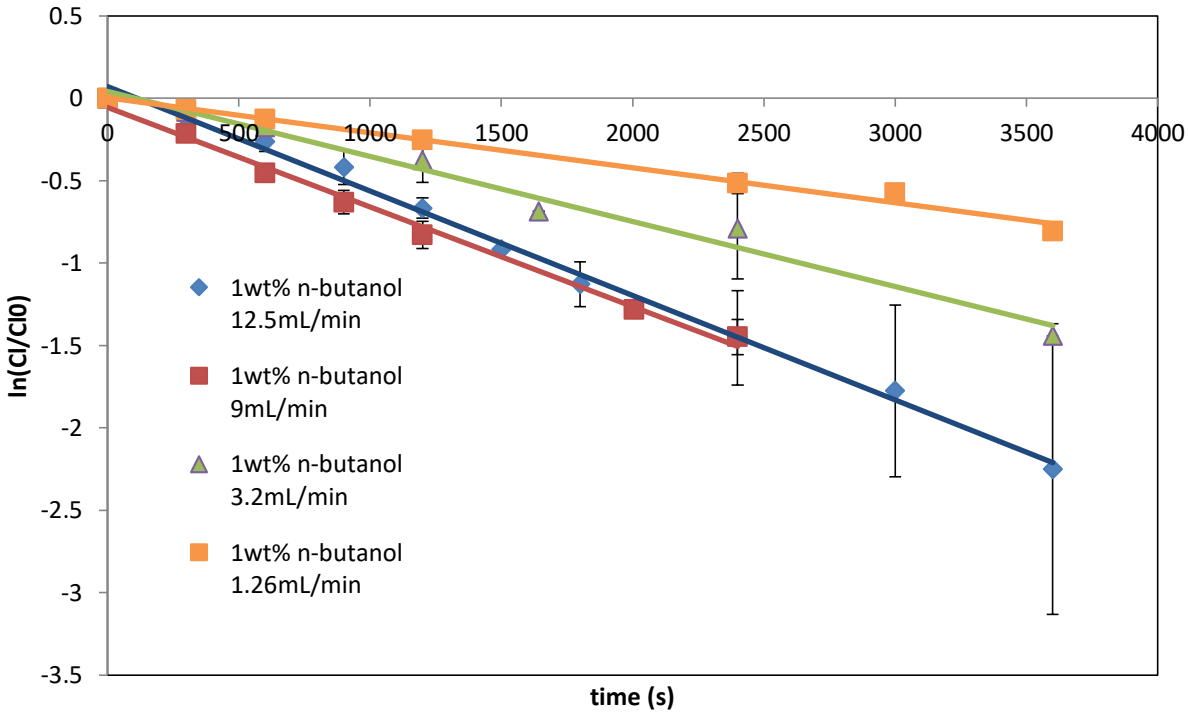

Graphs for finding the value of α_1. 1 wt% n-butanol at 400 rpm, 1.26 to 12.5 mL/min, 1500 psi, and 40°C.

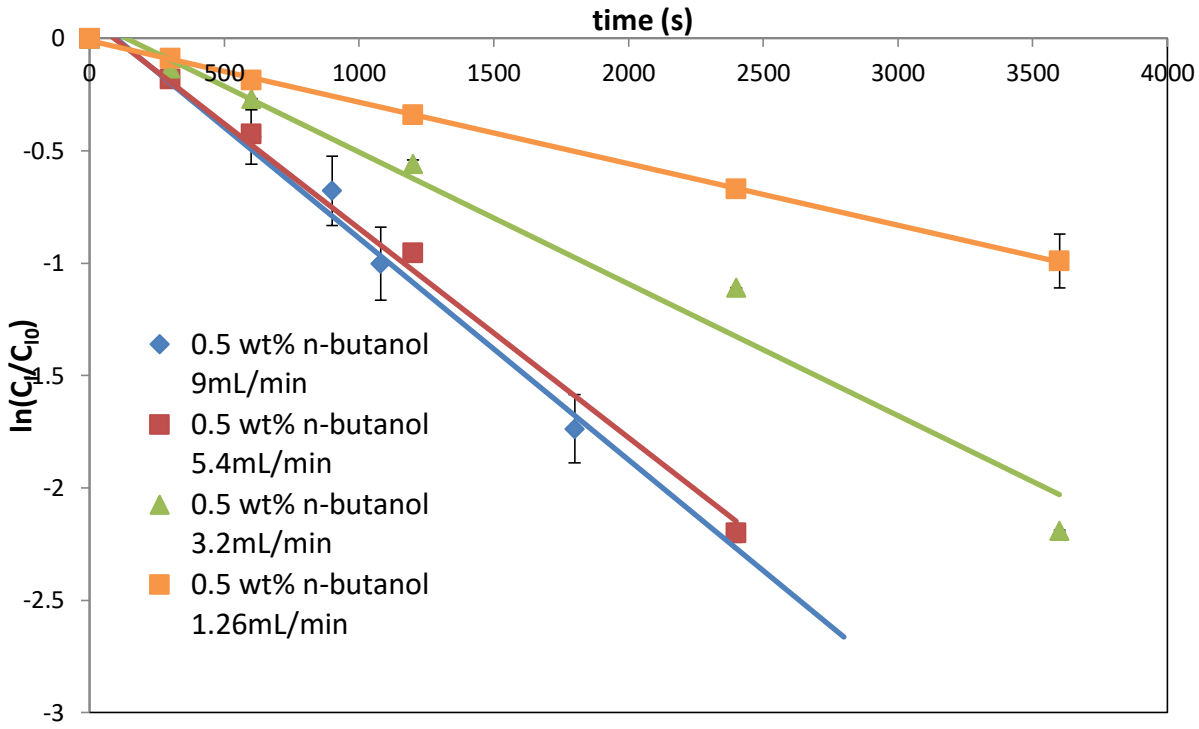

Graphs for finding the value of α_1. 0.5 wt% n-butanol at 400 rpm, 1.26 to 12.5 mL/min, 1500 psi, and 40°C.

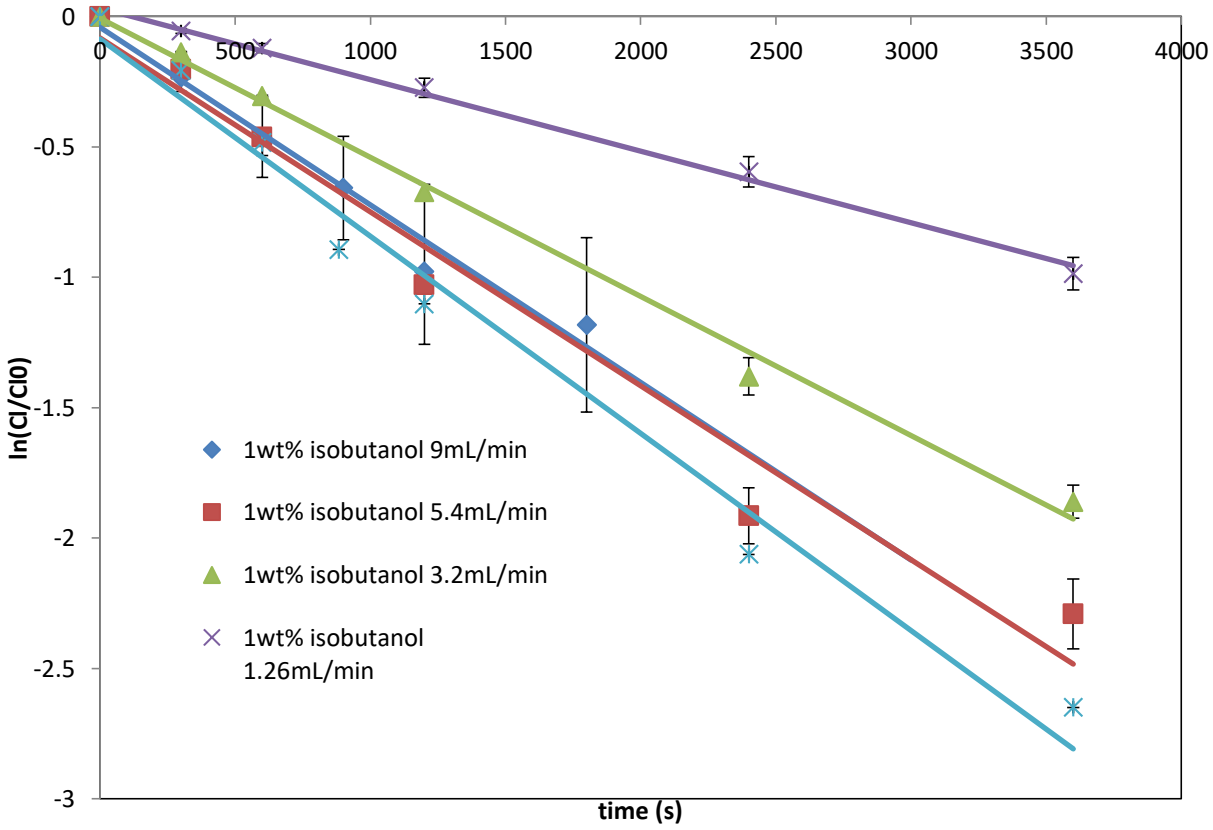

Graphs for finding the value of α_1. 1 wt% isobutanol at 400 rpm, 1.26 to 12.5 mL/min, 1500 psi, and 40°C.

Works Cited

1-butanol Safety Data Sheet. (2017). Retrieved from http://www.sigmaaldrich.com/MSDS/MSDS/DisplayMSDSPage.do?country=US&language=en&productNumber=437603&brand=SIAL&PageToGoToURL=http%3A%2F%2Fwww.sigmaaldrich.com%2Fcatalog%2Fproduct%2Fsial%2F437603%3Flang%3Den

1-hexanol Safety Data Sheet. (2017). Retrieved from http://www.sigmaaldrich.com/MSDS/MSDS/DisplayMSDSPage.do?country=US&language=en&productNumber=73117&brand=SIAL&PageToGoToURL=http%3A%2F%2Fwww.sigmaaldrich.com%2Fcatalog%2Fsearch%3Fterm%3D1-hexanol%26interface%3DAll%26N%3D0%26mode%3Dmatch%2520partialmax%26lang%3Den%26region%3DUS%26focus%3Dproduct

1-pentanol Safety Data Sheet. (2017). Retrieved from http://www.sigmaaldrich.com/MSDS/MSDS/DisplayMSDSPage.do?country=US&language=en&productNumber=398268&brand=SIAL&PageToGoToURL=http%3A%2F%2Fwww.sigmaaldrich.com%2Fcatalog%2Fsearch%3Fterm%3D1-pentanol%26interface%3DAll%26N%3D0%26mode%3Dmatch%2520partialmax%26lang%3Den%26region%3DUS%26focus%3Dproduct

Bernad, L., Keller, A., Barth, D., & Perrut, M. (1993). SEPARATION OF ETHANOL FROM AQUEOUS-SOLUTIONS BY SUPERCRITICAL CARBON-DIOXIDE - COMPARISON BETWEEN SIMULATIONS AND EXPERIMENTS. *Journal of Supercritical Fluids, 6*(1), 9-14. doi:10.1016/0896-8446(93)90004-h

Biosafety in Microbiological and Biomedical Laboratories. Retrieved from http://www.cdc.gov/biosafety/publications/bmbl5/index.htm.

Brennen, C. E. (1995). *Cavitation and bubble dynamics* (Vol. 44). New York: Oxford University Press.

Cardona, C., & Sanchez, O. (2007). Fuel Ethanol Production: Process Design Trends and Integration Opportunities. *Bioresource Technology, 98*, 2415-2457.

Chun, B. S., Lee, H. G., Cheon, J. K., & Wilkinson, G. (1996). Mass transfer in a countercurrent spray column at supercritical conditions. *Korean Journal of Chemical Engineering, 13*(3), 234-241. doi:10.1007/bf02705944

Conlon, C., Knutson, D., Overdevest, M., & Rivard, A. (2016). Extraction of Bio-Butanol using Supercritical Carbon Dioxide. In: Major Qualifying Project.

Dooley, K. M., Cain, A. W., & Carl Knopf, F. (1997). Supercritical fluid extraction of acetic acid, alcohols and other amphiphiles from acid-water mixtures. *The Journal of Supercritical Fluids, 11*(1), 81-89. doi:10.1016/S0896-8446(97)00026-0

Doran, P. M. (2013). *Bioprocess engineering principles, second edition* (Vol. 2nd). Waltham, Mass: Academic Press.

Errico, M., Tola, G., Rong, B.-G., Demurtas, D., & Turunen, I. (2009). Energy saving and capital cost evaluation in distillation column sequences with a divided wall column. *Chemical Engineering Research and Design, 87*(12), 1649-1657.

Fangrui, M., & Milford, H. (1999). Biodiesel Production: a review. *Bioresource Technology, 70*(1), 1-15.

Fox, E. A., & Gex, V. E. (1956). Single-phase blending of liquids. *AIChE Journal, 2*(4), 539-544. doi:10.1002/aic.690020422

Fuel Ethanol Overview. (2016).

Fuel Properties Comparison. (2014). Department of Energy Alternative Fuels Data Center Retrieved from http://www.afdc.energy.gov/fuels/fuel_comparison_chart.pdf.
Green, E. (2011). Fermentative production of butanol-the industrial perspective. *Current Opinion in Biotechnology, 22*, 1-7.
Guo, M. S., Weiping Buhain, Jeremy. (2015). Bioenergy and biofuels: History, status, and perspective *Renewable and Sustainable Energy Reviews, 42*, 712-725.
Haas, B. P. (2011). *Ethanol biofuel production*. New York: Nova Science Publishers.
Haugen, D. M., & Musser, S. (2012). *Renewable energy*. Detroit: Greenhaven Press.
Hunter, L. (2010). CO2 Flow Measurement Key in CCS Schemes.
Khosravi-Darani, K., & Vasheghani-Farahani, E. (2005). Application of supercritical fluid extraction in biotechnology. *Critical Reviews in Biotechnology, 25*, 231-242.
Kresta, S., & Wood, P. (1993). The Flow Field Produced by a Pitched Blade Turbine: Characterization of the Turbulence and Estimation of the Dissipation Rate. *Chemical Engineering Science, 48*, 1761-1774.
Lahiere, R. J., & Fair, J. R. (1987). MASS-TRANSFER EFFICIENCIES OF COLUMN CONTACTORS IN SUPERCRITICAL EXTRACTION SERVICE. *Industrial & Engineering Chemistry Research, 26*(10), 2086-2092. doi:10.1021/ie00070a026
Laitinen, A., & Kaunisto, J. (1998). Hydrodynamics and mass transfer in a rotating disk supercritical extraction column. *Industrial & Engineering Chemistry Research, 37*(6), 2529-2534. doi:10.1021/ie970658u
Laitinen, A., & Kaunisto, J. (1999). Oldshue-Rushton Column in Supercritical Fluid Extraction. *Separation Science and Technology, 34*(9), 1859-1872. doi:10.1081/SS-100100743
Laitinen, A., & Kaunisto, J. (1999). Supercritical fluid extraction of 1-butanol from aqueous solutions. *The Journal of Supercritical Fluids, 15*(3), 245-252. doi:10.1016/S0896-8446(99)00011-X
Laitinen, A., & Kaunisto, J. (1999). Supercritical fluid extraction of 1-butanol from aqueous solutions. *VIT Chemical Technology, 15*, 245-252.
Laitinen, A., & Kaunisto, J. (1999). Supercritical fluid extraction of 1-butanol from aqueous solutions. *Journal of Supercritical Fluids, 15*(3), 245-252. doi:10.1016/s0896-8446(99)00011-x
Landau, J., & Prochazka, J. (1961). Homogenization of Miscible Liquids by Rotary Impellers. *Collect. Czech Chem Commun, 26*, 2961-2974.
Li, S.-Y., Chiang, C.-J., Tseng, I.-T., He, C.-R., & Chao, Y.-P. (2016). Bioreactors and in situ product recovery techniques for acetone-butanol-ethanol fermentation. *FEMS Microbiology Letters, 363*(13).
Lim, J. S., Lee, Y.-W., Lee, Y. Y., Kim, J.-D., & Chun, H.-S. (1995). Mass-transfer and hydraulic characteristics in spray and packed extraction columns for supercritical carbon dioxide-ethanol-water system. *The Journal of Supercritical Fluids, 8*(2), 127-137. doi:10.1016/0896-8446(95)90025-X
Marrone, P. (1998). *Hydrolysis and Oxidation of Model Organic Compounds in sub- and supercritical Water:Reactor Design, Kinetics Measurements, and Modeling.* (PhD), MIT, Cambridge.
Masum, B., Masjuki, H., Kalam, M., Palash, S., & Habibullah, M. (2015). Effect of alcohol-gasoline blends optimization on fuel properties, performance and emissions of a SI engine. *Journal of Cleaner Production, 86*, 230-237.

Materials Measurement Laboratories. (2016). Retrieved from http://webbook.nist.gov/cgi/cbook.cgi?ID=C64175&Mask=4#Thermo-Phase

Mathews, J. (2008). Carbon-negative biofuels. *Energy Policy, 36*(3), 940-945.

Medina, I., & Martinez, J. L. (1997). Extraction of ethanol from aqueous solutions using subcritical and supercritical carbon dioxide. *Anales De Quimica, 93*(4), 267-270.

Methanol Safety Data Sheet. (2017). Retrieved from http://www.sigmaaldrich.com/MSDS/MSDS/DisplayMSDSPage.do?country=US&language=en&productNumber=322415&brand=SIAL&PageToGoToURL=http%3A%2F%2Fwww.sigmaaldrich.com%2Fcatalog%2Fproduct%2Fsial%2F322415%3Flang%3Den

Mohamed, R., & Mansoori, G. (2002). The use of supercritical fluid technology in food processing. *Food Technology*.

Moo-Young, M., Tichar, K., & Dullien, F. A. L. (1972). The blending efficiencies of some impellers in batch mixing. *AIChE Journal, 18*(1), 178-182. doi:10.1002/aic.690180133

Moreno, T., Tallon, S., Ryan, J., & Catchpole, O. (2012). Extraction of 1-butanol from aqueous solutions using supercritical CO_2. *Chemeca*.

Moreno, T., Tallon, S. J., & Catchpole, O. J. (2014). Supercritical CO2 Extraction of 1-Butanol and Acetone from Aqueous Solutions Using a Hollow-Fiber Membrane Contactor. *Chemical Engineering & Technology, 37*(11), 1861-1872. doi:10.1002/ceat.201300700

Moreno, T., Tallon, S. J., & Catchpole, O. J. (2014). Supercritical CO2 Extraction of 1-Butanol and Acetone from Aqueous Solutions Using a Hollow-Fiber Membrane Contactor *Chemical Engineering Technology, 37*(11), 1861-1872. doi:10.1002/ceat.201300700

Nadmin, F., Zack, P., Hoag, G., & Liu, S. (2001). United States experience with gasoline addatives. *Energy Policy, 29*(1), 1-5.

Norwood, K. W., & Metzner, A. B. (1960). Flow patterns and mixing rates in agitated vessels. *AIChE Journal, 6*(3), 432-437. doi:10.1002/aic.690060317

Oxygenates Fact Book. Clean Fuels Development Coalition.

Phelps, C., Smart, N., & Wai, C. (1996). Past, present and possible future applications of supercritical fluid extraction technology. *Journal of Chemical Education, 73*(12).

Primary Energy Consumption by Source. (2016).

Rakopoulos, D., Rakopoulos, C., Giakoumis, E., Papagiannakis, R., & Kyritsis, D. (2014). Influence of properties of various common bio-fuels on the combustion and emission characteristics of high-speed DI (direct injection) diesel engine: Vegetable oil, bio-diesel, ethanol, n-butanol,diethyl ether. *Energy, 73*, 354-366.

Shafiee, S., & Topal, E. (2009). When Will Fossil Fuel Reserves be Diminished? *Energy Policy, 37*(1), 181-189.

Shuler, M., & Kargi, F. (2002). *Bioprocess Engineering Basic Concepts* (2 ed.). Englewood Cliffs Pearson.

Stahl, E., Quirin, K. W., & Gerard, D. (1988). *Dense gases for extraction and refining*. United States U6 - ctx_ver=Z39.88-2004&ctx_enc=info%3Aofi%2Fenc%3AUTF-8&rfr_id=info%3Asid%2Fsummon.serialssolutions.com&rft_val_fmt=info%3Aofi%2Ffmt%3Akev%3Amtx%3Abook&rft.genre=book&rft.title=Dense+gases+for+extraction+and+refining&rft.au=Stahl%2C+E&rft.au=Quirin%2C+K.W&rft.au=Gerard%2C+D&rft.date=1988-01-01&rft.externalDocID=5831814&paramdict=en-US U7 - Book.

Sukumaran, R. K., Gottumukkala, L. D., Rajasree, K., Alex, D., & Pandey, A. (2011). *Butanol Fuel from Biomass: Revisiting ABE Fermentation*: Academic Press.
Tai, C. Y., & Wu, S.-Y. (2005). Kinetics of supercritical fluid extraction of ethanol from aqueous solution. *Chemical Engineering Communications, 192*(10-12), 1347-1360. doi:10.1080/009864490517133
Thompson, J., Prather, K., Timko, M., Freedman, A., Boock, J., & Tompsett, G. (2016). *Systems Biology Towards a Continuous Platform for Biofuels Production*. Retrieved from https://www.orau.gov/gsp2016/abstracts/thompson_janelle.pdf.
Tyner, E. W. (2008). The US Ethanol and Biofuels Boom: Its Origins, Current Status, and Future Prospects. *BioScience, 58*(7), 646-653.
van de Vusse, J. G. (1959). Residence times and distribution of residence times in dispersed flow systems. *Chemical Engineering Science, 10*(4), 229-233. doi:10.1016/0009-2509(59)80057-9
Visscher, F., van der Schaaf, J., Nijhuis, T. A., & Schouten, J. C. (2013). Rotating Reactors - A Review. *Chemical Engineering Research and Design, 91*, 1923-1940.
Wallner, T., Miers, S. A., & McConnell, S. (2009). A comparison of ethanol and butanol as oxygenates using a direct-injection, spark-ignition engine. *Journal of Engineering for Gas Turbines and Power, 131*(3), 032802.
Wang, S.-J., & Zhong, J.-J. (1996). A Novel Centrifugal Impeller Bioreactor. *Biotechnology and Bioengineering, 51*, 511-519.
Wankat, P. (2012). *Separation Process Engineering* (3 ed.). Saddle River: Pearson Education.
Westerterp, K. R., van Dierendonck, L. L., & de Kraa, J. A. (1963). Interfacial areas in agitated gas-liquid contactors. *Chemical Engineering Science, 18*(3), 157-176. doi:10.1016/0009-2509(63)85002-2
Xia, J.-Y., Wang, S.-J., Zhang, S.-L., & Zhong, J.-J. (2008). Computational Investigation of Fluid Dynamics in a Recently Developed Centrifugal Impeller Bioreactor. *Biochemical Engineering Journal, 38*, 406-413. doi:10.1016/j.bej.2007.08.006
Yusuf, C. (2007). Biodiesel from Microalgae. *Biotechnology Advances, 25*, 294-306.
Zwietering, T. N. (1958). Suspending of solid particles in liquid by agitators. *Chemical Engineering Science, 8*(3), 244-253. doi:10.1016/0009-2509(58)85031-9